CSMS

CONFERENCE

MICROSCOPY2024

20 - 22 MAY 2024

Hotel Atrium
Nový Smokovec
Slovakia

Microscopy 2024

Book of abstracts

Vladislav Krzyžánek, Kamila Hrubanová, Dušan Chorvát
(eds.)

Czechoslovak Microscopy Society

Brno 2024

Vladislav Krzyžánek, Kamila Hrubanová, Dušan Chorvát (eds.)

Microscopy 2024. Book of abstracts.

Brno, 2024

ISBN 978-80-909216-0-3

Annual CSMS conference Microscopy 2024, 20.-22.5.2024, Nový Smokovec, Slovakia

Content

Československá mikroskopická společnost, z.s.

Československá mikroskopická společnost je občanské sdružení vědeckých, pedagogických, technických a odborných pracovníků, kteří se zabývají a zajímají o jakýkoliv typ mikroskopie. Cílem tohoto sdružení je zvyšovat úroveň mikroskopických oborů, rozvíjet je a vzdělávat především nastupující vědeckou generaci. Společnost vytváří prostředí a podmínky pro vzájemnou odbornou spolupráci a výměnu znalostí mezi členy působícími ve vědě, školství, praxi a spolupracuje za tímto účelem také s firmami, vyvíjejícími a vyrábějícími mikroskopickou techniku. Společnost každoročně pořádá česko-slovenskou konferenci a vícero odborných kurzů a uděluje výroční cenu ČSMS významné osobnosti mikroskopie. Z mezinárodních aktivit společnost pravidelně spolupořádá Multinational Congres on Microscopy (MCM) a je členem European Microscopy Society (EMS) a International Federation of Societies for Microscopym (IFSM).

CSMS in short

The Czechoslovak Microscopy Society is a voluntary organisation gathering of scientists, pedagogical, technical and other specialists in the area of electron, optical, and other types of microscopy. Its purpose is to develop and advance standards in the field, to provide conceptual prognosis/assessment, and to promote the results of the research in the field. The Society fulfils the following objectives:

- Support of the progress in all branches and applications of microscopy, promotion of science and popularization of science to the public.
- Advancement and prognosis of achievements, encouragement and coordination of collaboration between members in research, education and praxis.
- Contribution to the growth of the academic level of members, particularly those who are novices in the field.
- Promotion of the relevant associated bodies related to scientific work to stimulate development in the field.
- Maintenance of the specialist expertise in projects involving microscopy techniques and equipment.
- The Society is a member of the International Federation of Societies for Microscopy (IFSM) and the European Microscopy Society (EMS). It collaborates also with other international organisations of similar goals.

Exhibitors and Sponsors

ADVASCOPE
accelerating particle detection

Altium

crytur

delong instruments®

JEOL

mt.eu měřicí technika morava

NenoVision

pragolab

SpeciOn

SVEN BIOLABS S.R.O.
WWW.SVENBIOLABS.CZ

TESCAN
PERFORMANCE IN NANOSPACE

ThermoFisher SCIENTIFIC

ZEISS
Seeing beyond

ČESKÝ OPTICKÝ KLASTR
Let's Make Optics for the Future. Together.

CSMS Conference - **MICROSCOPY 2024**

20 - 22 May 2024, Nový Smokovec, Vysoké Tatry
Hotel Atrium / Nový Smokovec, Vysoké Tatry

Monday 20th May 2024

8:00	**Trip to the mountains** *(expected arrival time 13:00)*
15:00	**Registration of participants** *(until 19:00)*
15:30	**Member meeting of CSMS**
17:00	**Conference opening**
17:10	**Announcement of the winners of scholarship competition by Thermo Fisher / CSMS**
17:15	Jan Hajduček: Comprehensive magnetic analysis from electron diffraction patterns in Transmission Electron Microscopy
17:30	**Announcement of the winners of scholarship competition by CSMS**
17:35	Tomáš Hrbek: Electrochemical atomic force microscopy as a tool for the study of degradation of iridium-ruthenium catalyst for the anode of a proton exchange membrane water electrolyzer
17:50	**Announcement of the winner of the best CSMS dissertation sponsored by ZEISS**
17:55	Jakub Pospíšil: Development of biomimetic surfaces for studying of cellular interactions
18:10	**Announcement of CSMS award for merit in microscopy**
18:15	Miroslav Šlouf: Lecture of the laureate
19:00	**Welcome party**

Tuesday 21th May 2024

9:00	**Plenary lecture** Jiří Materna: Where artificial intelligence is heading: applications in microscopy
9:45	**Session I - Material sciences** (chairs: Eliška Materna Mikmeková and Miroslav Šlouf)
9:45	**Invited talk** Tamás Csanádi: Strength enhancement and plasticity of high-entropy carbide grains at the micro-scale
10:15	Ivo Kuběna: Microstructural Damage Mechanisms in Additively Manufactured Ni-Based Superalloy
10:30	Mariana Klementová: Eveslogite - nanotubular silicate mineral
10:45	Lukáš Průcha: Transfer of graphene onto different substrates for specific applications
11:00	Saffana Kouka: Thermoplastic starch: Relations among processing conditions, morphology, rheology, and properties
11:15	**Poster session + coffee break**
11:45	**Technology news I** (chairs: Jana Nebesářová and Josef Lazar)
11:45	Thermo Fisher Scientific (Lukáš Kejík): Hydra PFIB platform for advanced material and life science applications
12:15	AdvaScope (Pavel Stejskal): Advancing Diffraction in SEM: Using Hybrid-Pixel Detectors for Ultrafast 4D STEM
12:30	Pragolab (Jan Vysloužil): Electron and holographic microscopes in practice
12:45	Specion (Andreas Nowak): Leica Microsystems is proud to present the next generation ultramicrotome for electron microscopy sample preparation
13:00	**Lunch**

14:00	**Technology news II** (chairs: Jana Nebesářová and Josef Lazar)
14:00	JEOL (Laurent Vassé): FIB Solutions from JEOL
14:30	TESCAN (Hana Tesařová): Empowering Innovation in Science with TESCAN Solutions
14:45	Altium International (Kateřina Lónová): Cellular Secrets Unveiled: Ever wondered what your cells are up to at night?
15:00	ZEISS (Pavel Krist): Easy and Perfect Scanning of Microscopy Slides
15:30	**Poster session + coffee break**
16:30	**Session II - Optics and Instrumentation** (chairs: Kamila Hrubanová and Dušan Chorvát)
16:30	**Invited talk** Ilya Belevich: Bridging the gap: AI-based segmentation tools for quantitative microscopy and the following analysis pathways
17:00	Radim Skoupý: Sixteen pixel electron ptychography
17:15	Pavlína Sikorová: 4D-STEM/PNBD: Powder electron diffraction in SEM microscopes
17:30	Michal Horák: Metal-insulator transition in vanadium dioxide studied by analytical transmission electron microscopy
17:45	Tereza Motlová: Production of polymer optical elements and their analysis by electron microscopy
18:00	**Break**
19:00	**Social evening with banquet (+ yCSMS activities)**

Wednesday 22th May 2024

9:00	**Workshops** Viktor Sykora: Electron Microscopy and Artificial Intelligence (in Czech) Ilya Belevich: Deep Learning for Image Segmentation: A Comprehensive Workflow from Raw Images to Complete Models
10:00	**News in microscopy community** (chairs: Vladislav Krzyžánek)
10:00	Martin Strnad: The Young Czechoslovak Microscopy Society: Mapping out future endeavors
10:10	Radka Martinková: Brnoregion microscopy
10:20	Martina Wernerová: Czech-BioImaging: Infrastructure dedicated to users
10:30	Jiri Novacek: Czech Infrastructure for Integrative Structural Biology
10:40	Petr Mikulík: New study program “Mikroskopie” at the Masaryk University
10:50	Petr Přikryl: Building the Czech optical ecosystem
11:00	**Poster session + coffee break**
11:30	**Session III – Biomedical sciences** (chairs: Veronika Huntošová and Jiří Týč)
11:30	**Invited talk** Martin Kundrát: Microscopy and X-ray Imaging in Paleontology: Slovak Integrative Paleobiology Lab
12:00	Josef Lazar: Novel genetically encoded biosensors for imaging molecular processes of cell signaling
12:15	Aleš Benda: Enhancing FLIM Data Analysis Through Deep Learning
12:30	Dominik Pinkas: The utility of EDS in biological transmission electron microscopy
12:45	Veronika Huntosova: Multimodal metal-organic framework nanoparticles for bioimaging and targeted treatment
13:00	**Conclusion**
13:10	**Lunch**

Plenary session

Where artificial intelligence is heading: applications in microscopy

Materna J.[1], Mikmeková Š.[2], Čermák J.[2], Jozefovič P.[2], Ambrož O.[2], Zouhar M.[2]

[1] Machine Learning College, s.r.o, Brno, Czech Republic
[2] Institute of Scientific Instruments of the Czech Academy of Sciences, Brno, Czech Republic

Email of the presenting author: jiri@mlcollege.com

In this talk, we delve into the exciting realm of artificial intelligence (AI) and its growing range of applications within microscopy. Beginning with a brief overview of the current landscape of AI in 2024, with particular emphasis on the strides made in generative AI, we set the stage for an exploration into the realm of machine learning for image processing and generation.

As AI continues its rapid evolution, its integration into microscopy holds immense promise for advancing our understanding of the microscopic world. By harnessing the power of generative AI, researchers can now analyze intricate microscopical structures and phenomena with unprecedented accuracy, revolutionizing experimental design and analysis. Our focus will shift to the pivotal role of machine learning in facilitating image-to-image translation. Through sophisticated algorithms and neural network architectures, AI can seamlessly convert images captured through various microscopy techniques, facilitating cross-modal analysis and enhancing data interpretation.

To conclude the talk, we will present a compelling use-case demonstrating the practical application of AI in microscopy within a research group at the Institute of Scientific Instruments of the Czech Academy of Sciences. Specifically, we will delve into our ongoing efforts in steel analysis, showcasing how AI-driven image processing techniques have revolutionized our approach to understanding material properties and structural characteristics at the microscale. This case study serves as a testament to the transformative potential of AI in microscopy and underscores its role in driving innovation across diverse scientific domains.

Acknowledgement:

This research was funded by the Czech Academy of Sciences, praemie Lumina Quaeruntur:
“Laboratory of advanced steels microstructural classification by artificial intelligence methods”.

Technology news

Hydra PFIB platform for advanced material and life science applications

Kejík L.[1], Hovorka M.[1], Wandrol P.[1], Ošťádal R.[1]

[1] Thermo Fisher Scientific, Brno, Czech Republic

Email of the presenting author: lukas.kejik@thermofisher.com

Plasma focused ion beam (PFIB) delivers several advantages with respect to the conventional gallium-based FIB. Material removal rate can be significantly larger as the PFIB generally offers much higher ion beam currents without the need to deal with the implanted gallium ions which can react with the milled material.

We introduce a Helios Hydra PFIB DualBeam platform which combines the innovative multiple ion species PFIB column with the monochromated Elstar SEM Column. The unique multiple ion species PFIB column enables the use of four ion species (Xe, Ar, O, N) as a primary beam with a fast and automated switching capability. The SEM column offers a wide range of working conditions to image the nanoscale details with sub-nanometer resolution. Additionally, utilization of the Cryo Stage accesses the cryogenic temperatures to work with vitrified biological samples or with unstable material science samples like polymers.

The choice of four different ion species grants the option of choosing the best fit for the desired use case or even combine different ions, e.g., to use Xe^+ to mill away large volume of materials while polishing with Ar^+ to have smooth cut faces. Nevertheless, the choice of the ion species depends on the milled material where, e.g., O^+ ions showed to be the best choice for carbon-based materials. One can also consider the differences in the damage done to the sample by the ions where heavier ions generally result in more damage events overall, but the damage is more localized within a thinner layer than in case of lighter ions.

The unique properties of the Hydra platform were demonstrated on two main use cases: high-resolution volume imaging (Fig.1) and lamella preparation for the follow up TEM analysis of the samples from the biological as well as material science domains. Additionally, Helios Hydra DualBeam can support several complete workflows for the TEM lamella preparation. From the life science domain, the cryo correlative targeting workflow is possible thanks to the Integrated Fluorescence Light Microscope (iFLM) which allows targeting a specific region of the cell based on the fluorescence data and the resulting lamella can then be transferred to the cryo TEM. From the material science domain, the Inert Gas Sample Transfer workflow allows working with air sensitive, e.g., battery electrode materials where the CleanConnect facilitates the inert gas transfer from the glove box, milling the lamella in the DualBeam, and the transfer to the TEM, preserving the pristine structure of the observed materials.

In conclusion, the Helios Hydra PFIB DualBeam platform offers a unique versatility and a broad range of applications from the life and material sciences contributing to advancements at the forefront of scientific exploration.

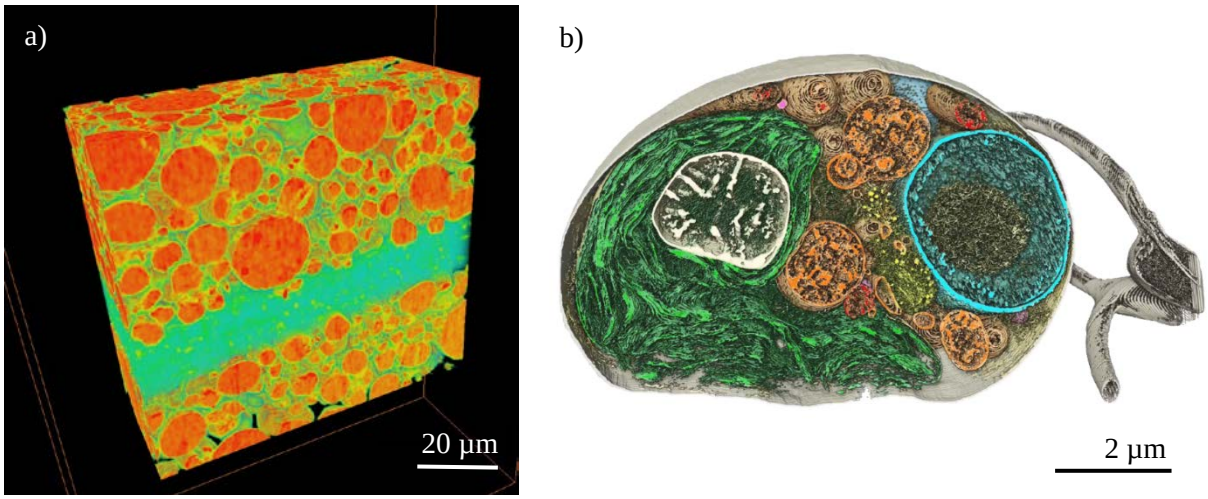

Fig.1: 3D reconstruction of the Auto Slice and View dataset: a) lithium nickel manganese cobalt oxide (NMC) cathode, b) plunge-frozen Chlamydomonas cell.

Advancing Diffraction in SEM: Using Hybrid-Pixel Detectors for Ultrafast 4D STEM

Stejskal P.[1], Motúz R.[2], Horák M.[3], Šikola T.[3]

[1] AdvaScope s.r.o., Brno, Czech Republic
[2] TESCAN Group, Brno, Czech Republic
[3] Brno University of Technology, Brno, Czech Republic

Email of the presenting author: pavel.stejskal@advascope.cz

4D Scanning Transmission Electron Microscopy (4D STEM) is a cutting-edge technique that involves scanning an electron beam across a 2D array on a sample. Simultaneously, a detector positioned below the sample records a 2D pattern for each point visited by the electron beam, resulting in a 4D dataset. This method is commonly used in Transmission Electron Microscopy (TEM) for various applications, including virtual imaging, orientation analysis, strain mapping, and differential phase contrast.

Recent advancements in detector technology, particularly in miniaturization and low-energy sensitivity, have made it feasible to apply this technique even in Scanning Electron Microscopes (SEMs). The primary objective of this work is to develop a dedicated 4D STEM detector specifically for SEMs.

The proposed 4D STEM solution relies on a Timepix3 pixelated detector. The Timepix3 detector comprises a matrix of 256 × 256 smart digital pixels (each with a pixel pitch of 55 μm). Within each smart pixel, advanced electronics handle signal processing, including digital registers. Upon detecting an electron, immediate digitization occurs, capturing complex information such as position, energy, and time. This process effectively suppresses unwanted signals, allowing only relevant events to be selected. Consequently, image quality improves significantly, noise is reduced, and resolution and contrast are enhanced in the acquired images.

One of the key advantages of this detector for 4D STEM applications is its data-driven readout. Instead of recording a full image for every probe position, the detector streams data directly from the chip for each detected event. As a result, dwell times can be as short as hundreds of nanoseconds, eliminating the traditional bottleneck associated with image acquisition.

Initial results from the in-situ setup are depicted in Figure 1, where a complete map of 1536 × 1024 points was acquired in just 80 seconds. The full dataset includes individual diffractograms for each point, enabling subsequent virtual diffraction imaging.

References:

[1] Ophus, C.: “Four-Dimensional Scanning Transmission Electron Microscopy (4D-STEM): From Scanning Nanodiffraction to Ptychography and Beyond” doi: 10.1017/s1431927619000497
[2] Tureček, D., Jakůbek, J. and Soukup, P.: "USB 3.0 readout and time-walk correction method for Timepix3 detector", doi:10.1088/1748-0221/11/12/C12065
[3] "Four-dimensional scanning transmission electron microscopy in a FIB-SEM instrument", ID: FW06010396, national TAČR grant

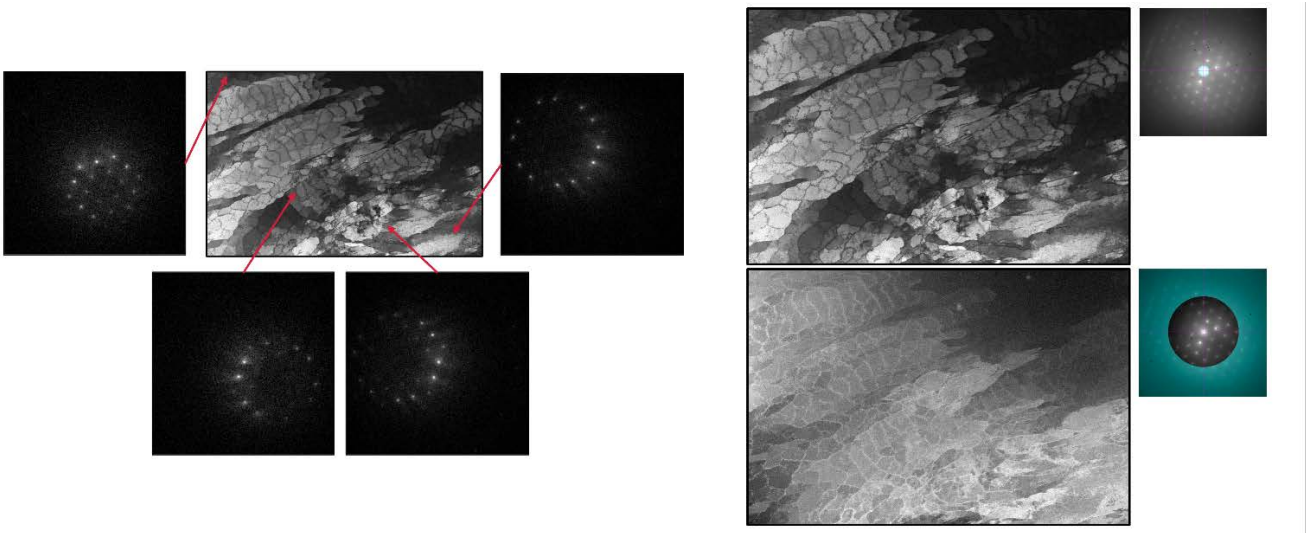

a) individual diffractograms for different locations b) reconstructed SEM images with bright field and HAADF masks applied

Figure 1: 4D-STEM image of a stainless steel sample, 1536 × 1024, 30 kV, 13 pA with a frame time 80 s.

Electron and holographic microscopes in practice

Vysloužil J.[1]

[1] Pragolab s.r.o., Prague, Czech Republic

Email of the presenting author: vyslouzil@pragolab.cz

Microscopic techniques are essential for research in both living and non-living sciences, and new imaging methods and increased resolution capabilities create opportunities for detailed studies of biological samples, including capturing the dynamics of living cells as well as material samples.

Electron microscopy enables the examination of cell and tissue ultrastructure on a nanometer scale. Within electron microscopy, including low-voltage microscopy, it is possible to combine TEM, SEM, STEM, ED, and EDS methods for routine and rapid work. High contrast and resolution offer utilization in a wide range of applications: nanomaterials, polymers, bacteria, viruses, tissue sections, chemistry, biochemistry, water purity, etc. Lens technology based on permanent magnets allows for the creation of a compact and easily transportable microscope for any laboratory without the need for structural modifications of laboratory.

QPI (Quantitative Phase Imaging) represents a new approach within microscopic methods for evaluating cell growth, differentiation, proliferation, necrosis, or apoptosis. The high detection sensitivity of the system enables precise and fully automated cell segmentation with subsequent analysis of data describing the properties and dynamics of cell populations. With its gentleness, it finds its place even in experiments with stem cells, in researching new drugs, in studying cell interactions, as well as in biomaterial research, with the choice between a label-free approach or a combination of QPI with fluorescence labeling.

Leica Microsystems is proud to present the next generation ultramicrotome for electron microscopy sample preparation

Nowak A.[1]

[1] Leica Microsystems, Vienna

Email of the presenting author: Andreas.Nowak@leica-microsystems.com

Building upon the Leica EM UC7 and 70 years of ultramicrotomy history, UC Enuity introduces a significant advancement to the field. With an emphasis on automation, UC Enuity lowers the barrier to entry for researchers and technicians, enabling users of all skill levels to achieve precise and reproducible results with minimal training. Moreover, its modular design not only enhances the user experience but also ensures the ultramicrotome is future-proof, offering the flexibility to upgrade and integrate new features according to your needs, such as Auto alignment and reliably target trimming based on µCT data.

Cellular Secrets Unveiled: Ever wondered what your cells are up to at night?

Lonova K.[1], Kobidova B.[1]

[1] Altium International s.r.o., Prague, Czech Republic

Email of the presenting author: katerina.lonova@hpst.cz

In recent years, the field of digital holographic microscopy has gained widespread popularity as a convenient tool for observing cell populations. Offering a user-friendly and hassle-free approach, digital holographic microscopy has emerged as a popular method for researchers, owing to its ability to provide high-quality images without the requirement for chemical staining or labels, which can introduce unwanted cytotoxic effects. By harnessing label-free technology and employing a fully automated workflow, digital holographic microscopy enables gentle yet precise imaging of cells, preserving their natural characteristics and dynamics. This non-invasive modality not only eliminates the need for disruptive sample preparation procedures but also maintains exceptional resolution, ensuring that even subtle cellular features can be accurately captured and analyzed. Moreover, digital holographic microscopy offers an innovative solution for continuous imaging, facilitating the real-time monitoring of cellular processes in their native environment. By enabling researchers to observe dynamic cellular behaviors over extended periods, digital holographic microscopy opens up new avenues for understanding complex biological phenomena and advancing various fields, including cell biology, microbiology, and tissue engineering.

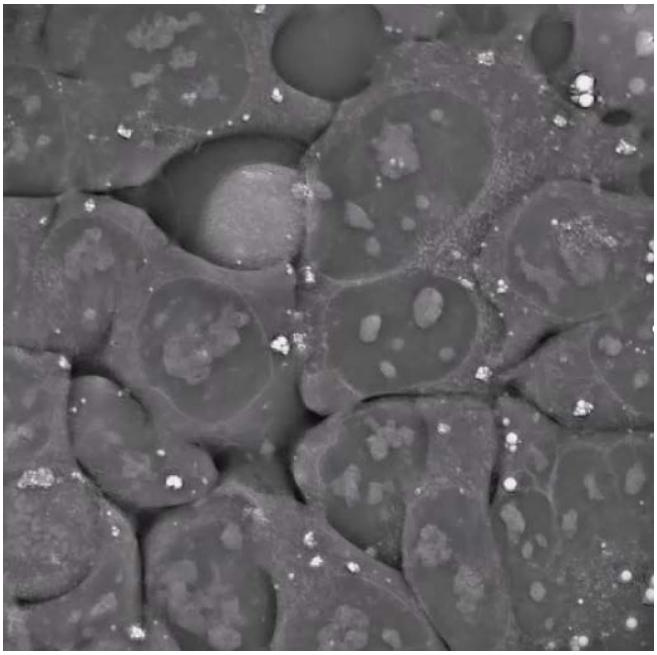

Easy and Perfect Scanning of Microscopy Slides

Krist P.[1]

[1] ZEISS Research Microscopy Solutions

Email of the presenting author: pavel.krist@zeiss.com

The most challenging research tasks as well as your routine scanning applications are supported by powerful hardware and perfectly featured software of ZEISS Axioscan 7. Capture virtual slides quickly with high-speed scanning, while retaining consistently high quality, whether you want to capture brightfield, fluorescence or polarized light images. ZEISS Axioscan 7 repeatedly produces digitized slides at dramatically improved speed, thanks to hardware components designed for extended, uninterrupted operation. A fully motorized condenser, powerful light sources and sensitive cameras ensure 24/7 scan performance, whether you have many similar slides or mixed applications to process. Easily assigned scan profiles allow acquisition runs to be set up quickly. Axioscan 7 software is built to flawlessly process large amounts of raw data – in the range of several terabytes.

References:

[1] https://www.zeiss.com/microscopy/en/home.html
[2] https://www.zeiss.com/microscopy/en/products/imaging-systems.html

Fig. 1: ZEISS Axioscan 7

CSMS awards

Comprehensive magnetic analysis from electron diffraction patterns in Transmission Electron Microscopy

Hajduček J.[1], Štindl J.[2], Rusz J.[3], Uhlíř V.[1,2]

[1] CEITEC BUT, Brno University of Technology, Brno, Czech Republic
[2] Institute of Physical Engineering. Brno University of Technology, Brno, Czech Republic
[3] Department of Physics and Astronomy, Uppsala University, Uppsala, Sweden

Email of the presenting author: jan.hajducek@ceitec.vutbr.cz

A high-resolution understanding of magnetic textures and their physics allowed magnetic materials to transform numerous technological fields, such as data storage, sensing, or computing devices. However, the ongoing demand for performance enhancement and miniaturization requires combining multiple types of magnetic orderings; apart from conventionally used ferromagnets (FM), antiferromagnets (AF) are increasingly exploited. AF ordering is characteristic of its alternating magnetic moments between neighboring atoms, making their internal magnetic textures unresolvable for most conventional magnetic imaging techniques [Che20].

Transmission electron microscopy (TEM) has dominated the field of sub-nm spatial resolution and has shown its ability to resolve numerous FM features, such as domain walls and skyrmions, including the direction of the magnetization vector [Wol22]. Recently, it has been shown that TEM can resolve even AF features [Kri22, Koh22]; however, with a very limited picture of their exact magnetic configuration. TEM-based techniques sensitive to AF order are typically linked to analyzing electron diffraction patterns in various experimental configurations [Lou12], including the energy-filtered analysis [Yua97].

This work aims to provide a more complete picture of how AF ordering of the studied specimen translates to the distribution of inelastically scattered electrons in the TEM diffraction patterns. We demonstrate the semiquantitative theoretical approach of how the different configurations of AF magnetic moments project to energy-filtered diffraction patterns and the experimental platform for validating these results, namely freestanding films of AF NiO and FeRh.

We demonstrate that understanding inelastically scattered electrons in TEM diffraction patterns could open broad experimental possibilities for high-resolution deciphering of AF order, thus further solidifying their fundamental understanding and strengthening their application potential.

References:

[Che20]: S.-W. Cheong, et al. *npj Quant. Mat.* **5**:3 (2020).
[Wol22]: D. Wolf, et al. *Nat. Nano.* **17**, 250-255 (2022).
[Kri22]: F. Křížek, et al. *Sci. Adv.* **8**, eabn3535 (2022).
[Koh22]: Y. Kohno, et al. *Nature* **602**, 234–239 (2022).
[Lou12]: J. C. Loudon. *Phys. Rev. Lett.* **109**, 267204 (2012).
[Yua97]: J. Yuan, et al. *Journ. of Appl. Phys.* **81**(8) (1997).

Acknowledgement:

JH acknowledges the financial support from the TFS & CSMS Scholarship (2023). JH, JŠ, and VU acknowledge CzechNanoLab Research Infrastructure supported by MEYS CR (LM2023051).

Electrochemical atomic force microscopy as a tool for the study of degradation of iridium-ruthenium catalyst for the anode of a proton exchange membrane water electrolyzer

Hrbek T.[1], Khalakhan I.[1], Kúš P.[1], Matolínová I.[1]

[1] Charles University, Faculty of Mathematics and Physics, Department of Surface and Plasma Science, V Holešovičkách 2, 180 00 Prague 8, Czech Republic

Email of the presenting author: tomas.hrbek@matfyz.cuni.cz

Introduction

Proton Exchange Membrane Water Electrolyzers (PEM-WEs) are poised for commercial-scale production, yet the challenge persists regarding developing an effective iridium-based catalyst for the anode [1]. Our previous investigation showcased a thin-film iridium-ruthenium catalyst (comprising 25% Ir, equivalent to 158 µg cm-2, and 75% Ru) fabricated onto the surface-enhanced PEM-WE anode using magnetron sputtering [2]. This catalyst exhibited remarkable activity and durability within single-cell PEM-WE setups, achieving a current density of 1 A cm-2 at 1.606 V and operating at 80 °C, with a degradation rate of merely -1.3 µV h-1 sustained over 500 hours [3]. Despite its superior electrochemical performance, the precise mechanisms underlying its efficacy remain unknown.

Materials and methods

The materials under investigation comprise bimetallic alloys comprising iridium and ruthenium, fabricated via magnetron sputtering. Primary investigations of these layers will be conducted using an electrochemical atomic force microscope to elucidate the correlation between morphology and applied potential. Additionally, the twin counterparts of the prepared layers intended for electrochemical atomic force microscopy analysis will undergo examination within a specialized electrochemical setup to accurately assess their performance. Comprehensive characterization of all samples will entail the application of a diverse array of analytical techniques, including X-Ray Photoelectron Spectroscopy, Energy Dispersive X-Ray Spectroscopy, and Scanning Electron Microscopy.

Results

The preliminary investigation of the electrochemical activity in the half-cell confirms our previous results, demonstrating the superior activity of Ir-Ru 25.75, compared to Ir-Ru 50:50 and pure Ir. Pure Ru 100 shows excellent activity but has inferior stability.

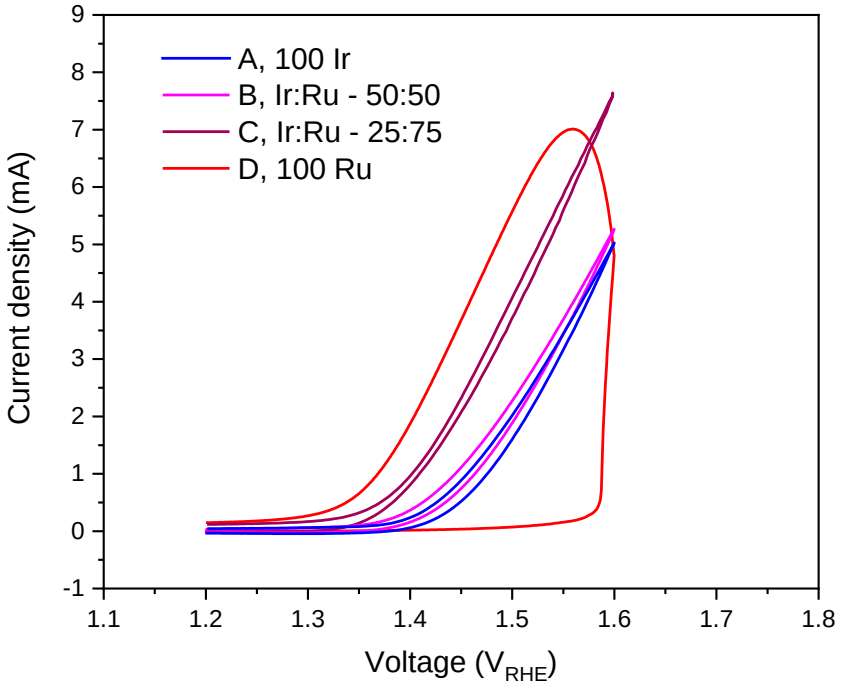

Fig. 1: The activities of Ir-Ru bimetallic catalyst in rotating disk electrode.

Conclusion

The Ir-Ru catalyst prepared by magnetron sputtering demonstrates excellent catalytical properties for oxygen evolution reactions in proton exchange membrane water electrolyzers. However, the mechanism behind its operation still needs to be well described. We employ an electrochemical atomic force microscope to understand them more thoroughly.

References:

1. Carmo, M., et al., *International Journal of Hydrogen Energy*. 2013. p. 4901-4934.
2. Hrbek, T., et al., *International Journal of Hydrogen Energy*. **47**(49): p. 21033-21043.
3. Hrbek, T., et al., Journal of Power Sources, 2023. **556**.

Acknowledgement:

Tomáš Hrbek acknowledges funding from the CSMS scholarship.

Development of biomimetic surfaces for studying of cellular interactions

Pospíšil J.[1,2], Hovádková Z.[5], Hrabovský M.[5], Mlčoušková J.[7], Bidmanová Š.[3], Paruch K.[4], Damborský J.[3], Hampl A.[1, 6], Jaroš J.[1,6]

[1] Core Facility Cellular Imaging, CEITEC Masaryk University, Brno, Czech Republic
[2] Department of Histology and Embryology, Faculty of Medicine, Masaryk University, Brno, Czech Republic
[3] Loschmidt Laboratories, Department of Experimental Biology and Research Centre for Toxic Compounds in the Environment, Masaryk University, Brno, Czech Republic
[4] Department of Chemistry, Faculty of Science Masaryk University, Brno, Czech Republic
[5] TESCAN Brno s.r.o.
[6] International Clinical Research Center (ICRC), St. Anne's University Hospital, Brno, Czech Republic
[7] LORD, Faculty of Medicine, Masaryk University, Brno, Czech Republic

Email of the presenting author: jakub.pospisil@ceitec.muni.cz

Intercellular interactions and cellular engagement with the extracellular matrix are essential for maintaining tissue and organ homeostasis during development and into adulthood. This research overcomes the limitations of current technologies that cannot precisely manipulate molecular domain distributions in experimental settings. It does so by employing a cutting-edge electron beam lithography (EBL) technique that modifies cultivation surfaces at the nanoscale and enables covalent bonding of protein domains, thereby facilitating cellular interactions (Fig. 1).

The study places a special emphasis on advanced microscopy techniques, specifically structured illumination microscopy (SIM) and expansion microscopy (ExM). These super-resolution methods are pivotal in analyzing the effects of nanoscale bio-domain configurations on cellular behavior, using the Ephrin family of proteins as a model system. Observations made on the hESC stem cell line (CCTL14) reveal that precise nanoscale arrangements significantly influence cellular responses.

By integrating SIM (Fig. 2) and ExM, this work not only provides a deeper insight into the nanometer-scale interactions but also demonstrates the utility of biomimetic nanostructured surfaces. These surfaces are adaptable and can be employed to explore various biological questions, thereby enabling a detailed examination of the mechanisms driving cellular interactions at the nanoscale. This approach offers a significant advancement in the field of cellular and molecular biology, pushing the boundaries of what can be studied and understood about cell behavior.

Acknowledgement:

This work was supported by the European Regional Development Fund─project INBIO (CZ.02.1.01/0.0/0.0/16_026/0008451). The authors would like to acknowledge the Ministry of Education, Youth and Sport of the Czech Republic (MEYS CR) for financial support (European Strategy Forum on Research Infrastructures [ESFRI] Research Centre for Toxic Compounds in the Environment [RECETOX] LM2018121). This project has received funding from the European Union's Horizon 2020 research and innovation program under grant agreement 857560. The article reflects the authors' views, and the agency is not responsible for any use that may be made of the information it contains. D.B. was supported by funds from Alzheimer nadační fond, Prague, Czech Republic, and by Career Restart Grant (MUNI/R/1697/2020). The authors acknowledge the core facility CELLIM supported by the Czech-BioImaging large RI project (LM2018129, funded by MEYS CR) for their support with obtaining scientific data presented in this paper. The authors gratefully acknowledge the Czech Infrastructure for Integrative Structural Biology (CIISB), the Instruct-CZ Centre of Instruct-ERIC EU consortium, funded by MEYS CR infrastructure project LM2018127, and the European Regional Development Fund project UP CIISB (CZ.02.1.01/0.0/0.0/18_046/0015974) for financial support of the experiments performed at the CF Nanobiotechnology. The authors also acknowledge the support provided by CZ-OPENSCREEN, National Infrastructure for Chemical Biology (LM2018130), and by Bader Philanthropies, Inc.

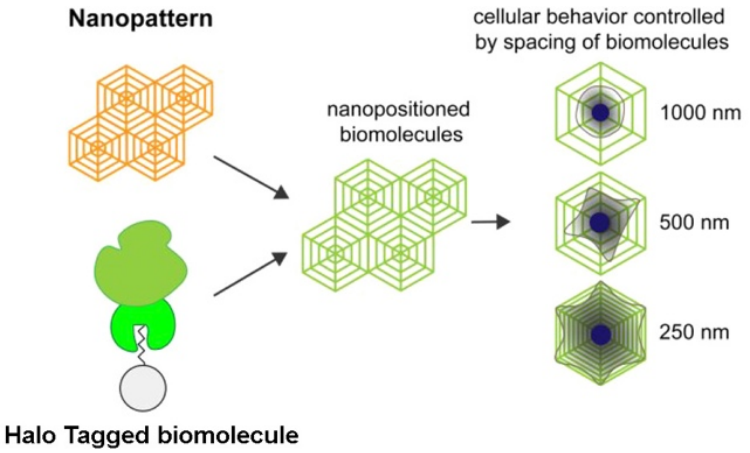

Fig. 1: Nanoscale modification and modulation of cellular interactions

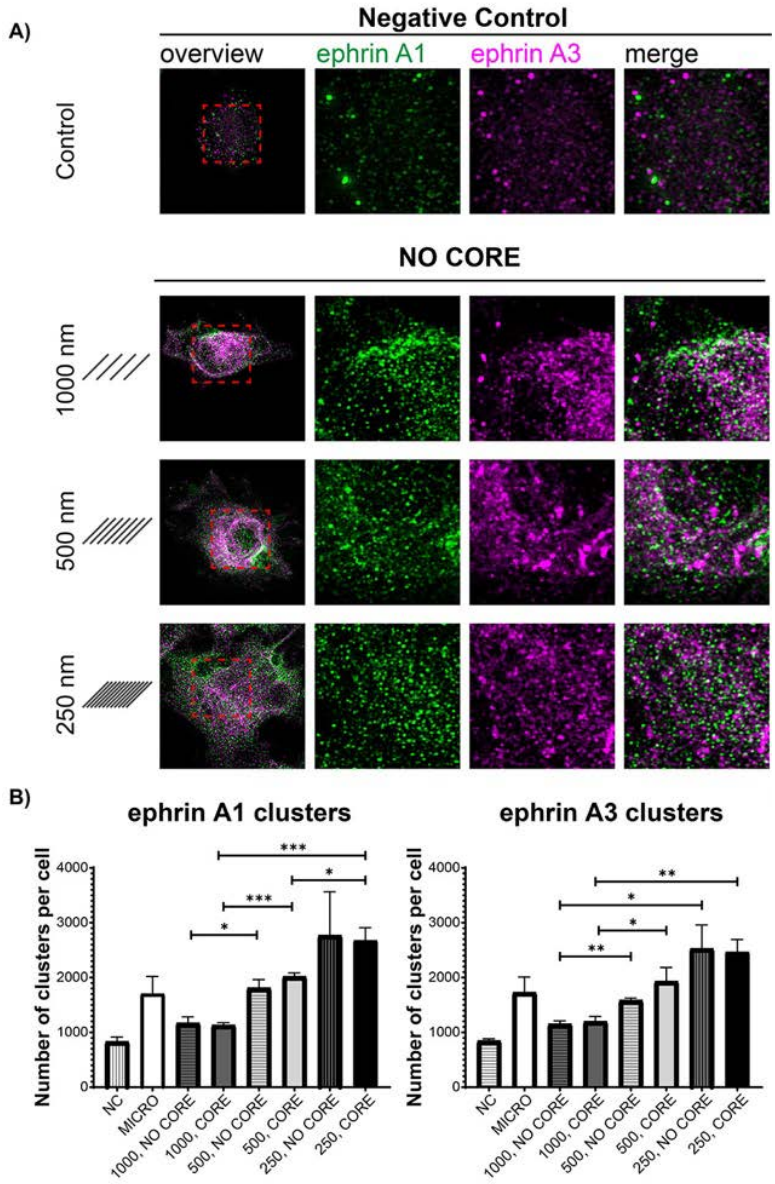

Fig. 2: Nanopatterned EphA2 Influences Intracellular Localization of the Ephrin A Ligands in Human Pluripotent Stem Cells

Thirty Years in Materials Science: From Diffraction to Microscopy, Micromechanical Properties, and Back Again

Slouf M.[1]

[1] Institute of Macromolecular Chemistry CAS, Prague, Czech Republic

Email of the presenting author: slouf@imc.cas.cz

In this contribution, I summarize my experience and achievements after 30 years of work in materials research. Materials science is defined as an interdisciplinary field of researching, modifying and/or discovering materials. It incorporates the elements of chemistry, physics, and engineering. The main focus is set on the understanding of the relations among the processing, structure, and properties of materials.

My way through the realm of materials science started in the field of diffraction (Charles University in Prague; single crystal X-ray diffraction; deformation electron densities), then it continued with microscopic methods (Institute of Macromolecular Chemistry CAS; electron microscopy of synthetic polymers and biopolymers; bulk polymer systems for biomedical applications), later it brought me to the micromechanical properties of the investigated materials (microindentation; structure-properties relations in polymer systems), and recently it lead back to the diffraction techniques (4D-STEM-in-SEM; development of novel, fast and user-friendly method of electron diffraction in SEM microscopes, which was named 4D-STEM/PNBD and called *electron diffraction for everyone*).

During the presentation, we will go through all above-listed topics. We will demonstrate the surprisingly close connections among diffraction, microscopy and microindentation techniques in materials science. We will illustrate the steeply increasing importance of automated data processing and programming in contemporary data analysis. Last but not the least, we will exemplify the power and the necessity of collaborations in modern research.

Material sciences

Strength enhancement and plasticity of high-entropy carbide grains at the micro-scale

Csanádi T.[1]

[1] Institute of Materials Research, Slovak Academy of Sciences, Košice, Slovak Republic

Email of the presenting author: tcsanadi@saske.sk

Introduction: Strengthening and plasticity are known in general as mutually exclusive properties of materials. This phenomenon has been investigated in grains of a recently developed (Hf-Ta-Zr-Nb)C high-entropy carbide and compared with the binary (Hf-Ta)C and constituent monocarbides of TaC and HfC subjected to nanoindentation and micropillar compression.

Materials and methods: The samples were prepared by spark plasma sintering and the crystallographic orientation of grains was determined by electron backscatter diffraction (EBSD). Micropillars and micro-cantilevers were milled out from grains of specific orientations using a focused ion beam (FIB) technique.

Results and conclusion: Nanoindentation tests exhibited a significantly enhanced hardness (36.1±1.6 GPa,) compared to the hardest monocarbide (HfC, 31.5±1.3 GPa) and the binary (Hf-Ta)C (32.9±1.8 GPa). Micropillar compression test of near {001} oriented grains revealed that (Hf-Ta-Zr-Nb)C had a significantly enhanced yield (6.2 GPa) and failure strength compared to the corresponding base monocarbides (3.0-3.9 GPa) while maintaining a similar ductility to the least brittle monocarbide (TaC) during the operation of {110}<1-10> slip systems. Nanohardness anisotropy was correlated to the activated slip systems during nanoindentation determined by EBSD and TEM analyses. The strength enhancement obtained in binary (Hf-Ta)C and high-entropy (Hf-Ta-Zr-Nb)C systems was explained by the increased Peierls stress of an a/2<1-10>{110} edge dislocation due to larger atomic randomness with the increasing number of elements at the dislocation core.

Keywords: high-entropy carbide, nanohardness, strength, plasticity

Microstructural Damage Mechanisms in Additively Manufactured Ni-Based Superalloy

Gálíková M.[1], Šulák I.[1], Fintová S.[1], Kuběna I.[1]

[1] Institute of Physics of Materials, Czech Academy of Sciences, Zizkova 22, 61600 Brno, Czech Republic

Email of the presenting author: kubena@ipm.cz

Introduction

Nickel-based superalloys are primary material for components that are required to withstand high-temperature exposure and loading. Since they exhibit exceptional resistance to oxidation, elevated temperatures, creep, and possess remarkable mechanical strength, these alloys find extensive use in various fields, particularly in engines, hot section of turbines, nuclear reactors, and aerospace components [1,2]. Typical degradation mechanism accompanied in these critical components is low cycle or thermomechanical fatigue. The applications with high number of operation cycles and high stresses that frequently exceed the material yield strength imply large plastic deformation due to mechanical loading and/or thermal gradients. Nowadays, traditional preparation routes such as casting or forging are in some cases replaced by additive manufacturing (AM) techniques [3–5]. Until recently, the IN939 was considered as not suitable for L-PBF manufacturing, however after optimizing printing parameters, it became possible to manufacture a defect-free bulk material. Although the process of additive manufacturing still faces several challenges. The AM promises a possibility of production of Ni-based superalloy component with fine microstructure with pre-defined texture and containing almost no defects, that should increase the strength and fatigue properties of such components. Nevertheless, the influence of L-PBF manufacturing on the damage mechanisms operating during low cycle or thermomechanical fatigue has not been properly addressed yet.

The present contribution refers to the isothermal high-temperature low cycle and thermomechanical fatigue behaviour of polycrystalline nickel-based superalloy IN939 manufactured by laser powder bed fusion (L-PBF). Coffin-Manson curves were measured for three types of loading. Microstructural analysis was performed before and after loading and differences in microstructure were addressed.

Experiment

The material microstructure consists of elongated grains with a preferential orientation <001> parallel to building direction (Fig. 1-left). IN939 incorporates a considerable amount of a reinforced γ' phase that is embedded coherently within the matrix. γ' phase is present in microstructure in bimodal distribution (size of γ' phase ~10 nm and ~150 nm) which increases material strength through the interaction with dislocations (Fig. 1-right). To achieve such microstructure, the IN939 was exposed to three-step heat treatement – solution annealing at 1175°C for 45 minutes followed by two step precipitation hardening 1000°C/6h + 800°C/4h.

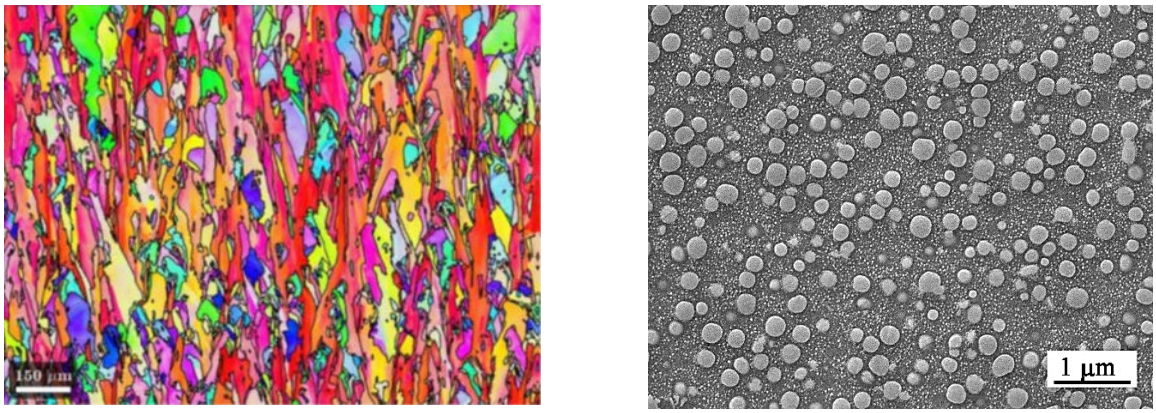

Fig. 1: Microstructure of L-PBF IN939 with relation to building direction and strain axis (left) and Gamma prime (γ') strengthening phase precipitation (right)

After heat treatment, the samples with electrolytically polished gauge length were subjected to thermomechanical loading both in-phase and out-of-phase conditions in temperature range from 400°C to 800°C with consistent heating and cooling rate of 10 °C/s. Secondly, the isothermal fatigue tests at constant temperature of 800°C were performed.

Results

The fatigue tests suggest that TMF loading is more detrimental than isothermal loading performed at 800 °C (Fig. 2-left). In-Phase loading with dominant fatigue-creep interaction appears to be the most damaging in very low cycle region. With increasing number of cycles to failure, the differences among loading cycles are very small and it seems that Out-of-Phase loading is the most detrimental. The typical EBSD micrograph taken after In-Phase loading with large total strain amplitude is shown in Fig 2-right. No significant grain coarsening or texture reduction were observed. It is obvious that fatigue crack propagates predominantly along grain boundaries which confirms the presence of the creep contribution to the damaging mechanisms.

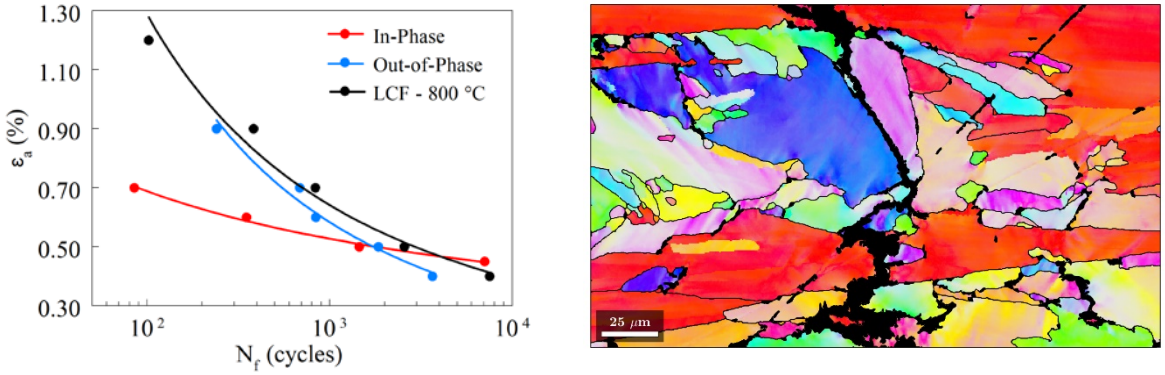

Fig. 2: Fatigue life curves measured in AM IN939 (left), EBSD micrograph showing the texture and the path of fatigue crack (right), loading axis and building direction is oriented horizontally.

Conclusions

Based on the experiments, following conclusions can be drawn:

- The microstructure after AM process consist of elongated grains in building direction with crystallographic <001> texture
- AM IN939 exhibit the highest resistance to LCF and Out-of-Phase loading in the very low cycle fatigue region, while with increasing number of cycles to failure, the differences in fatigue life among individual types of loading diminish.
- The fatigue crack growth along grain boundaries was revealed indicating the contribution of creep mechanism the damaging mechanism.

Acknowledgement:

The authors are grateful for financial support of the Czech Science Foundation by the project 23 - 06167S

References

[1] R.C. Reed, Cambridge University Press, 2008.
[2] B. Blakey-Milner et al., Mater. Des. 209 (2021) 110008.
[3] S. Sanchez et al., Int. J. Mach. Tools Manuf. 165 (2021) 103729.
[4] J. Xu et al., Acta Mater. 240 (2022) 118307.
[5] V. Kalyanasundaram et al., Addit. Manuf. Lett. 5 (2023) 100119.

Eveslogite - nanotubular silicate mineral

Götz E.[1], Klementová M.[2], Depmeier W.[3], Krivovichev S.V.[4,5], Czank M.[3], Schowalter M.[6], Palatinus L.[2], Rozhdestvenskaya I. V.[5], Yakovenchuk V.N.[4], Kolb U.[1,7]

[1] Technical University of Darmstadt, Darmstadt, Germany
[2] FZU - Institute of Physics of the Czech Academy of Sciences, Prague, Czech Republic
3 Kiel University, Kiel, Germany
4 Kola Science Centre, Russian Academy of Sciences, Apatity, Russia
5 St. Petersburg State University, St. Petersburg, Russia
6 Institute of Solid State Physics, University of Bremen, Bremen, Germany
7 Johannes Gutenberg University, Mainz, Germany

Email of the presenting author: klemeari@fzu.cz

Naturally occurring minerals provide examples of unique nanoscopic tubular units based upon silicate oxyanions. The crystal structure of eveslogite (first described in [1]), a chemically and structurally complex natural Ca-K-Ba-Ti-Fe-Nb silicate from the Eveslogchorr Mt., Khibiny massif, located in the Russian Arctic, solved using innovative electron crystallography techniques provides an amazing example of binary nanotubular structure formed by two type of tubules, one of which is an analogue of the yuksporite [2] nanorod with elliptical cross-section, whereas the other is new and represent a Nb-modified variety of the charoite [3] tubule. The tubules are packed in a tight arrangement and linked through secondary interactions involving Ca^{2+} and Na^{+} cations. The interiors of the tubules are occupied by K^{+} and Ba^{2+} cations as well as H_2O molecules. The topological analysis of interpolyhedral connectivity shows that the walls of the nanotubules possess topologies of lamprophyllite and delhayelite-group minerals and most probably were formed through the natural exfoliation processes well-known in current 'soft-chemistry' nanotechnology. The information-based structural complexity calculations indicate that eveslogite is the seventh most complex mineral known so far. Our study further demonstrates the enormous potential of mineralogy to discover structures unprecedented among the currently known synthetic materials and to serve as an inspiration for the preparation of novel types of artificial nanostructures.

Many attempts have been made to collect X-ray diffraction data on the eveslogite crystals using both in-house and synchrotron radiation sources. All the attempts failed due to the small size of the crystals and their curved and fibrous morphology. 3D electron diffraction experiments were therefore undertaken. Most datasets came from twinned crystals, but a few corresponded to untwinned crystals. The unit cell refined against the powder diffraction data differed only slightly from the 3D ED cell, namely a = 14.2358(2) Å, b = 44.8239(5) Å, c = 15.9058(4) Å, β = 109.658(2). Figure 1 shows the resulting crystal structure of eveslogite in projection along *a* axis. The unit cell contains 345 independent atom positions. The skeleton of the structure consists of 62 SiO_4 tetrahedra, which form chains and two different kinds of tubules that run parallel to [100]. Adjacent to the tubules, there are 13 polyhedra. Four of them contain highly scattering species, which were attributed to a mixed-occupancy Ba/Sr sites and the remaining nine were interpreted as K atoms. Seven K atoms at 0.5 occupancy were located in the interior of the tubules. Two octahedra of one tubule are occupied by Ti/Nb. The other tubule contains eight $(Ti,Nb,Fe,Mn)O_6$ octahedra. The ratio of cations in these positions was set and fixed to the values corresponding to the average chemical composition estimated by EDS, leading to an occupancy for each M position of 0.740, 0.048, 0.134 and 0.079 for Ti, Nb, Fe and Mn, respectively. The same procedure was followed with the $(Fe,Mn)O_5$ square pyramid, where the occupancies were set to 0.63 and 0.37 for Fe and Mn, respectively. The tubules are inter-connected by forty independent (Ca,Na)Ox polyhedra that form ribbons parallel to [100].

The eveslogite structure model was compared with a filtered HAADF image. The image is oriented along [100] and shows the different tubules (Fig. 2A). By overlying the structure onto the HAADF image it can be seen that the atom positions agree very well (Fig. 2B). The minor discrepancies in atom positions could be attributed to a slight sample mistilt relative to the electron beam during the acquisition of the image.

References:

[1] Menshikov Yu.P. et al. Obshch. 132(2003), 59-67 (in Russian, English abs.).
[2] Krivovichev S.V. et al. Amer. Miner. 89(2004) 1561–1565.
[3] Rozhdestvenskaya, I. V. et al. IUCrJ 4(2017) 223–242.

Acknowledgement:

CzechNanoLab project LM2023051 funded by MEYS CR is gratefully acknowledged for the financial support of the measurements at LNSM Research Infrastructure.

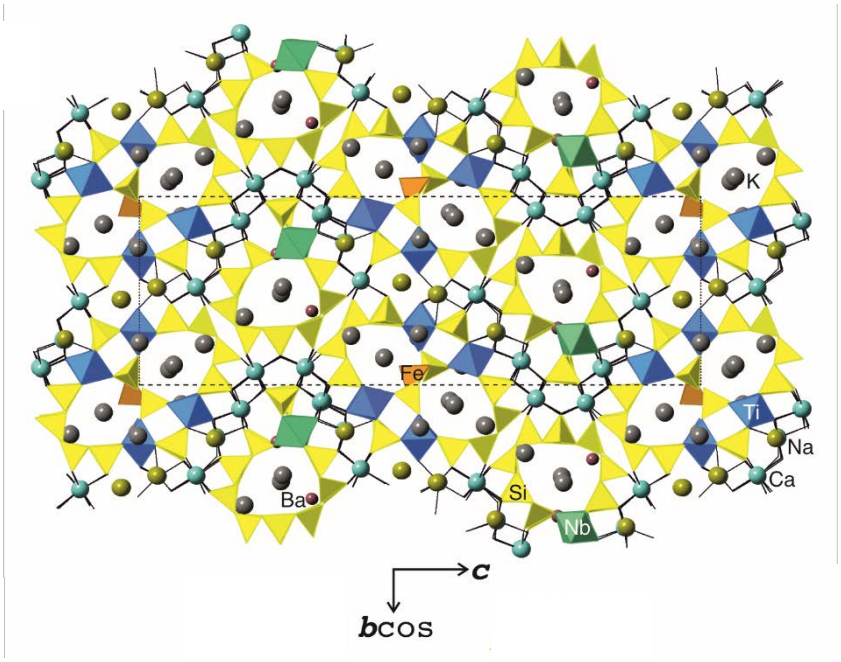

Fig. 1: The crystal structure of eveslogite - projection of the full crystal structure along a axis.

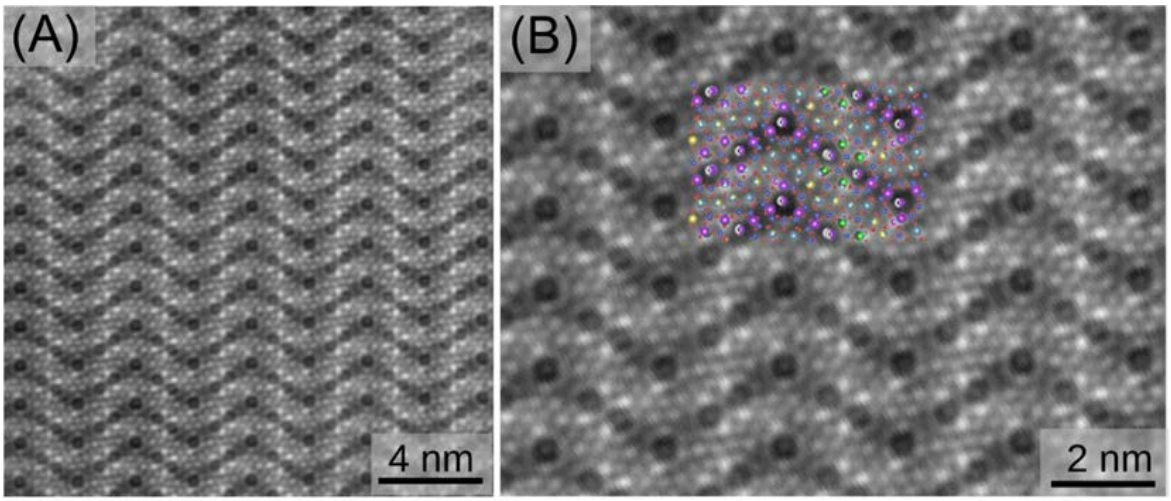

Fig. 2: HAADF image analysis of the eveslogite structure. (A) Filtered STEM HAADF image of eveslogite along the a-axis, (B) zoomed in view overlayed with the structure of eveslogite.

Transfer of graphene onto different substrates for specific applications

Průcha L.[1], Lejeune M.[2], Materna Mikmeková E.[1]

[1] Institute of Scientific Instruments of the CAS, Brno, Czech republic
[2] Université de Picardie-Jules Verne, Amiens, France

Email of the presenting author: prucha@isibrno.cz

One of the biggest challenges nowadays is still the transfer of graphene to the desired substrate. Although many works try to unify the approach to graphene transfer, the same transfer procedure still has not been applied to all types of substrates. Different graphene transfer is used if graphene is transferred to a solid substrate, if a free-standing sample is desired, or if graphene is transferred to polymer substrates [1, 2].

The most common method used today for graphene transfer is using an auxiliary PMMA layer [1]. Here, the metal on which the graphene has grown is etched off with an etchant and the graphene with PMMA is then transferred to the desired substrate. The PMMA is then etched away using a solvent. This method, of the many others used, is relatively simple, time-saving and does not require specialized equipment.

The goal of this work is to demonstrate that this method is sufficiently unified in itself that with minor modifications it is possible to transfer graphene with PMMA on solid samples as well as to create free-standing graphene and graphene on a polymer substrate and then clean the PMMA layer off, which has not been done in the known literature to date for polymers.

This transfer method was used to create samples on solid substrates, both conductive and non-conductive. The preparation of such substrates with graphene is nowadays quite simple compared to other more difficult methods. For free-standing samples, the cleanliness of the transferred graphene can be very well seen, due to the fact that the substrate underneath the graphene does not interfere with the STEM analysis. Therefore, the final cleanliness of the graphene can be better enhanced this way. At the same time, it is important to use graphene removal methods other than conventional acetone immersion for free-standing graphene, as acetone is a volatile and aggressive substance that will in most cases tear free-standing samples. The resulting cleanliness of graphene after PMMA removal is shown in Fig. 1 through STEM analysis.

For the transfer of graphene to polymer substrates using PMMA, acetone cannot be used as a PMMA solvent, due to the fact that it reacts strongly with most plastics as well. Thus, another solvent was used - acetic acid. The acid was diluted to dissolve PMMA, with which it reacts strongly, while not reacting with the polymer substrate. In this work, base plastics such as PET, PE or PS were used, which are supposed to be substrates for flexible electronic devices [3, 4]. The Raman spectra of graphene on polymer substrates can be seen in Fig. 2. At the end of the transfer, a conductive layer of single-layer high-quality graphene (no D peaks in the Raman spectra) was formed on all substrates. This made it possible to observe the non-conducting substrates even under an electron microscope.

All samples were analysed using different types of microscopes (confocal, SEM, STEM) as well as Raman spectroscopy. All these analysis methods complement each other very well in the analysis of graphene and give a very good picture of the quality and purity of the graphene transferred.

References:

[1] Reina A. et al.: Journal of Physical Chemistry C 112(2008), 17741-17744.
[2] Bae S. et al.: Nature Nanotechnol. 5(2010), 574-578.
[3] Anagnostopoulos G. et al.: ACS Appl Mater Interfaces 8(2016), 22605-22614.
[4] Du Z. et al.: ACS Appl Mater Interfaces 9(2017) 43696-43703.

Acknowledgement:

The authors acknowledge funding from Czech Science Foundation GA22-34286S.

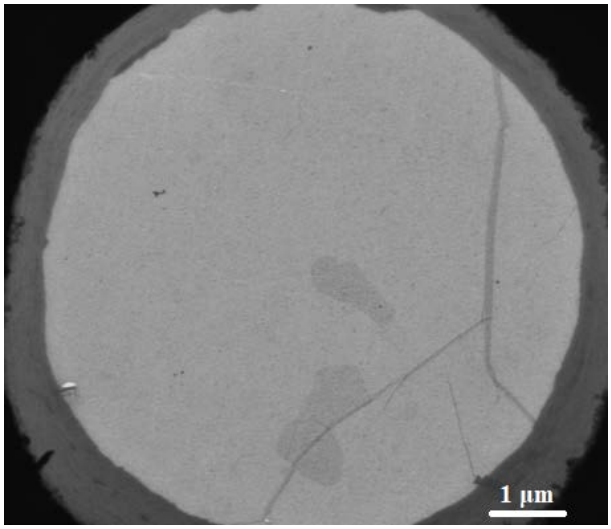

Fig. 1: Free-standing sample of graphene after all cleaning procedures

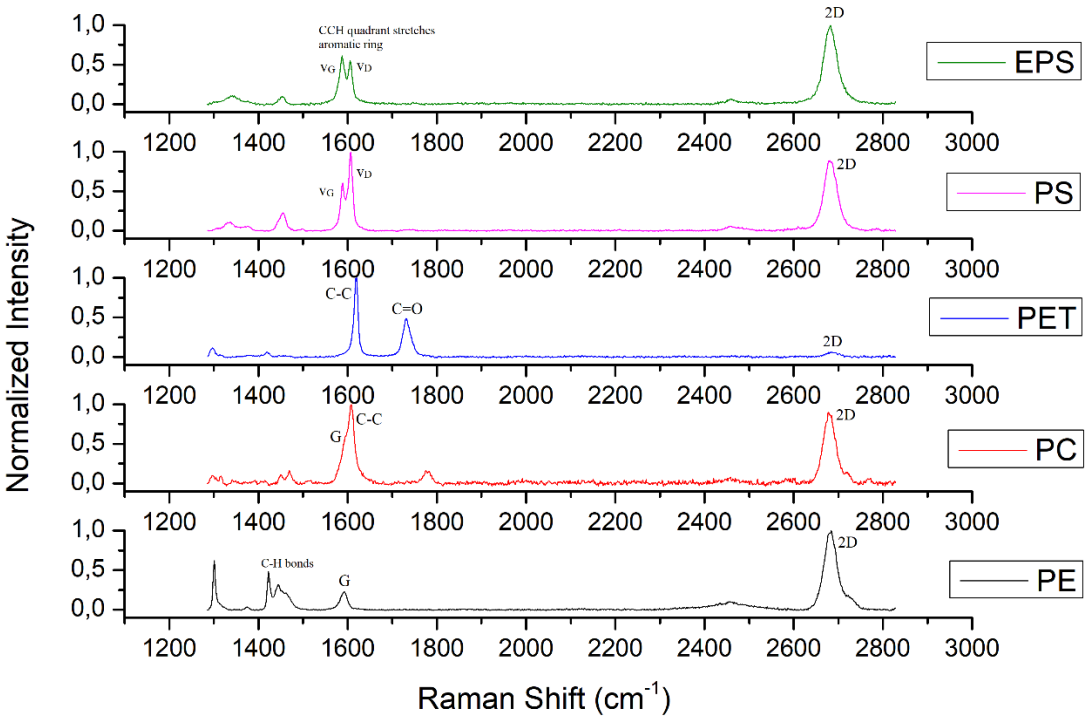

Fig. 2: Raman spectrum of graphene on various polymers after cleaning the PMMA layer

Thermoplastic starch: Relations among processing conditions, morphology, rheology, and properties

Kouka S.[1], Gajdosova V.[1], Strachota B.[1], Rana L.[1], Konefal M.[1], Stary Z.[1], Ocelic-Bulatovic V.[2], Kucic-Grgic D.[2], Vidovic E.[2], Slouf M.[1]

[1] Institute of Macromolecular Chemistry CAS, Prague, Czech Republic
[2] University of Zagreb, Zagreb, Croatia

Email of the presenting author: kouka@imc.cas.cz

Introduction. Thermoplastic Starch (TPS) has been traditionally prepared by different routes such as extrusion, film blowing, or solution casting. Processing methods or parameters as well as the botanical origin of starch influence the TPS end product in terms of its homogeneity and mechanical properties [1]. In our previous studies, we have shown that highly homogeneous wheat thermoplastic starch (TPSw) can be prepared by a two-step preparation procedure [2]. In this contribution, two additional issues were studied. First, the reliability and reproducibility of our two-step preparation procedure, and second, the influence of the starch type and the final TPS homogeneity on its rheological, thermomechanical, and micromechanical properties.

Experimental. We applied our two-step plasticization protocol to four types of starch (wheat, potato, bean, and tapioca) in two different laboratories (one in the Czech Republic and the other in Croatia). The homogeneity of all obtained TPSs was characterized by polarized light microscopy (PLM) and scanning electron microscopy (SEM). The influence of starch homogeneity on the macro and micromechanical properties was studied by dynamic mechanical analysis (DMA) and instrumented microindentation hardness testing (MHI).

Results and conclusion. From the macroscopic point of view, all the obtained materials looked similar regardless of the starch type and the laboratory involved in processing. However, the microscale homogeneity of TPS's was different as documented on PLM micrographs (Fig. 1). Wheat starch exhibited a nearly perfect homogeneity (Fig. 1a), while the other starch types contained non-plasticized granules, which appear bright in PLM due to their anisotropic nature. Based on the PLM results, we compared the macro- and micromechanical properties of the best and the least homogenized TPS's, which were those obtained from wheat and potato, respectively. Both macroscale DMA measurements (Fig. 2) and microscale MHI measurements (Fig. 3) were in agreement that the non-plasticized starch granules in potato starch stiffened the final material (higher values of G', G'', E_{IT} and H_{IT}) and increased its viscosity (higher values of $|\eta^*|$ and lower C_{IT}). We conclude that the non-plasticized granules are a disadvantage for bio-medical applications, where the best possible homogeneity should be achieved, but they may be an advantage in technical applications, where they can act as a bio-compatible filler that increases the stiffness and hardness of the material.

References:

[1] Liu H et al.: Thermal Processing of Starch-Based Polymers. Progress in Polymer Science 2009, 34 (12), 1348–1368. https://doi.org/10.1016/j.progpolymsci.2009.07.001.

[2] Ostafinska A. et al.: Thermoplastic Starch Composites with TiO_2 Particles: Preparation, Morphology, Rheology and Mechanical Properties. International Journal of Biological Macromolecules 2017, 101, 273–282. https://doi.org/10.1016/j.ijbiomac.2017.03.104.

Acknowledgment: Projects TN02000020 (TA CR) and NU21-06-00084 (AZV CR).

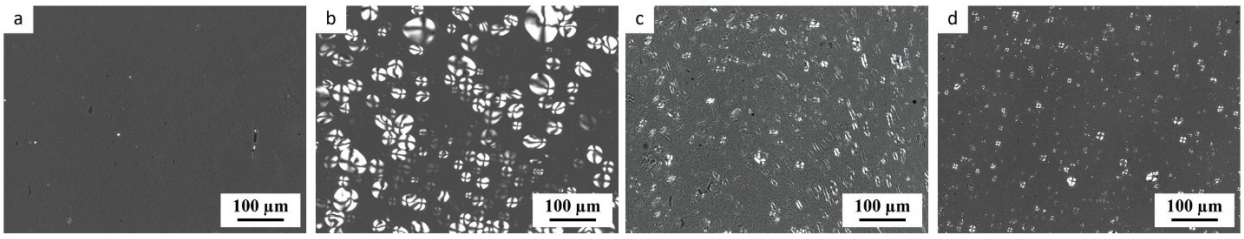

Figure 1: *PLM micrographs showing thin sections of all of prepared TPS's: (a) wheat, (b) potato, (c) bean, and (d) tapioca starch.*

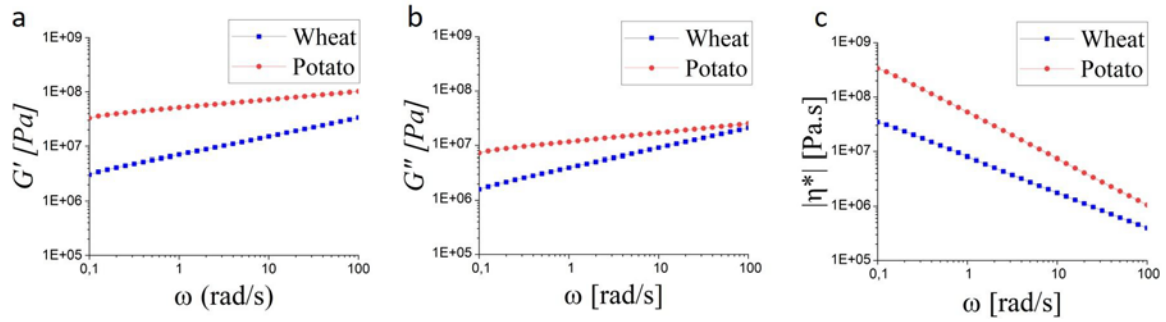

Figure 2: *Macromechanical properties of TPSw and TPSp. The plots show (a) Storage modulus (G'), (b) loss modulus (G''), and (c)absolute value of the complex viscosity (|η*|) as a function of oscillatory shear angular frequency (ω) during the oscillatory shear measurements for TPSw and TPSp.*

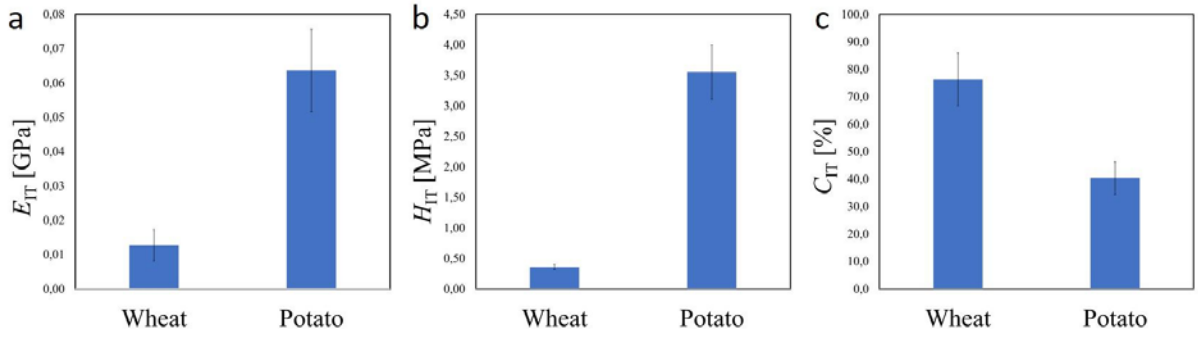

Figure 3: *Micromechanical properties of TPSw and TPSp. The plots show (a) indentation modulus, (b) indentation hardness, and (c) indentation creep.*

Optics and Instrumentation

Bridging the gap: AI-based segmentation tools for quantitative microscopy and the following analysis pathways

Belevich I.[1]

[1] University of Helsinki, Helsinki, Finland

Email of the presenting author: ilya.belevich@helsinki.fi

Introduction: Advancements in microscopy techniques have led to the generation of ever-increasing amount of data, necessitating efficient processing methods. In this landscape, the development of image segmentation tools, especially those harnessing the power of artificial intelligence (AI), has become a critical component. Yet, segmentation is merely one piece of the puzzle; there is an urgent demand for methodologies that enable quantitative data analysis.

Materials and methods: Over the past decade, our team has addressed these challenges by developing Microscopy Image Browser, an open-source software for image segmentation. In the last three years, we have been expanding it with solutions for image segmentation using deep learning, encompassing various 2D, 2.5D, and 3D workflows focusing on userfriendliness and suitability for biological researchers.

Results and conclusion: In this talk, I will highlight our recent developments in creating AI-based image segmentation workflows that bring us closer to achieving quantitative analysis of biological effects. Analyzing biological organelles, which can exhibit diverse shapes, can be challenging, requiring specific analysis algorithms to address this complexity. Additionally, we recognize the untapped potential within large-volume electron microscopy datasets. These datasets contain a wealth of information that extends beyond the original research project's scope. To unlock this potential, we must emphasize data sharing and encourage the responsible reuse of these valuable datasets. During the talk, I will also discuss the role of data sharing in encouraging the responsible reuse of these valuable datasets.

Sixteen pixel electron ptychography

Skoupy R.[1], Grando Stroppa D.[2], Guizar-Sicairos M.[1,3], Mueller E.[1], Fabbri E.[1] and Poghosyan E.[1]

[1] Paul Scherrer Institute, Villigen PSI, Switzerland
[2] Dectris LTD., Baden-Daettwil, Switzerland
[3] École Polytechnique Fédérale de Lausanne, Lausanne, Switzerland

Email of the presenting author: radim.skoupy@psi.ch

Electron ptychography is a great method, recently gaining popularity due to its high contrast and its dose efficient imaging capabilities for a wide variety of both biological and materials specimens [1-4]. However, it suffers from several practical limitations which restrict its wider use, including expensive detectors needed for rapid data acquisition as well as huge size of the data sets, resulting in extreme data storage requirements and long reconstruction time. An optimal experimental approach suggests a sampling of the area of interest with high spatial overlap of the probes (typically > 60 %) together with the acquisition of large diffraction patterns at each beam position. In turn, the costs are long acquisition and processing time, as well as significant storage requirements. In many cases, slightly sub-optimal image quality is still sufficient, which allows to mitigate the above-mentioned challenges by down-sampling in both, real and reciprocal space to reduce the size of the datasets to a computationally more affordable size.

In this work we demonstrate that limitations caused by extreme size of the datasets can be reduced, while preserving adequate image quality, by using a very small pixel number for the diffraction patterns combined with adequate real space sampling. The ratio between real and reciprocal space sampling is adjustable in case of ptychographic imaging since it is possible to trade the real-space sampling for the diffraction-space sampling and vice versa [5]. In this study, the specimen of interest is a lamela prepared from a beam tolerant, SmB_6 crystal along the [110] crystallographic axis, where we aimed to distinguish individual B columns along with Sm atom positions (shorter B-B distance 1.21 Å and Sm-Sm 2.92 Å). The dateset was taken on a probe corrected TEM, JEOL ARM-200F, equiped with the very fast pixelated STEM detector Arina [6] (DECTRIS).

As a part of pre-processing, we have applied various combinations of binning the diffraction pattern as well as reduced the overlap in real space by skipping some of the scan positions. As a result, we got diffraction pattern sizes from originally 192×192 pixels per pattern down to 2×2 pixels and beam overlaps droping down from an overlap of 80 % to non-overlapping beams. From these datasets, phase images were then reconstructed using software package *ptychoShelves* [7]. As visible in Fig. 1, the structure of the specimen can – despite the reduced image quality – still be retrieved down to a binning of 32 in reciprocal space resulting in a 6×6 pixel diffraction array using homogeneous ilumination (geometrically 60 % overlap; marked in yellow). With real space oversampling (real space overlap of ~80 %) we can bin diffraction patterns even more, i.e. down to the size of 4×4 pixels (marked in blue), recover the phase image and still benefit from high contrast of both light and heavy atomic species. Here, notice the lower contrast of boron atoms in the differencial phase contrast image (DPC) computed from the very same datasets (marked in red).

In conclusion, we can significantly reduce dataset sizes if a somewhat reduced image quality is acceptable, which opens space for superfast iterative reconstructions running on-the-fly hand-in-hand with data acquisition, or use of unconventional detection systems like avalanche photodiode arrays, and still preserving most of the ptychographic reconstruction advantages.

References:

[1] Guanxing, L. et al.: ACS Central Science 8 (2022), 1579-1588.
[2] Jiang, Y. et al.: Nature 559 (2018), 343-349.
[3] Pennycook, T.J. et al.: Ultramicroscopy 196 (2019), 131-135.
[4] Chen, Z. et al.: Nature Communications 11 (2020), 2994.
[5] Cesar da Silva J. and Menzel A.: Optics Express 23(2015), 33812-33821.

[6] ARINA [Online], https://www.dectris.com/en/detectors/electron-detectors/for-materials-science/arina/ (accessed 18 03, 2024).
[7] Wakonig, K. et al.: Journal of Applied Crystallography. 53 (2020), 574–586.

Acknowledgement:

The authors acknowledge funding from the Swiss national science foundation (206021_177020) for co-financing the TEM ARM-200F and PSI Research Grant 2021 (R.S.). We are very grateful to DECTRIS for having the chance of using their detector and for their support with detector integration (ARINA) and experiments.

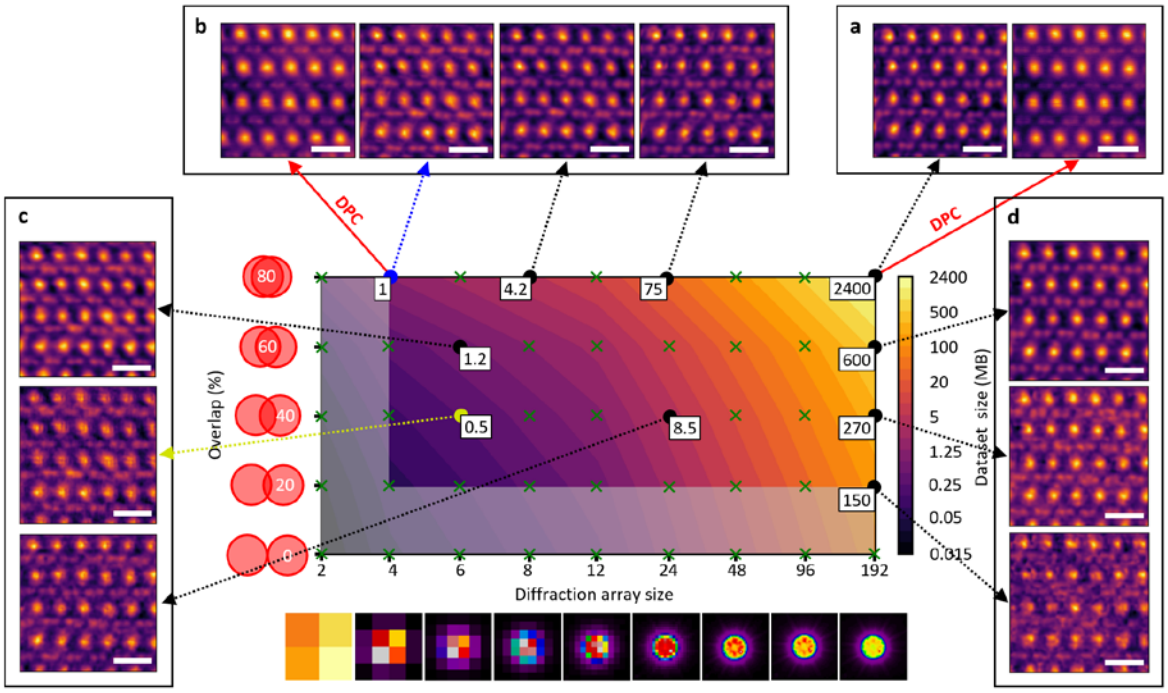

Fig. 1: Reconstruction quality change with reduced real and reciprocal space sampling. (a) Original dataset reconstruction (128×128 beam positions with a step size of 0.159 Å, and diffraction patterns of 192×192 pixels). Reconstructed phase images with various diffraction pattern size (b), real space sampling (d) and a combination of both (c), respectively. Reasonable reconstructions may be achieved down to diffraction arrays of 6×6 pixels and 40 % beam overlap (giving a dataset size reduction of 4800 times) or high 80 % beam overlap and diffraction patterns of 4×4 pixels (dataset size reduction 2400 times). Gray area indicates inadequate reconstruction results with just real or reciprocal-space sampling reduction. For all reconstructions, the scale bar corresponds to 5 Å.

4D-STEM/PNBD: Powder electron diffraction in SEM microscopes

Sikorova P.[1], Skoupy R.[1], Pavlova E.[2], Krzyzanek V.[1], Slouf M. [2]

[1] Institute of Scientific Instruments, Czech Academy of Sciences, Brno, Czech Republic
[2] Institute of Macromolecular Chemistry, Czech Academy of Sciences, Praha, Czech Republic

Email of the presenting author: pavlinasik@isibrno.cz

Introduction: This work is focused on our recent improvements of 4D-STEM/PNBD method (Four-Dimensional Scanning Transmission Electron Microscopy/Powder NanoBeam Diffraction) [1-3]. The method provides a user-friendly way to use a modern SEM microscope as a fast powder electron diffractometer. The only necessary hardware requirements are an SEM microscope with a 2D-array detector of transmitted electrons (4D-STEM-in-SEM).

Materials and Methods: The principle of the 4D-STEM/PNBD method is shown in Figure 1. First, a standard STEM/BF image of the sample is acquired with a scanning submatrix. From each position within the scanning submatrix, a diffraction pattern is captured using a 2D-array STEM detector. The sum of the post-processed individual diffraction patterns is then used to obtain the powder diffractogram.

The reduction of 4D-STEM dataset (Fig. 1a-b) to 2D-powder diffractogram (Fig. 1c) can be automated by means of our open-source Python package named STEMDIFF (https://pypi.org/project/stemdiff). The conversion of 2D-powder diffractogram to 1D-radially averaged profile (Fig. 2) and its comparison with theoretically calculated powder X-ray diffraction pattern (PXRD) can be performed with the sister Python package EDIFF (https://pypi.org/project/ediff). Both packages have support for Jupyter, which is a significant step towards user-friendliness and makes the software fast and intuitive to use.

The current development aims to improve individual diffraction patterns so that even very difficult samples can be processed satisfactorily. Images of such samples suffer from high levels of noise and background artifacts that cannot be easily removed by conventional image processing methods. Therefore, a denoising neural network is currently being developed to sufficiently suppress not only the background but also the noise. Due to the lack of training data, various simulations of individual diffractograms with artificially introduced noise and background (Figure 3) had to be performed to obtain the required clean data on which the network can then be trained. The exact form of the simulations still needs to be determined so that they are as close as possible to the real data and the performance of the pilot network is comparable for both simulated and real datasets.

Results and Conclusions: The 4D-STEM/PNBD method introduces a new electron diffraction technique that is now also available to SEM users. Therefore, in addition to the classical SEM imaging modes, the use of pixelated STEM detectors enables the acquisition of electron diffraction. Such datasets can be easily collected and by using freeware packages (STEMDIFF, EDIFF) that reduce 4D-data to 2D-diffractograms, the data become more accessible to a wider range of users and can be accessed even by less experienced crystallographers. In order to expand the possibilities of use even further, the packages are under constant development and are being extended with additional utilities, such as the possibility of using artificial intelligence to be able to process even samples, which have so far been a challenge for the software.

Acknowledgement: Project TN02000020 (TA CR) and Thermo Fisher Scientific company for a high-resolution SEM with pixelated detector installed at ISI CAS.

References:

[1] Nanomaterials 11 (2021) 962; doi: 10.3390/nano11040962
[2] Materials 14 (2021) 7550; doi: 10.3390/ma14247550
[3] Small Methods 7 (2023) 2300258; doi: 10.1002/smtd.202300258

Figures:

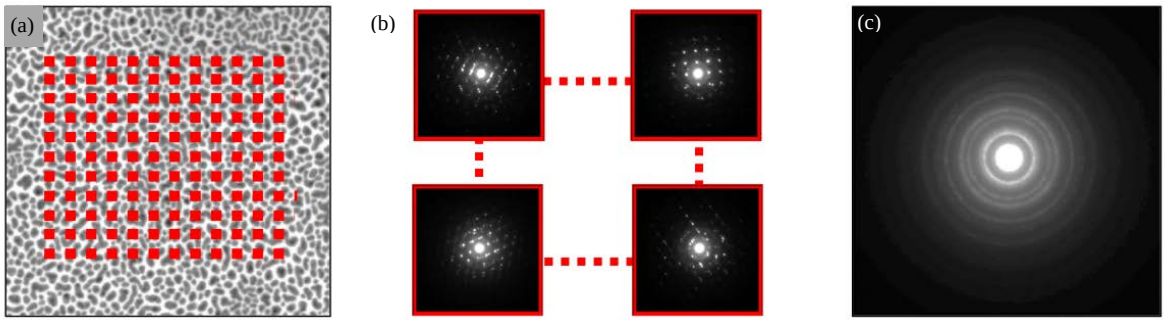

***Figure 1: The workflow of 4D-STEM/PNBD**: acquisition of STEM/BF micrograph (a), set of diffraction patterns (b), final powder diffractogram (c). [Source: Nanomaterials 2021, 11, 962. https://doi.org/10.3390/nano11040962]*

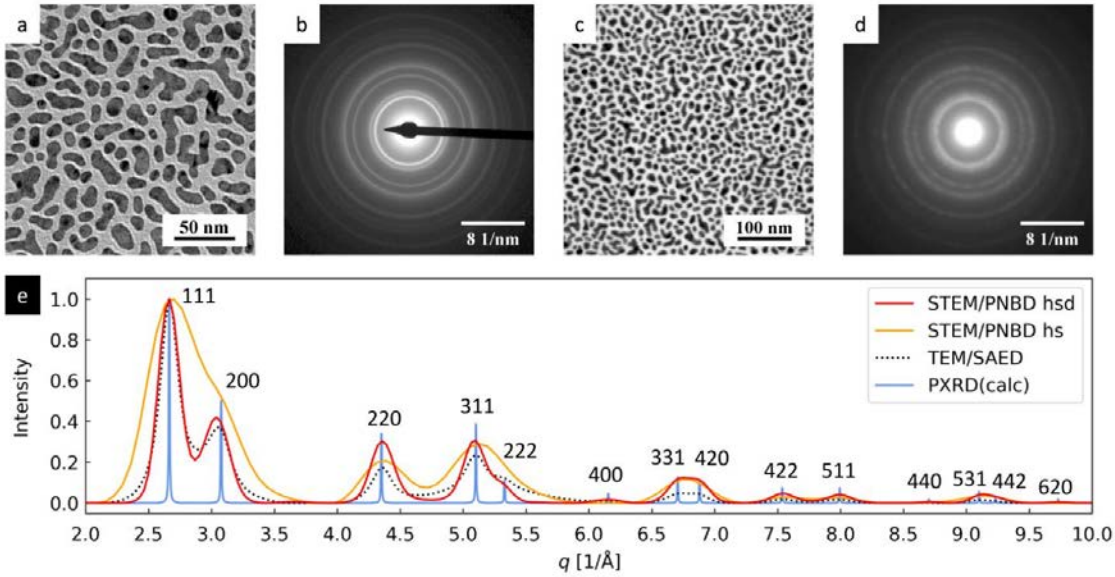

***Figure 2: Comparison of 4D-STEM/PNBD, TEM, and PXRD results for Au nanoislands:** (a) TEM/BF, (b) TEM/SAED, (c) STEM/BF, (d) 4D-STEM/PNBD, (e) radially averaged results from 4D-STEM/PNBD with deconvolution (red), 4D-STEM/PNBD without deconvolution (orange), TEM/SAED (black), theoretically calculated PXRD (blue). [Source: Materials 2021, 14, 7550, https://doi.org/10.3390/ma14247550]*

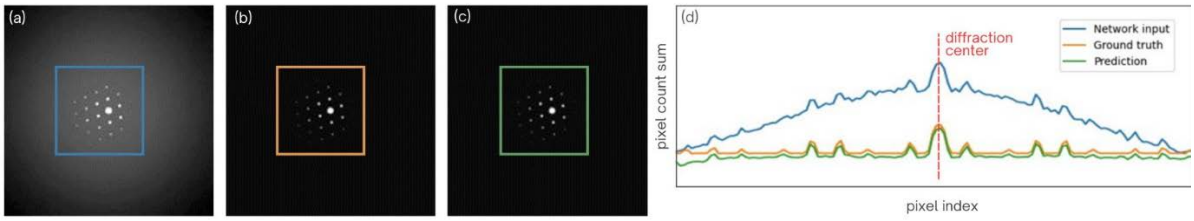

***Figure 3: Performance of the proposed U-NET on simulated data:** (a) simulated low-quality diffractogram (network input), (b) simulated high-quality diffractogram (ground truth), (c) network output (prediction), (d) comparison of 1D profiles*

Metal-insulator transition in vanadium dioxide studied by analytical transmission electron microscopy

Horák M.[1], Kepič P.[1], Konečná A.[1], Šikola T.[1], Křápek V.[1]

[1] Brno University of Technology, Brno, Czech Republic

Email of the presenting author: michal.horak2@ceitec.vutbr.cz

We present a comprehensive study of vanadium dioxide, a phase-changing material with a low transition temperature with a dielectric low-temperature and metallic high-temperature phase, using optical microscopy and analytical scanning transmission electron microscopy combined with in-situ heating. We have explored the metal-insulator transition (MIT) in the single vanadium dioxide nanoparticle caused by in-situ heating. We have identified the dielectric and the metallic phase of the nanoparticle by imaging, diffraction, electron energy loss spectroscopy, and optical transmission. The differences in high-resolution images and diffraction patterns obtained at high and low temperatures confirmed that the MIT is related to a modification of the crystal lattice. In low-loss EELS, the MIT is manifested by the emergence of the plasmon peak in the high-temperature metallic phase (Fig. 1). In core-loss EELS, we observed an energy shift of the oxygen K-edge and varied intensity of the vanadium $L_{2,3}$-edge with the temperature and attributed them to MIT. Moreover, our results show that the transition can be observed directly using imaging techniques such as STEM-ADF and DF-TEM with no need for in-situ spectroscopy. The convergent beam electron diffraction (CBED) patterns recorded in 4D-STEM confirmed that the contrast change in STEM-ADF comes from the crystallographic change during MIT. Fig. 2 shows STEM ADF and corresponding CBED patterns together with DF-TEM and corresponding SAED patterns at room temperature (RT, 22°C), at high temperature (HT, 86°C), and back at room temperature (RT, 22°C). The contrast change in images indicates the MIT. This finding allowed us to study the hysteresis of the MIT in vanadium dioxide with a high spatial resolution. We have observed that the transition from the dielectric to metallic phase is smooth and spans a rather large temperature range while the backward transition is abrupt. Our results therefore provide a comprehensive analysis of the MIT in the single vanadium dioxide nanoparticle and pave the way to phase-changing devices made of vanadium dioxide.

References:

[1] Krpenský J. et al.: arXiv:2309.11980v2 (2024).

Acknowledgement:

This research has been supported by GACR (22-04859S) and MEYS CR (project CzechNanoLab, LM2018110).

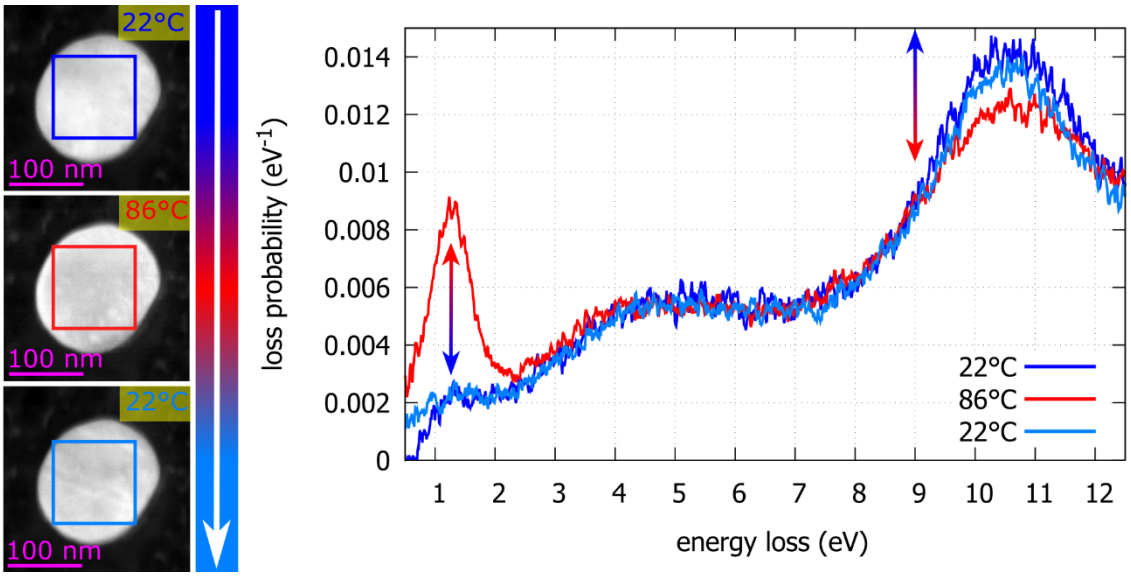

Fig. 1: Low-loss EELS of the insulator-metal-insulator transition in the VO2 nanoparticle. (a-c) STEM-ADF micrographs of the VO2 nanoparticle at 22°C (a), at 86°C (b), and back at 22°C (c). (d) Measured EEL spectra of the low-loss region at these three states indicate the insulator-metal-insulator transition by the presence of localized surface plasmon peak around 1.2 eV in the metallic phase (86°C, red line) which is absent in the dielectric phases (22°C, blue lines).

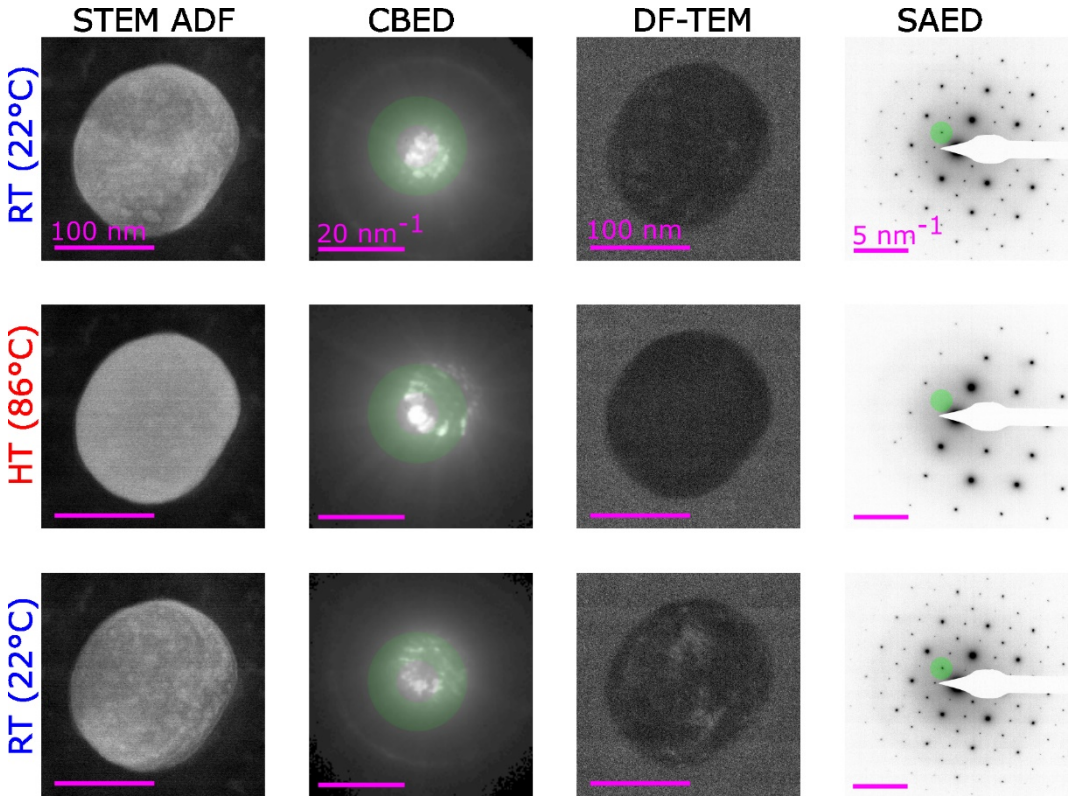

Fig. 2: MIT in a VO2 nanoparticle: STEM ADF and corresponding CBED followed by DF-TEM and corresponding SAED of the initial dielectric (RT, 22°C), metallic (HT, 86°C), and final dielectric (RT, 22°C) phase of the VO2 nanoparticle during the heating induced MIT. The green area in CBED shows the position of the STEM-ADF detector and the green area in SAED shows the position of the objective aperture used in the DF-TEM, respectively.

Production of polymer optical elements and their analysis by electron microscopy

Motlová T., Pokorná Z., Šerý M., Mika F.

Czech Academy of Sciences, Institute of Scientific Instruments, Brno, Czech Republic

Email of the presenting author: tereza.motlova@isibrno.cz

There is a great demand nowadays for optical components with high quality and efficiency, yet as lightweight and low-priced as possible. This demand has led to a trend towards miniaturization, not only in technology and science, but also in everyday life.
Inspired by this downsizing trend, we decided to design and manufacture a micro-optical element [1] that will improve the optical parameters of a Czerny-Turner crossed spectrometer (Fig. 1). The spectrometer was built at the Institute of Scientific Instruments and serves as an analytical tool for a custom-built reactive ion etching system [2]. The aim of this micro-optical element is to correct certain optical aberrations of the Czerny-Turner spectrometer and increase the signal-to-noise ratio.

To produce this element, we used two-photon lithography and then nanoimprint lithography. We did not have to buy off-the-shelf corrective elements, but were able to design and manufacture one that was specifically tailored to our needs (Fig. 2). Surface quality, profile verification and the presence of defects were checked using confocal microscopy and scanning electron microscopy at the Laboratories of Electron Microscopy, a member of the Czech BioImaging Infrastructure. In our evaluation, we focused particularly on geometric defects and the homogeneity of the material, especially the presence of bubbles and inclusions that change the refractive index of the material (Fig. 3).
Based on these measurements, the manufacturing process can be fine-tuned and the manufacturing parameters required to produce the best possible corrective element can be adjusted. The know-how acquired will be used at the Institute of Scientific Instruments in future for the production of micro-optical elements for various applications.

References:

[1] Motlova T.: Výroba polymerních optických prvků a jejich analýza elektronovou mikroskopií. Brno: Vysoké učení technické v Brně, Fakulta strojního inženýrství, 2023. 71 pages.
[2] Šilhan, L.: Konstrukce spektroskopického systému pro systém reaktivního iontového leptání. Brno: Vysoké učení technické v Brně, Fakulta strojního inženýrství, 2019. 45 pages.

Acknowledgement:

The authors acknowledge funding from project Quantum engineering and nanotechnology, reg. n.: CZ.02.01.01/00/22_008/0004649. Co-financed by the European Union. Electron microscopy and Raman spectroscopy analysis provided at Core Facility Electron microscopy and Raman spectroscopy, ISI CAS, Brno, CR, is supported by MEYS CR (LM2023050 Czech-BioImaging).

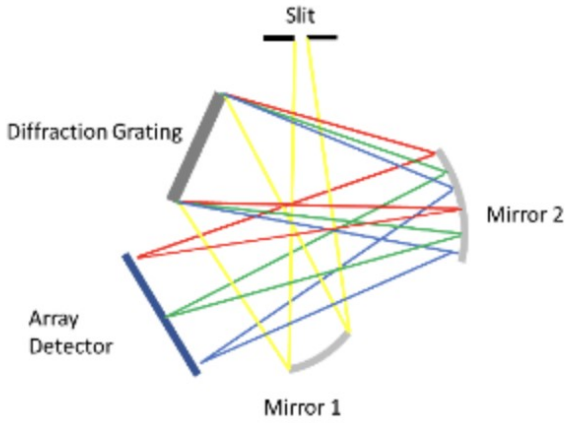

Fig. 1: Schematic of a crossed Czerny-Turner spectrometer [2]

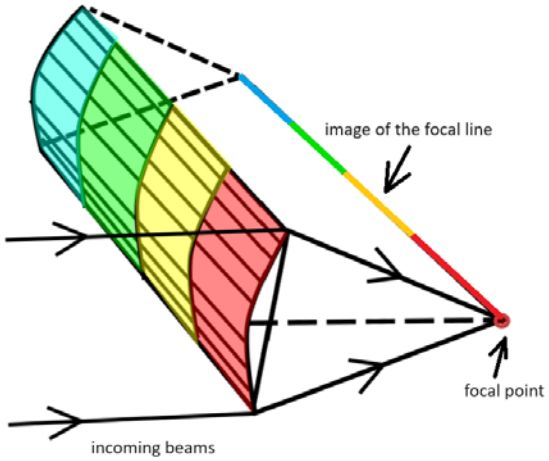

Fig. 2: Scheme of corrective element (linear Fresnel lens) [1]

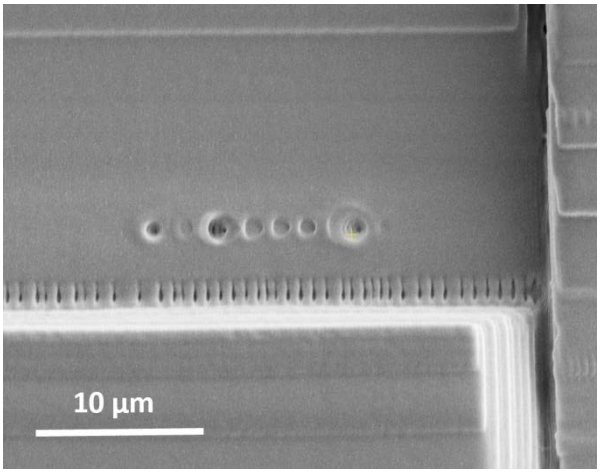

Fig. 3: One of the defects on the top of the manufactured lens observed in the electron microscope [1]

Biomedical sciences

Microscopy and X-ray Imaging in Paleontology: Slovak Integrative Paleobiology Lab

Kundrát M.[1]

[1] Center for Interdisciplinary Biosciences, Technology and Innovation Park, Pavol Jozef Šafárik University, Košice, Slovak Republic

Email of the presenting author: martin.kundrat@upjs.sk

Microscopy is a ubiquitous tool for investigating the morphological structure of extant and extinct organisms. For many decades, transmitted light microscopy (TLM), polarized light microscopy (PLM), and ultraviolet light (UV) have been frequently used to search for information preserved in objects that fossilized tens to hundreds of millions of years ago. When fossilized remains such as tree trunks, leaves, and fruits, as well as bones, teeth, eggs, and eggshells became available for physical sectioning, TLM enabled the first analysis of their microstructure. Later on, PLM turned out to be a complimentary tool as it highlighted detectable fluorescence in fossilized shells (Fig. 1A), hard tissues (Fig. 1B), and soft tissues to some extent; for example, the distribution of collagen fibers in bone (Fig. 1C). A higher flux of UV of different wavelength on fossils can enhance image contrast and reveal fossilized objects that are not seen under white light.

Recently, paleobiology has made significant scientific advances in developing numerous semi-invasive or non-invasive imaging techniques. For example, scanning electron microscopy has been often applied to study the hard-eggshell microstructure or to recognize pigment-packed organelles in fossilized integumentary structure (Fig. 1D; Kundrát et al. 2020). However, X-ray technologies are those that revolutionized our possibilities to peer inside fossilized organismal remains with an exceptional level of detail.

Since their first discovery, X-rays have been used to image objects that are defined as not transparent to visible light while taking advantage of their inhomogeneous absorption. Historically, radiography was the first X-ray technique used by paleontologists as early as 1896 (Hohenstein 2004). Although this approach was useful for numerous cases to map the distribution of fossil remains inside rocks, it has become insufficient to give meaningful data on specimens preserved inside the high-density rocks that absorb most of the X-ray photons.

Tremendous progress was made when computer-assisted tomographic (CT) technology, providing a 3D imaging perspective, became a more common diagnostic tool for medicine. Medical CT scanners have limited spatial resolution adapted for human clinical mapping; it is difficult, even with the most enhanced scanners, to properly image structures smaller than 0.5 mm. This limit was exceeded 40 years ago when the X-ray computed microtomography (µCT) with a spatial resolution better than 20 microns emerged (Flannery et al. 1982). Current µCT facilities (e.g. Zeiss X-ray microscopes, Zeiss X-radia synchrotrons) can rich even higher spatial resolution and provide thus experimental benchmark for a wide variety of applications useful for paleontological imaging. The X-ray tube scanners, however, are considerably limited to sharply visualizing micron-level structures preserved within high-density objects like in-rock embedded fossilized tissues (e.g. *in ovo* preserved dinosaur embryos; Fig. 1E). This is the reason why the so-called synchrotron paleontology became the leading technology in virtual paleohistology.

Synchrotron is a particle accelerator that generates electromagnetic radiation through deviation of the direction of ultra-relativistic electrons by the magnetic field. The generated photon beams (synchrotron light) are channeled by optic elements to experimental laboratories called beamlines. The synchrotron light used for X-ray µCT in structural biology and paleobiology at the third-generation synchrotrons, such as Spring-8 in Japan, possesses four main properties that significantly enhance data quality and imaging applications: monochromaticity, parallel geometry, high beam intensity, and partial coherence (Ueki and Yamamoto 1999). It is quite common that the fossilization process reduces the contrast between the density of fossilized tissues and associated rock. The third-generation synchrotrons enable to increase of the lost contrast virtually using the new imaging modality: the propagation-based phase contrast µCT (Fitzgerald 2000). The propagation-based phase contrast (pph-c) imaging significantly increases the signal-to-noise ratio and thus dramatically enhances the detection of fine density contrasts between fossilized tissues and surrounding rock (Fig. 1F) and considerably increases the final quality of scans (e.g. dinosaur embryonic tooth microstructure by Varricchio et al. 2018; virtual

osteology and histology of *Archaeopteryx* by Kundrát et al. 2019, and virtualization of 3D preserved dinosaur embryonic skull by Kundrát et al. 2020).

Based on 15 years of experience with carrying on experiments at different synchrotrons (France: ESRF; Switzerland: PSI SLS; Italy: Elettra; Australia: ANSTO, and Japan: Spring-8 JASRI) the first Slovak laboratory of synchrotron paleontology was set at Pavol Jozef Šafárik University in Košice. Starting in 2016, a Japan-Slovak research platform in integrative paleobiology was established at SPring-8. This platform aims to utilize synchrotron radiation to detect information about the life of extinct organisms accessible in fossilized remains. Several pilot projects were carried out to test imaging technology at SPring-8 on different kinds of fossil objects such as individual bones of extant and extinct birds of Brazil, New Zealand, Slovakia, and Madagascar and of non-avialan and avialan dinosaurs from the Mesozoic of China (Fig. 1G), Kanada, USA, and Uzbekistan, as well as objects more challenging for scanning, including high-density dinosaur eggs containing embryos and flattened fossils associated with soft tissues.

References:
[1] Kundrát M et al.: Gondwana Research 80 (2020), 1-11.
[2] Hohenstein P: British Journal of Radiology 77 (2004), 420-425.
[3] Flannery BP et al.: Science 237 (1987), 1439-1444.
[4] Ueki T and Yamamoto M: Ways & Means 7 (1999), R183-187.
[5] Fitzgerald R: Physics Today 53 (2000), 23-26.
[6] Varricchio et al.: Scientific Reports 8 (2018), 12454.
[7] Kundrát M et al.: Historical Biology 31 (2019), 3-63.
[8] Kundrát M et al.: Current Biology 30 (2020), 1-7.

Acknowledgment: The author acknowledges funding from the Slovak Research and Development Agency (APVV-18-0251, APVV-21-0319) and the Scientific Grant Agency VEGA of the Ministry of Education, Science, Research and Sport of the Slovak Republic (Grant #1/0075/22).

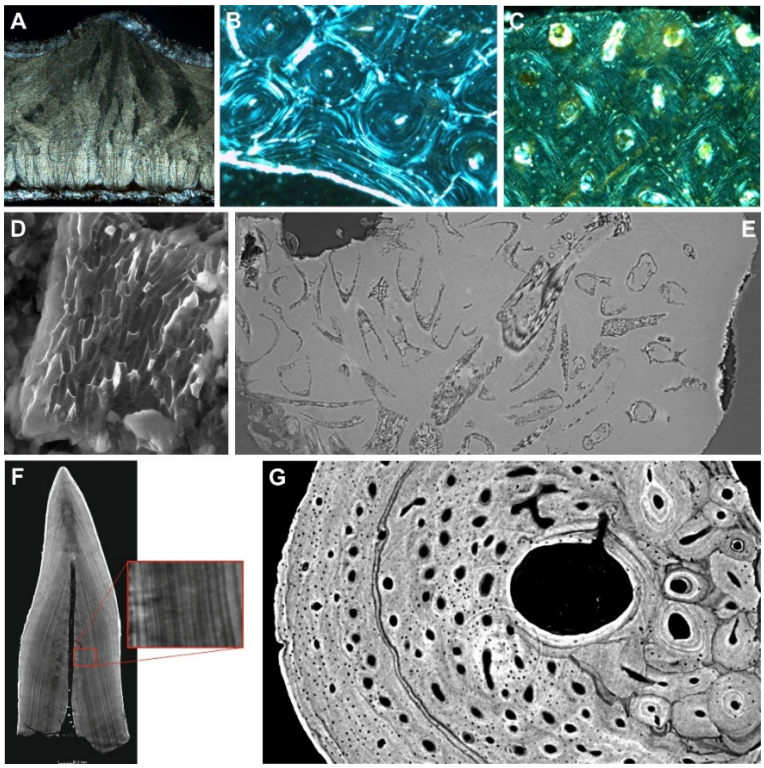

Figure 1. A. *Eggshell microstructure of a theropod dinosaur (Cretaceous, China) shown in circularly polarized light (CPL).* ***B.*** *Bone microstructure of a pterosaur (Cretaceous, China) viewed with PLM.* ***C.*** *Distribution of collagen fibers within the cortical bone of a pterosaur (Cretaceous, China) viewed with PLM.* ***D.*** *Eumelanosomes visualized in the fossilized feather of a polar dinosaur (Cretaceous, Australia) using scanning electron microscopy.* ***E.*** *Propagation phase-contrast synchrotron µCT (pph-c sµCT) reveals embryonic bones inside a dinosaur egg (Cretaceous, China).* ***F.*** *Dentine increments of a theropod dinosaur (Cretaceous, USA) visualized using pph-c sµCT.* ***G.*** *High-resolution synchrotron-generated virtual osteohistology of a theropod dinosaur (Cretaceous, China).*

Novel genetically encoded biosensors for imaging molecular processes of cell signaling

Miclea P.[1], Nagy Marková V.[1], Sakhi A.[1], Bondar A. [1,2,3], Lazar J.[1]

[1] First Faculty of Medicine, Charles University, Prague, Czech Republic
[2] Inst. Of Entomology, Biology Centre, České Budějovice, Czech Republic
[3] University of South Bohemia, České Budějovice, Czech Republic

Email of the presenting author: josef.lazar@lf1.cuni.cz

Genetically encoded fluorescent biosensors convert specific biomolecular events into optically detectable signals. By revealing biochemical processes *in situ*, they have revolutionized cell biology. However, imaging molecular processes often requires modifying the proteins involved, and many molecular processes are still to be imaged. Here we present a novel, widely applicable design of genetically encoded biosensors [1] that notably expand the observation possibilities, by taking advantage of a hitherto overlooked detection principle: directionality of optical properties of fluorescent proteins [2, 3]. The probes offer an extremely simple design, high sensitivity, multiplexing capability, ratiometric readout and resilience to bleaching artifacts, without requiring any modifications to the probe targets. We illustrate their performance on numerous molecular processes of cell signaling. By demonstrating a novel detection principle and allowing many more cellular processes to be visualized, the biosensors are likely to inspire numerous future developments and insights.

References:

[1] Lazar J., Bondar A.: EPO patent application 19831301.7 (2020).
[2] Myšková J. et al.: PNAS 117(2020), 32395- 32401.
[3] Lazar J. et al.: Nature Methods 8(2011), 684-690.

Acknowledgement:

The authors acknowledge funding from EIC PathFinder grant ‘UniSens’.

Enhancing FLIM Data Analysis Through Deep Learning

Benda A.[1], Čočková Z.[1], Backová L.[1,2], Pánek D.[1]

[1] IMCF at BIOCEV, Faculty of Science, Charles University, Vestec, Czech Republic
[2] current address: Instituto Biofisika CSIC, UPV/EHU, Leioa, Spain

Email of the presenting author: ales.benda@natur.cuni.cz

Fluorescence Lifetime Imaging Microscopy (FLIM) captures the decay rate of fluorescence from excited molecules, revealing intricate cellular processes. Unlike intensity-based fluorescence microscopy, FLIM's temporal resolution uncovers environmental and molecular dynamics within cells. Model-free FLIM phasor analysis is often used for simplified interpretation of complex lifetime data.

Managing FLIM data is challenging due to its size, often surpassing 16 GB (2048 x 2048 x 4 detectors x 1024 TCSPC channels x 8 bit), necessitating specialized photon counting data formats. These formats, however, are not readily compatible with standard segmentation tools, leading to the need for custom software to process the data into common formats. In addition, whole image analysis frequently encounters challenges due to background noise or parasitic contributions. To ensure reliable data analysis, it is essential to select specific regions (ROIs) containing the desired signal from individual cells or organelles. Deep learning (DL) -driven segmentation can significantly enhance the process of compartmentalization analysis by precisely identifying and delineating relevant ROIs.

Our current workflow involves processing of raw FLIM data using custom-developed software, which generates both intensity and RGB-encoded lifetime images. These images then serve as novel channels to train neural networks, enabling precise segmentation of ROIs in complex biological samples. Upon segmentation, we extract ROI-based lifetime information and compute phasors for individual objects (ROIs). Phasor data are visualized with scatter plots and evaluated for statistically significant differences among experimental datasets. The segmentation-first strategy prior to phasor analysis allows us to discern even subtle variances in fluorescence lifetimes, thereby enhancing the sensitivity and specificity of our investigations.

We demonstrate the DL-enhanced FLIM analysis in three applications. The first two employ NAD[P]H imaging to compare the metabolic activity in subcellular compartments. In the first application cell segmentation allows to obtain reliable metabolic data for cancer cell experiments by rejecting autofluorescence signal from melanin-dense granules. In the second metabolic activity of sperms between healthy individuals and patients is compared. Segmenting sperm heads and midpieces allowed us to spot significant metabolic differences in particular compartments between groups, which would otherwise be hindered in full image analysis. The third application is analysis of membrane tension using the Flipper-TR probe. Membrane-specific analysis was possible by training neural networks to segment membranes in individual cells on stained Yeast cultures. However, we needed to correct for underlying autofluorescence. For that purpose, use of transformation neural network allowed us to simulate the membrane signal in unstained Yeast samples with poorly visible membranes, and use this data to depict membrane areas with previously trained network to measure autofluorescence.

Acknowledgement:

The authors acknowledge funding from the MEYS CR (LM2023050 Czech-BioImaging).

The utility of EDS in biological transmission electron microscopy

Pinkas D.[1], Vlcak E.[1], Raabova H.[1], Filimonenko V.[1,2]

[1] Electron microscopy core facility, Institute of molecular genetics, Prague, Czechia
[2] Laboratory of Biology of the Cell Nucleus, Institute of molecular genetics, Prague, Czechia

Email of the presenting author: Dominik.pinkas@img.cas.cz

Greyscale images traditionally produced by electron microscopy carry valuable data about biological samples, be it when embedded in resin and stained with heavy metals or in frozen hydrated state. There is, however, no direct information about what exactly produces the contrast which leaves space for misinterpreting the images. The signals produced by the sample upon electron beam irradiation contain much more information than what can be captured on a camera.

Energy dispersive X-ray spectroscopy (EDS) is a well-established method for determining elemental composition of samples based on X-rays emitted by sample upon electron beam irradiation. It is used extensively in material science and predominantly coupled with scanning electron microscopy. It's use in biological TEM is much less common but can provide valuable insights in multiple areas. Most obvious use is tracking and identification of heavy metal contaminants that are sometimes easily masked by precipitations of contrasting agents used during sample preparation, allowing researchers to describe mechanism of toxic effect of various nanoparticles on cellular level, track presence and accumulation of heavy metal pollutants within cells and tissues. But even light elements such as nitrogen and oxygen (in biological samples mostly consisting of carbon) can be reasonably distinguished and mapped enabling study of metabolism of elements like S, N and P. Due to small interaction volume of the STEM probe with an ultrathin sample, it is possible to observe local variations in concentrations of elements in near nanometer scale. This can be used to better understand subcellular morphology for example by tracking protein rich and DNA rich regions of cell nuclei via P and N concentration. Our facility also successfully employed EDS analysis for localization of metal nanoparticles in frozen hydrated samples.

On top of that, EDS helps validate results obtained by other indirect methods of sample characterization and can verify that basic inputs such as drug delivery systems or above-mentioned nanoparticles are indeed what researchers expect them to be.

200kV cryo (S)TEM is available in the Electron microscopy core facility of the Institute of Molecular Genetics of the Czech Academy of Sciences in Prague, Czechia, and can be accessed through Euro-BioImaging as well as Czech-BioImaging research infrastructures.

Acknowledgement:

Electron Microscopy Core Facility, IMG ASCR, Prague, CR, is supported by MEYS CR (LM2023050 Czech-BioImaging),OP RDE (CZ.02.1.01/0.0/0.0/18_046/0016045, CZ.02.1.01/0.0/0.0/16_013/0001775) and IMG grant (RVO: 68378050).

Multimodal metal-organic framework nanoparticles for bioimaging and targeted treatment

Huntošová V.[1,2], Migasová A.[3], Zauška Ľ.[3], Benziane A.[4], Vámosi G.[4], Almáši M.[3]

[1] Center for Interdisciplinary Biosciences, Technology and Innovation Park, P.J. Šafárik University in Košice, Košice, Slovak Republic
[2] Institute of Animal Biochemistry and Genetics, Centre of Biosciences, Slovak Academy of Sciences, Bratislava, Slovak Republic
[3] Department of Inorganic Chemistry, Faculty of Science, P. J. Šafárik University in Košice, Košice, Slovak Republic
[4] Department of Biophysics, Institute of Physics, Faculty of Science, P.J. Šafárik University in Košice, Košice, Slovak Republic
[5] Department of Biophysics and Cell Biology, Faculty of Medicine, University of Debrecen, Debrecen, Hungary

Email of the presenting author: veronika.huntosova@upjs.sk

Metal-organic frameworks (MOFs) are porous, ordered network hybrid materials that assemble by self-organisation of metal ions or metal clusters with organic ligands under controllable conditions [1]. They are gaining increasing attention due to their structural diversification, large specific surface area, high porosity and well-defined pore shapes. In our work, we have prepared MIL-101(Al)-NH_2 particles filled with hypericin, a promising antiviral agent of natural origin that has been reported to inhibit coronavirus replication by targeting the viral 3-chymotrypsin-like protease (3CLpro) [2, 3].

SARS-CoV-2 enters the cells by binding the viral spike protein to the angiotensin-converting enzyme 2 receptor (ACE-2) of the host cell [4]. The viral envelope attaches to the cell membrane, and the viral genome is released into the cytoplasm. It captures the host ribosomes and is translated into a large polypeptide chain (8000 kDa), which is further autoproteolytically cleaved by proteases (papain-like proteases and 3CLpro) encoded by the viral genome to form several non-structural proteins required for viral replication. For this reason, 3CLpro is one of the main targets of treatment against SARS-CoV-2.

In the present work, the pores of MOFs (MIL-101(Al)-NH_2) were filled with hypericin and their interaction with cells was analysed. Confocal fluorescence microscopy and time-resolved fluorescence microscopy (FLIM) were used to monitor the release of hypericin towards two types of cells. HEK cells (human embryonic kidney cells) and GFP-labelled HEK cells with high expression of ACE-2 receptors were used as a model system for the SARS-CoV-2 target. MIL-101(Al)-NH_2 particles were clearly visible inside the cells thanks to the bright fluorescence emitted < 490 nm at 405 nm excitation. While clusters of the particles were observed outside of the cells, the hypericin fluorescence > 600 nm at an excitation of 560 nm (Fig. 1). GFP fluorescence (in the green region at 488 nm excitation) was mainly detected in the plasma membrane of HEK cells expressing ACE-2 receptors. FLIM measurements showed that GFP fluorescence is influenced by the presence of hypericin in these cells. In addition, immunofluorescent labelling of mitochondria showed differences between HEK and GFP-HEK cells, confirming their importance in the autophagy process, which has been proposed as an important signalling pathway affected by SARS-CoV-2 [5].

To summarise, the prepared particles have promising properties for bioimaging and drug delivery. By further modifying the surface, they can be precisely targeted to cells with increased expression of ACE-2 receptors.

References:

[1] Steenhaut T. et al.: Journal of Materials Chemistry A 9 (2021), 21483-21509.
[2] Matos A. et al.: Frontieres in Microbiology 13 (2022), 828984.
[3] Bajrai L. et al.: Scientific Reports 12 (2022), 21723.
[4] Randhawa P. at al.: Frontiers in Physiology 11 (2020), 611275.
[5] Rein T.: Journal of Cellular Biochemistry 123 (2022), 155-160.

Acknowledgement:

The authors acknowledge funding from the APVV-20-0340 project and Euro-BioImaging for providing access to imaging technologies and services via the Cellular Imaging Hungary Node (Debrecen, Hungary) and ISIDORe support by grant ISD_d005.

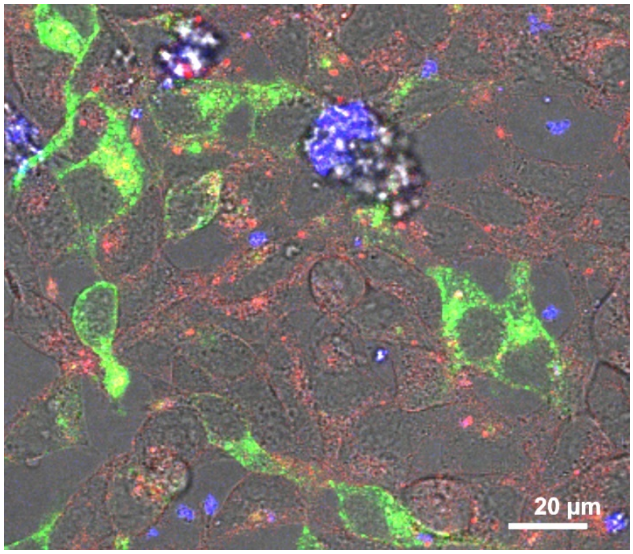

Fig. 1: Fluorescence image of HEK cells subjected to MIL101(Al)-NH_2 particles (blue) loaded with hypericin (red) that was released from the particles and taken by cells. GFP-HEK expressing high level of ACE-2 receptors are labelled in green.

News in microscopy community

The Young Czechoslovak Microscopy Society: Mapping out future endeavors

Mrázová K.[1], Ďurinová E.[1], Průcha L.[1], Pevná V.[1], Strnad M.[1]

[1] Council members of the Young Czechoslovak microscopy society

Email of the presenting author: martin.strnad.cze@gmail.com

Join us for an introductory lecture on the present and future endeavors of the newly established Young Czechoslovak Microscopy Society (yCSMS). Our society is a dynamic hub for microscopy enthusiasts, encompassing students, early-career scientists with a fervent interest in microscopy. At yCSMS, we foster connections among like-minded individuals, providing a platform for networking, knowledge exchange, and skill enhancement through a range of avenues including workshops, webinars, industry visits and potential collaborative research endeavors. Whether you're taking your first steps into microscopy or you're already a seasoned microscopist, yCSMS offers an avenue to broaden your horizons and become part of a supportive community dedicated to nurturing your passion for microscopy.

References:

[1] https://ycsms.org/

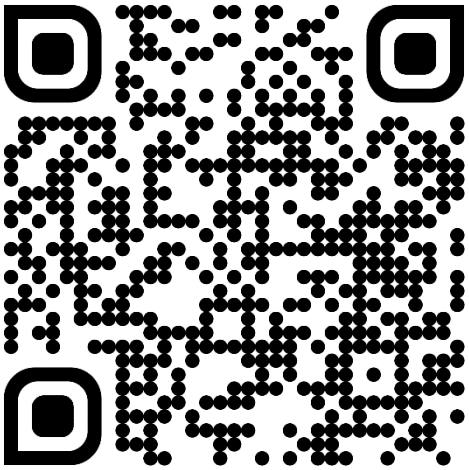

Fig. 1: registration form for the yCSMS

Czech-BioImaging: Infrastructure dedicated to users

Wernerová M.[1], Hozák P.[1]

[1] Institute of Molecular Genetics of the Czech Academy of Sciences, Prague, Czech Republic

Email of the presenting author: martina.wernerova@img.cas.cz

Czech-BioImaging, the national research infrastructure for biological and medical imaging, has been dedicated to serving users for nine years. In 2023, our network expanded to include 16 participating core facilities across five cities in the Czech Republic.

We offer open access to a wide range of services, including both routine and highly specialized devices in light and electron microscopy, medical imaging, and cutting-edge tools for data processing and analysis. Users are provided comprehensive technical support, expertise, and guidance throughout the entire process, from designing experiments to analyzing and interpreting acquired data for project solutions. Our specialization extends across various fields, encompassing cell and molecular biology, genetics, physiology, parasitology, tumor biology, neuroscience, developmental biology, and pathology.

Excitingly, Czech-BioImaging has secured significant financial resources once again. These funds will fuel infrastructure development from 2024 to 2026, focusing on the replacement and modernization of outdated yet still highly demanded equipment. Additionally, we plan to acquire new technologies to enrich our portfolio and better meet the evolving needs of our users.

During the conference, we will provide attendees with a glimpse into the array of services offered by Czech-BioImaging and unveil the exciting developments planned for 2024. Join us as we continue to push the boundaries of imaging technology and empower researchers across the Czech Republic and beyond.

Acknowledgement:

National Infrastructure for Biological and Medical Imaging is co-funded by the Ministry of Education, Youth and Sports of the Czech Republic (project LM 2023050 and OP JAK infrastructure project "Modernisation of the VVI Czech-BioImaging" CZ.02.01.01/00/23_015/0008205).

Czech Infrastructure for Integrative Structural Biology

Novacek J.[1]

[1] CEITEC Masaryk University, Kamenice 5, 62500 Brno, Czech Republic

Email of the presenting author: jiri.novacek@ceitec.muni.cz

The Czech Infrastructure for Integrative Structural Biology (CIISB) is a national research infrastructure that provides access to high-end technologies and methodologies related to structural biology. Its mission is to support the scientific and research community by offering state-of-the-art equipment and expertise in areas such as X-ray crystallography, nuclear magnetic resonance (NMR) spectroscopy, mass spectrometry (MS), cryo-electron microscopy (cryo-EM), atomic force microscopy (AFM), and wide range of other biophysical techniques. These technologies enable detailed studies of the structure and dynamics of biological molecules, which are crucial for understanding their function in health and disease. Our primary goals include facilitating access to high-end instrumentation, R&D support, education, and training.

New study program “Mikroskopie” at the Masaryk University

Mikulík P.[1], Kubíček K.[1,2], Munzar D.[1]

[1] Department of Condensed Matter Physics, Faculty of Science, Masaryk University, Brno, Czech Republic
[2] CEITEC, Masaryk University, Brno, Czech Republic

Email of the presenting author: mikulik@physics.muni.cz

We present new study programme “Mikroskopie” (Microscopy) as a two-year follow-up master's degree study to start in the Autumn semester 2024 [1]. The programme is accredited at Masaryk University, Faculty of Science. In addition to academic staff from this faculty and CEITEC MU, other Brno institutions and companies will participate in courses as well. “Mikroskopie” starts in Czech language, and an English version “Microscopy” is supposed to follow in the near future.

The aim of the study programme is to obtain the professional qualification of an expert in the field of microscopic methods. It will focus on electron and light microscopy and other imaging methods useful for research, development and applications. The study is aimed both at consolidating and deepening the education obtained by students in their previous bachelor's programme with physical, mathematical-physical or biophysical focus. The programme will deal with areas of light and particle optics, properties of materials and the structure of biological samples, physics related to the properties and construction of imaging devices. The students will get particular knowledge and skills in the field of physics and structural biophysics required for the profession of development and application specialists. The aim is to prepare qualified experts theoretically, with an emphasis on the ability to follow the development of related physics methods, as well as practically through practical training at standard and development workplaces of manufacturing companies and at academy.

References:

[1] https://www.sci.muni.cz/pro-uchazece/navazujici-magisterske-studium/26987-mikroskopie

Acknowledgement:

We thank all the people, institutions and companies supporting this new study programme.

Fig. 1: Flyer of the Microscopy programme.

Building the Czech optical ecosystem

Přikryl P.[1]

[1] Czech optical cluster, Olomouc, Czechia

Email of the presenting author: petr.prikryl@optickyklastr.cz

Czech Optical Cluster was created with the aim to improve the conditions for optical industry development in the Czech Republic through cooperation of companies, public sector and educational sector in the entire value chain in the field of optics, optomechatronics, photonics, optoelectronics and fine mechanics, including related production, technology and service development in supplier's and customer's domain. Our ambition is to achieve technological milestones, but also the need to create an industrial ecosystem that will be able to withstand the challenges of the current and future world. Not only to promote innovation, but also to maintain stability and competitiveness in the ever-changing global market environment. Photonics is acknowledged at the EU Level as a Key Enabling Technology and Advanced Technology for Industry This domain has comprehensive and transversal applications to a wider range of sectors, while being critical for Europe's economic security and strategic autonomy in sensitive and relevant value chains, such as Semiconductor industry, Agrifood, Health, Manufacturing and Mobility. Ultimately, a widespread deployment of Photonics technologies into businesses can strengthen the resilience (economic and environmental) of the Czech Republic and Europe.

Acknowledgement:

The authors acknowledge funding from project: OPTAK Spolupráce: Česká optika pro budoucnost. The project duration 1.7.2023 - 30.6.2026.

Posters

Atomic oxygen beam etching of single domain graphene real-time observations in an ultrahigh vacuum scanning electron microscopy

Mikerásek V.[1,2], Piastek J.[1,2], Supalová L.[1,2], Špaček O.[1,2], Bartošík M.[1,2], Mach J.[1,2] and Šikola T.[1,2]

[1] Institute of Physical Engineering, Brno University of Technology, Faculty of Mechanical Engineering, Brno, Czech Republic
[2] CEITEC - Central European Institute of Technology, Brno, Czech Republic

Email of the presenting author: vojtech.mikerasek@vutbr.cz

Introduction:

Graphene has gained popularity due to its unique mechanical, electrical and optical properties. It is studied not only in the context of fundamental physics, but also for its use in various applications, such as transparent and flexible electronics, sensor and biosensors. However, common applications require modifying the properties of graphene either by opening the band gap to achieve semiconductor properties or by modifying the surface to ensure selectivity of different sensors. The modifications can be a variety of adding defects, ribbons, layering or modifying atoms.[1]

One way of increasing sensitivity is by covalent and non-covalent binding of different organic molecules to oxygen group, which can be used to identify different compounds.[2] Instead of commonly used chemically prepared graphene oxide or reduced graphene oxide, pure graphene can be modified by oxidation methods (oxygen plasma, ozone, atomic oxygen).[3] Currently, the best preparation method is CVD, which allows mass production of large, high-quality graphene.

In this paper we focus on the treatment of graphene with atomic oxygen. This can be supported by other experiments[4,5] or DFT simulations[6] or molecular dynamics[7] that have been devoted to demonstrating the mechanism of carbon atom removal in the form of CO or CO_2 gases. The causes are due to the influence of defects and inhomogeneities in the graphene structure and the supersaturation of the surface with oxygen atoms, which interact to weaken the bonding between carbon atoms.

The objective was to obtain a more detailed insight into the evolution of the reaction of atomic oxygen with graphene.

Materials and methods:

The samples were graphene single crystals grown on Cu-foil using CVD methods under low pressure and gas flows (CH_4 and H_2). Individual monolayer graphene crystals were up to 40 µm in size. The transfer is completed on SiO_2 substrate with a support layer - polymethyl methacrylate (PMMA). Raman spectroscopy showed that most of the grains are single layer, with several defects in the centre.

Atomic oxygen was produced by the high-thermal dissociation of molecular oxygen, which was released into the instrument chamber ($p_{O2} \approx 1\times10^{-4} - 1\times10^{-3}$ Pa), on the surface of an iridium filament (dia. 0.125 mm) that was heated by current. This filament was positioned adjacent to the sample (distance >8 mm), when oxygen atoms fly from it to the surroundings after dissociation.

The process was observed in-situ by a scanning electron microscope under ultrahigh vacuum (UHV-SEM). After each experiment, the final state was measured by Raman spectroscopy (532 nm laser, objective 100×, <5 mW) and the chemical composition was determined by X-ray photoelectron spectroscopy.

Results:

The observations were carried out in the UHV-SEM chamber over tens of minutes, with images of individual graphene monocrystals taken at five-minute intervals. The oxidation process was still active at that time. From the calculation based on pressure, the distance of the Ir filament from the sample and the dissociation efficiency estimation, the dose was estimated flux of about $(1\text{-}3)\times10^{14}$ atom.cm^{-2}s^{-1}.

The study of the interaction of graphene with atomic oxygen showed that it was gradually etched away. The effect of scanning by electron on the evolution of the reaction can be neglected because similarly sized graphene crystals outside the observed region are in the same etching stage or have the same contrast with the substrate. Observations have shown that the phase of the reaction depends on the distance from the iridium filament, which corresponds to the size of the atomic oxygen dose (in Fig. 1).

It has been shown that after 30 min there is a disappearance of the flake boundaries. We also observe that the contrast is reversed (the flakes are lighter). This phenomenon was noticed only on graphene on

pure Si with a native oxide layer. Thus, it is concluded that it was a prooxidation of the graphene-uncovered surface. We are able to confirm that the graphene is ultimately etched off during the process, according to the data measured by XPS (in Fig. 2a).

After UHV-SEM measurements, the size of individual graphene flakes could be located and remeasured using Raman spectroscopy to reveal the localization of the defect (in Fig. 2c).

The high doses probably cause the sample to become oversaturated with oxygen, which, according to the processes described[7], etches away the carbon atoms.

In further experiments, it would be valuable to examine graphene samples more precisely at lower doses of atomic oxygen and to investigate the effect of the heat from the heated Ir-filament on the reaction as described. Alternatively, an experiment should be prepared to measure at atomic resolution.

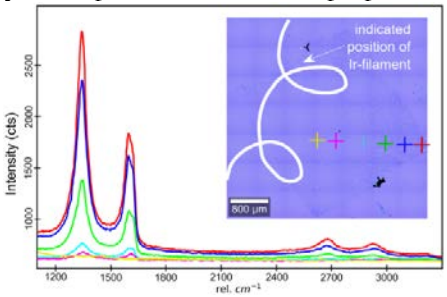

Fig. 1: Raman measurements of a sample coated with graphene individual crystals on SiO_2/Si measured after deposition of atomic oxygen. The decrease of the D peak with respect to G correlates with the distances of the measured points from the Ir-filament and the dose of atomic oxygen, respectively.

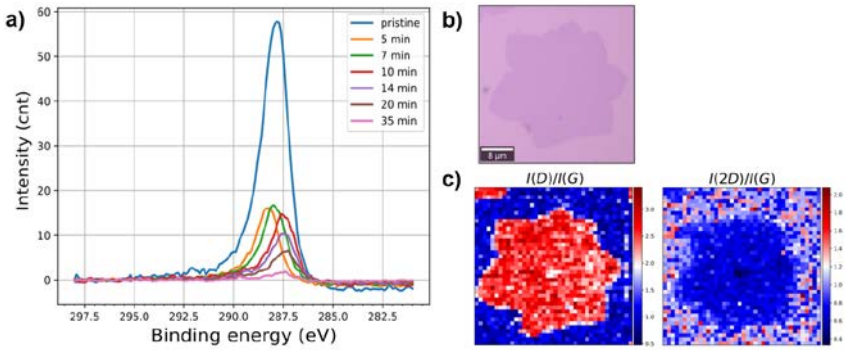

Fig. 2: Chemical and structural analysis of graphene after interaction with atomic oxygen: a) Observed etching of monolayer graphene on SiO_2 by analysis of XPS spectra and b) optical microscope image of graphene single-layer monocrystal and c) spatial distribution of defects in graphene grains shown by Raman spectroscopy mapping.

Conclusion:

In conclusion, the reaction of atomic oxygen with CVD graphene single-layer crystals was observed, leading to a gradual etching. These processes are tracked in real time using a scanning electron microscope, which has detected the initiation of the reaction at the edges and in the centre of the grains, where there is an increased number of defects resulting from the growth process. Almost complete etching of graphene crystals was observed after 30 min of exposure to a low flux of atomic oxygen.

References:

[1]Lee G., Kim J., Kim K., et al.: *J. Vac. Sci. Technol. A* 33, (2015), 060602.
[3]Fiorani, A., el.al.: *Current Opinion in Electrochemistry*, 16, (2019), 66-74.
[4]Kapitanova O. O., et.al.: *J. Phys. Chem. C*, 121, 50 (2017), 27915–27922.
[5]Hossain M. Z., Johns J. E., Bevan K. H., et.al.: *Nature Chemistry*, 4, (2012), 305–309.
[6]Vinogradov N. A., Schulte K., Ng M. L., et.al.: *J. Phys. Chem. C*, 115, 19, (2011), 9568–9577.
[7]Sun T., Fabris S. and Baroni S.: *J. Phys. Chem. C*, 115, 11, (2011), 4730–4737.
[8]Srinivasan S. G. and van Duin A. C. T..: *Phys. Chem. A* 2011, 115, 46 (2011), 13269–13280.

Acknowledgement:

Part of the work was carried out with the support of the CzechNanoLab research infrastructure (ID LM2018110, MŠMT, 20202020 and ID LM2023051, MŠMT, 20232023) CEITEC Brno University of Technology.

Nanoscale Optoelectronic Insights into $CsPbBr_3$: Advanced Characterization of Charge Carrier Dynamics

Klok P.[1, 2], Dvořák P.[1, 2], Liška P.[1, 2], Kratochvíl M.[3], Gavranović S.[3], Ulč F.[1], Spousta J.[1, 2], Šikola T.[1, 2]

[1] Institute of Physical Engineering, Faculty of Mechanical Engineering, Brno University of Technology, Brno, Czech Republic
[2] Central European Institute of Technology, Brno University of Technology, Brno, Czech Republic
[3] Faculty of Chemistry, Brno University of Technology, Brno, Czech Republic

Email of the presenting author: 208733@vutbr.cz

Cesium lead bromide ($CsPbBr_3$) has attracted significant attention [1] for its exceptional optoelectronic properties, including high photoluminescence yield [2] and low non-radiative lifetimes [3]. Additionally, its cost-effective synthesis methods [4] make it particularly promising for applications in light-harvesting devices like photovoltaics [5] and radiation detection [6]. However, achieving comprehensive understanding of charge carrier behavior at the nanoscale in $CsPbBr_3$ remains a challenge.

This study utilizes advanced high-resolution techniques, such as Kelvin probe force microscopy (KPFM), steady-state and time-resolved photoluminescence (PL and TRPL), in combination with aperture-type near-field optical microscopy (a-SNOM), to delve into properties of $CsPbBr_3$. A novel contribution introduced by our group is the utilization of near-field time-resolved photoluminescence measurements. This approach provides unprecedented nanoscale insights into radiative recombination and charge carrier processes, as illustrated in Figure 1.

Preliminary findings reveal a strong correlation between regions of intense radiative recombination and areas with reduced charge accumulation, as confirmed by KPFM measurements conducted both in darkness and under light exposure. These insights provide valuable information about the spatial variability of electronic properties in $CsPbBr_3$, pushing the boundaries of nanoscale characterization and supporting the development of next-generation $CsPbBr_3$ devices.

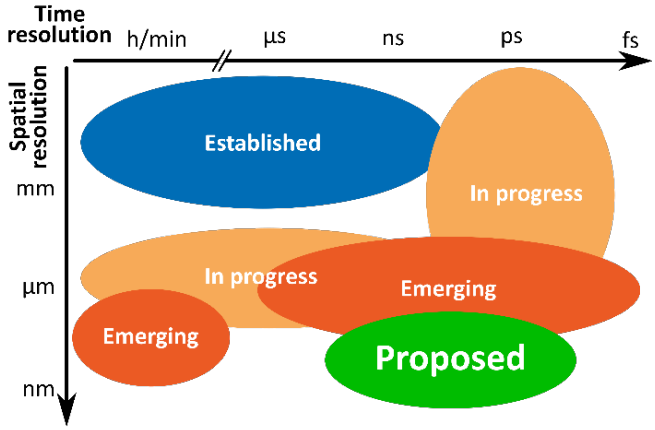

Fig. 1: Table summarizing the main techniques used for investigating charge carrier recombination and diffusion in perovskites. Adapted from [7].

References:

[1] Stoumpos C. et al: Crystal Growth & Design 13(2013), 2722-2727.
[2] Stasio F. D. et al: Chemistry of Materials 29(2017), 7663-7667
[3] Diroll V. G. et al: Advanced Functional Materials 28(2018), 1800945.
[4] Li F. et al: Science 381(2023), 1468-1474.
[5] Ullah S. et al: Materials Advances 2(2021), 646-683.
[6] He Y. et al: Nature Photonics 15(2021), 36-42.
[7] Delport G. et al.: Advanced Energy Materials 10(2020), 13.

Acknowledgement:

The author acknowledges funding support from Specific Research, Brno University of Technology project FCH/FSI-J-24-8521. Additionally, the research benefited from the CzechNanoLab Research Infrastructure supported by MEYS CR (LM2023051). The author also acknowledges the Brno Ph.D. Talent Scholarship – Funded by the Brno City Municipality.

Probing electron scattering phenomena of graphene at very low energies

Materna Mikmeková E.[1], Konvalina I.[1], Müllerová I. [1], Průcha L.[1], Paták A.[1]

[1] Institute of Scientific Instruments of the CAS, v. v. i., Královopolská 147, 612 00 Brno, Czech Republic

Email of the presenting author: eliska.mikmekova@isibrno.cz

Detailed knowledge of mechanisms of electron scattering and its practical consequences for very low energies are of prime importance for not only measurement techniques but also development of new materials for next-generation electronic devices.

Determining inelastic mean free path (IMFP) of electrons in bulk materials is an ongoing topic in spectroscopy. Information on IMFP for very low electron energies, $E \leq 100$ eV, is not satisfactory and it is often missing in case of 2D materials, which are promising in the semiconductor industry.

Low thickness of 2D crystalline materials motivated us to develop the unique UHV device analyzing samples via transmitted electrons in a standard microscopic regime (energy range 0 – 5 keV), and also via time-of-flight (ToF) method (focusing on energy range $E \leq 300$ eV). [1]

Graphene is one of the most well-known 2D materials, it is lightweight and strong, and its other unique properties such as excellent electrical and thermal conductivity and transparency make it an ideal candidate for study at very low energies in the transmission mode of our device. We performed experiments with multilayered graphene to obtain electron energy loss spectra (EELS). Both plasmon peaks (π and $\pi+\sigma$) are present in the measured spectra for 2 layer and 3-5 layers graphene samples (Figure 1). The position of the plasmon peaks increases with both the number of layers of 2D samples and the momentum transfer value [2, 3]. The experimental EELS data are used to derive IMFP values.

The measured data are supported by simulated momentum-resolved EELS spectra using many-body perturbation theory (Yambo code), on top of density-functional theory (DFT), Quantum Espresso [4].

References:

[1] I. Konvalina et al., Nanomaterials 11, (2021), 2435. https://doi.org/10.3390/nano11092435
[2] M. P. Seah and W. A. Dench, Surf. Interface Anal. 1 (1979), p. 2. https://doi.org/10.1002/sia.740010103
[3] P. Wachsmuth et al., Phys. Rev. B 90, (2014), 235434.https://doi.org/10.1103/PhysRevB.90.235434
[4] P Giannozzi et al., J. Phys. Condens. Matter 21 (2009), 395502. http://dx.doi.org/10.1088/0953-8984/21/39/395502

Acknowledgement:

The authors acknowledge funding from the Technology Agency of the Czech Republic, grant number TN02000020.

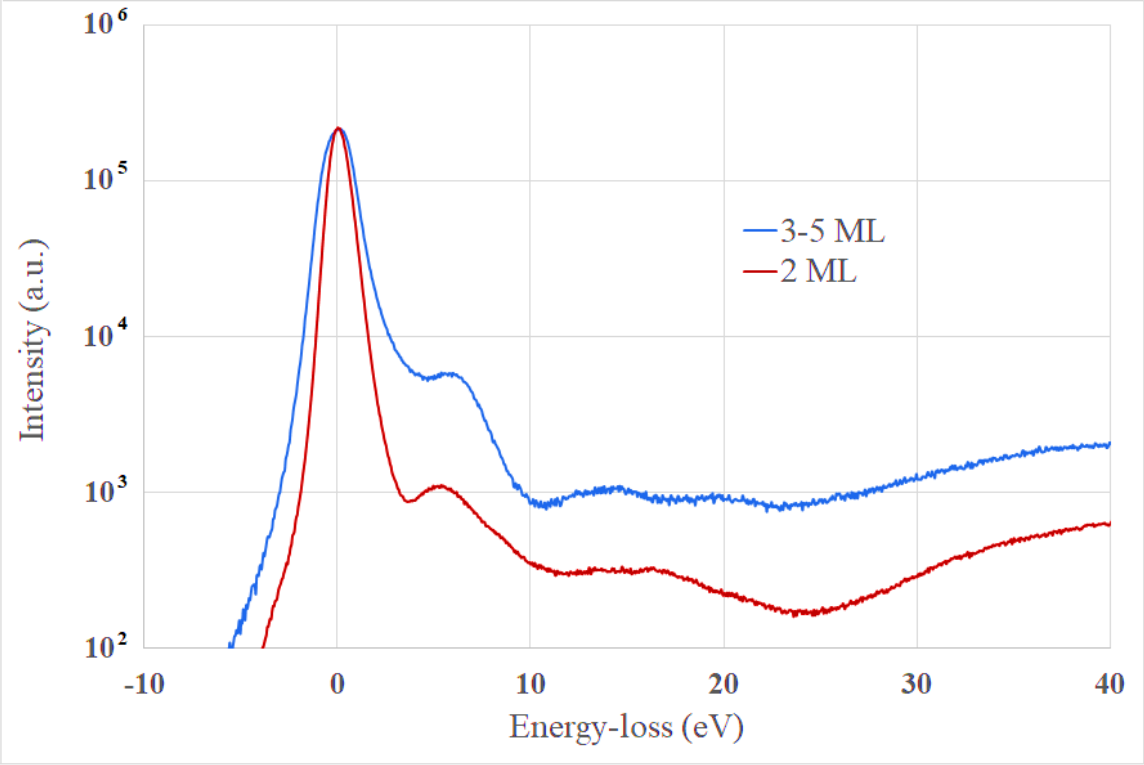

Fig. 1 : Experimental energy loss spectra of 2 layer and 3-5 layer graphene samples for a landing energy of 100 eV.

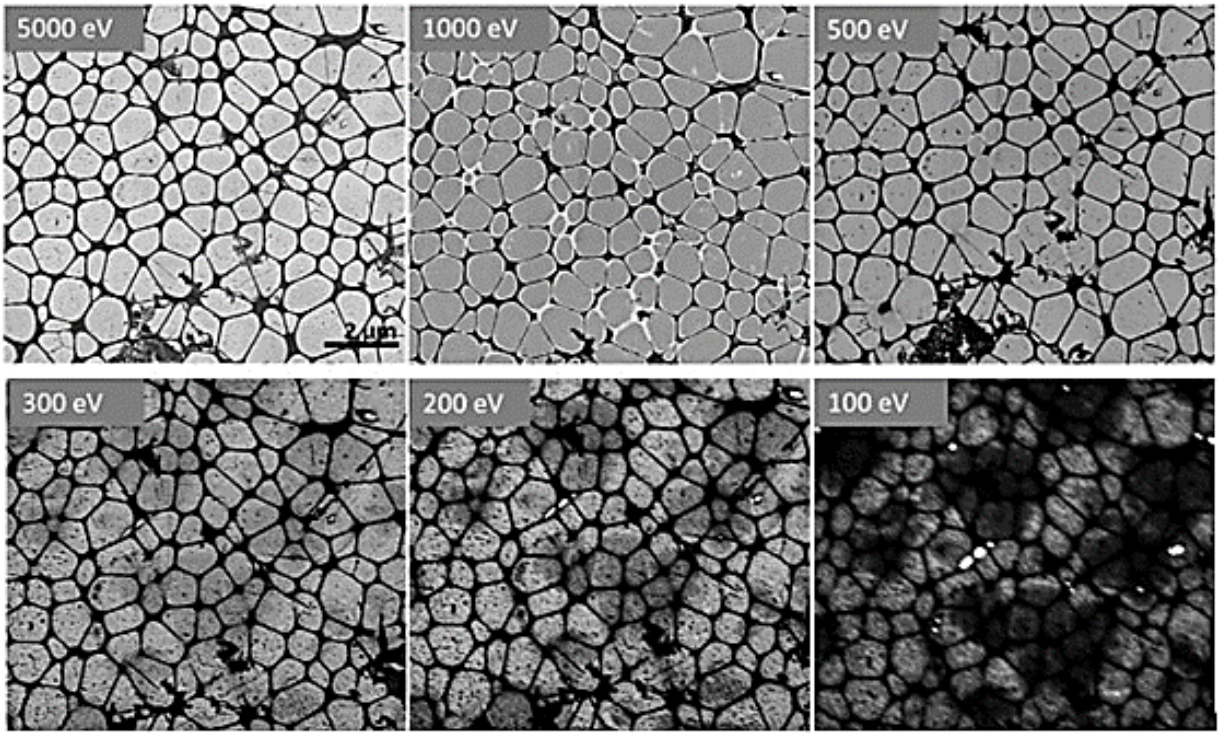

Fig. 2. : Micrographs of multilayered graphene (nominally 3 to 5 layers) observed from 5000 eV to 100 eV.

Investigation of optical dichroism with vortex electron beams

Zálešák M.[1,2], Ošmera M.[1], Hrtoň M.[1,2], Konečná A.[1,2]

[1] Institute of Physical Engineering, Faculty of Mechanical Engineering, Brno University of Technology, Brno, Czech Republic
[2] Central European Institute of Technology, Brno University of Technology, Brno, Czech Republic

Email of the presenting author: Marek.Zalesak@ceitec.vutbr.cz

Introduction:

Low-energy excitations in matter, such as phonons, excitons, or plasmons, can be significantly influenced by material interfaces and boundaries. For instance, by nanostructuring bulk plasmonic materials, it is possible to engineer localized plasmonic resonances both spectrally and spatially, which is vital for light manipulation at the nanoscale. However, a detailed analysis of the plasmonic excitations in nanostructures requires probes that can provide high spectral (meV) and spatial (~ nm) resolution. Focused electron beams in scanning transmission electron microscopes (STEMs) in connection with electron energy-loss spectroscopy (EELS) can perfectly fulfill these requirements. STEM-EELS has thus become one of the essential techniques for probing plasmons (and other low-energy excitations) in confined geometries [1,2].

STEM-EELS can also be used when probing nanoscale specimens that exhibits chiral behaviour. Chiral structures are those who can be distinguished from its mirror image (e.g. proteins, amino acids, or carbohydrates). However, to fully analyse chiral structures one needs to have a chiral probe as well. For this purpose, we can employ vortex electron beams (VEBs). VEBs featuring spiraling wavefronts have been suggested as exciting alternatives to conventional beams in retrieving dichroic signal for various samples, including chiral plasmonic nanoparticles or their assemblies [3]. Because of the azimuthally varying phase of VEBs, the interaction with a chiral nanostructure yields different EEL spectra than with standard electron probes with a flat phase profile.

Materials and Methods:

However, despite theoretical predictions, unambiguous experimental evidence of optical dichroism in low-loss EELS acquired with VEBs is still missing [4]. We performed a comprehensive theoretical analysis of dichroic EELS signal for a prototypical chiral plasmonic nanoparticle – a single-twist metallic helix – to reveal experimental parameters' influence on the robustness and strength of the dichroism. We explored the role of convergence and collection beam angles, acceleration voltage, beam position, and pre- or post-selected orbital angular momentum.

For the theoretical modeling, we considered the quantum description of the shaped electron beam as a wave function that interacts with the specimen described classicaly by quasi-electrostatic modes. These modes can be obtained by solving the Laplace equation with the specified geometry of the nanoparticle and local dielectric function.

We investigated the EEL spectra for two models of VEBs interacting with a single-twist metallic helix. The first model utilizes the numerical calculations of the electrostatic nanostructure modes via MATLAB plugin MNPBEM. We explored helices with different thicknesses and pitches. The second model is semi-analytical with an approximated distribution of mode charges corresponding to an infinitesimally thin metallic wire. In this contribution, we will compare the results from both models and explore the limitations of the simplified model.

Conclusions:

We will introduce the theoretical models used for the calculations of dichroic EEL spectra and results obtained by numerical and semi-analytical simulations of the prototypical chiral plasmonic nanoparticle excited by vortex electron probes. We will examine the robustness of the VEB excitation with respect to probe misalignments and positioning and further discuss optimal parameters for future experiments.

References:

[1] Wu Y. et al.: Chemical Reviews, Probing Nanoparticle Plasmons with Electron Energy Loss Spectroscopy, 118 (2018), 2994-3031.
[2] García de Abajo F.J. et al.: Reviews of Modern Physics, Optical excitations in electron microscopy, 82 (2010), 209-275.
[3] Asenjo-García A. et al.: Physical Review Letters, Dichroism in the Interaction between Vortex Electron Beams, Plasmons, and Molecules, 82 (2010), 066102.
[4] Harvey T.R. et al.: https://arxiv.org/pdf/1507.01810.pdf

Acknowledgement:

We acknowledge the support of the Czech Science Foundation GACR under the Junior Star grant No. 23-05119M and Brno Ph.D. Talent Scholarship – Funded by the Brno City Municipality.

Resonant Raman spectroscopy of GaN/graphene nanostructures; on the way to ultra-violet photodetectors

Kostka M.[1,2], Mach J.[1,2], Bartošík M.[1,2], Šikola T.[1,2]

[1] Brno University of Technology, Institute of Physical Engineering, Technická 2896/2, 616 69 Brno, Czech Republic
[2] Brno University of Technology, Central European Institute of Technology, Purkyňova 123, 612 00 Brno, Czech Republic

Email of the presenting author: 209403@vutbr.cz

Introduction

The development of light detectors is focused on high performance, fast response and simple fabrication. These parameters are affected by the charge carrier mobility, which is sensitive to perturbations in the crystal lattice, namely defects and phonons [1]. Gallium nitride is a polar III-V semiconductor, where a strong interaction between free electrons and phonons is observed [2]. The interaction lowers the efficiency of charge carrier collection upon light illumination, as well as it reflects on the presence of defects. The substrate for GaN growth is graphene, a two-dimensional material which exhibits ideal properties to form a conducting channel in photodetectors [3]. The structure of GaN nanocrystals grown on graphene substrate thus takes advantage of the sensitivity of GaN to ultra-violet light, thanks to the broad bandgap of 3,4 eV, alongside with the high electron mobility of graphene, which collects the photogenerated charge carriers.

Materials and methods

For a substrate, silicon wafer with 280 nm SiO_2 was used, covered by CVD graphene. The growth of GaN nanocrystals was performed by Molecular Beam Epitaxy at low temperatures of 200 °C. For the study of the exciton-phonon interaction, the Resonant Raman Spectroscopy was utilized, with the 355 nm excitation laser. The observations of nanostructures were done using SEM Fei Verios at 2 kV and 50 pA imaging conditions.

Results

The studied nanostructures are shown in the Fig. 1. The SEM image gives an information about the crystallinity, which is crucial for further applications. Given by the low acceleration energy used for the SEM imaging, the graphene substrate is visible in the image as a grey layer in the background. The optical properties of the nanostructures were studied using Resonant Raman Spectroscopy. The resulting spectrum is shown in the Fig. 2. Two different effects are observed: photoluminescence due to the radiative transition of the photoexcited electrons over the bandgap, forming a broad peak in the background; and the multi-phonon scattering in the form of a series of equally separated overtones of the A1(LO) phonon. In the non-resonant case (excitation laser 532 nm) these peaks are not observed. As they arise only with the sufficient excitation energy, their presence is an evidence of the exciton-phonon interaction. Such a strong interaction (overtones observed up to the 4th order) indicates on a good crystalline quality of the nanocrystals.

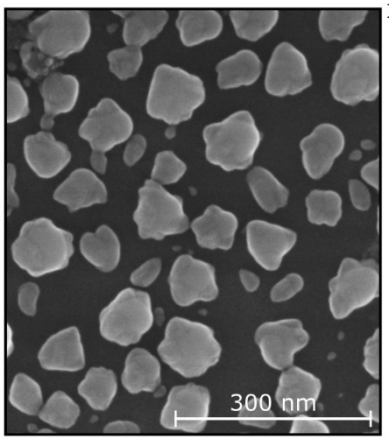

Fig. 1: SEM image of GaN nanocrystals with graphene substrate.

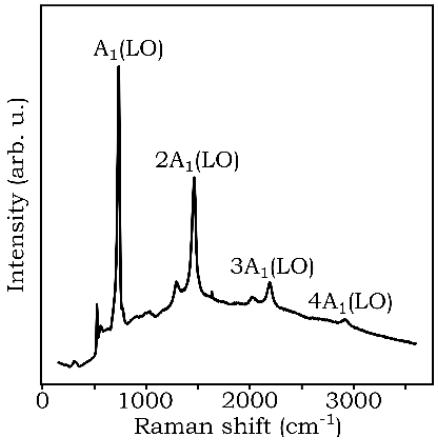

Fig. 2: Resonant Raman spectrum of GaN nanocrystals on graphene (λ_{exc} = 355 nm). The peak A_1(LO) and its overtones corresponds to the multi-phonon scattering, which arises during the exciton-phonon interaction.

Conclusion

In this work, we fabricated a structure of GaN nanocrystals grown on graphene substrate. The measurements of resonant Raman spectra displayed how the photoexcited electrons interact with the lattice vibrations. The observed effects help us understand the photodetection mechanism, in order to optimize the photodetector, in which these findings are applied. The confirmation of a good crystallinity of the nanocrystals is a key factor in fabricating highly sensitive photodetectors.

References:

[1] Sanders N. et al.: *Appl. Phys. Lett.*, 119(2021), 6.
[2] Behr D. et al.: *Appl. Phys. Lett.*, 15(1996), 2406-2406.
[3] Ferrari A. C. et al.: *Nat. Photonics*, 4(2010), 611-622.

Acknowledgement:

This research was supported by MEYS CR under project CzechNanoLab (LM2023051) at CEITEC Nano Research Infrastructure, and by Brno University of Technology (FSI-S-23-8336).

Optical polarization anisotropy of photoluminescence for CsPbBr3 nanorods

Gaizura F.[1], Dvořák P.[1,2], Bouchal P. [1,2], Liška P. [1,2], Balabán M.[1], Kratochvíl M.[3], Bačovský J.[4]

[1] Institute of Physical Engineering, Brno University of Technology, Technická 2, 616 69 Brno, Czech Republic
[2] Central European Institute of Technology, Brno University of Technology, Purkyňova 123, 612 00 Brno, Czech Republic
[3] Institute of Physical and Applied Chemistry, Brno University of Technology, Purkyňova 118, 612 00 Brno, Czech Republic
[4] Delong Instruments a. s., Palackého třída 153, 612 00 Brno, Czech Republic

Email of the presenting author: gaizurafilip@seznam.cz

Introduction:

Low-dimensional lead halide perovskites (LHPs) are promising nanomaterials due to their exceptional optoelectronic properties such as strong exciton resonances that can be controlled by an external electric field or charge injection.[1] Moreover, the preparation of all-inorganic perovskite nanoparticles (CsPbBr3) can be carried out using chemical synthesis utilizing the hot injection method. In the scientific community, the hot injection method is preferred for its precision in controlling nanoparticles' morphology, ensuring their adaptability. Furthermore, the method yields a liquid solution that can be effortlessly deposited across various substrates using a simple one-step spin-coating technique. Thanks to the inorganic composition, the nanoparticles provide long-term stability, enabling them to withstand environmental factors, thus enhancing their versatility for sensing applications. In addition, the optical properties of CsPbBr3 nanoparticles can be controlled by surface passivation, where the ligand-assisted reprecipitation (LARP) synthesis method is most often used.

CsPbBr3 nanorods show great application potential in optical detection or imaging because they show spatial optical anisotropy[2] of photoluminescence that is caused by the quantum confinement in nanoparticles. However, if we want to make full use of this interesting optical effect, then this places high demands on the precise production of nanorods and their subsequent accurate characterization.

Materials and Methods:

The synthesis of perovskite nanorods was carried out using room temperature method with Cs-oleate and $PbBr_2$ solution as precursors. Cs-oleate was introduced to $PbBr_2$ solution under vacuum at room temperature forming colloidal solution of monodisperse nanowires. Dissolution of the nanowires in non-polar solvent, such as cyclohexane, toluene or hexane, established new equilibrium and chemical cutting of nanowires occurred. Subsequently, these solutions ware put on Si substrates or TEM membranes by the drop casting method.

Results:

The newly synthesized CsPbBr3 nanorods showed consistent dimensions with little to no variation in length or diameter according to TEM analysis. Their dimensions are heavily influenced by the final concentration of nanorods in the solution showing direct proportionality with concentration. The ratio of capping ligands to Cs-oleate showed to be a crucial factor in altering the nanorods' dimensions where ratio favouring the capping ligands yielded smaller dimensions. The stoichiometry quality of our prepared nanorods, we measure by EDX spectroscopy that is also constituent of TEM microscope. Moreover, we observed for our samples two photoluminescence (PL) peaks at 520 nm and at 480 nm of wavelength which are shown reciprocally orthogonal polarization dependence of PL emission. We assign this effect to quantum confinement of excitons in shorter size of nanoparticles and it causes a blue spectral shift of one PL peak and its polarization anisotropy.

Conclusion:

We prepared the CsPbBr3 nanorods with variable size and shape by the hot injection method and by LARP. The morphology of nanoparticles was characterized by high lateral resolution low-energy TEM in cooperation with the Delong Instruments company. Moreover, this microscope can investigate the chemical composition and stoichiometry of individual nanorods utilizing EDX spectroscopy. Furthermore, we have shown that these CsPbBr3 nanorods evince two energy-separate strong exciton resonances at the blue and green colour. We have proved that the transversal exciton mode (resp. longitudinal) corresponds to the green peak (resp. blue) and therefore, it indicates the orientation of the long axis of CsPbBr3 nanorods.

References:

[1] ZHAO, Shiyu; WU, Jian; CHI, Xiaochun; SUI, Ning; KANG, Zhihui et al. Optical Properties of Inorganic Halide Perovskite Nanorods: Role of Anisotropy, Temperature, Pressure, and Nonlinearity. Online. The Journal of Physical Chemistry C. 2022, vol. 126, pages: 10.

[2] WANG, Yongkai, Xiaoyu LIU, Qiqian HE, et al. Reversible Transformation between CsPbBr 3 Perovskite Nanowires and Nanorods with Polarized Optoelectronic Properties. Advanced Functional Materials [online]. 2021, pages: 9.

Acknowledgement:

This work has been supported by the Czech Science Foundation grants no. 20-01673S. We would like to acknowledge CEITEC for providing the facilities necessary for the synthesis of materials used in this study. We are grateful to Delong Instruments for granting access to their transmission electron microscopy (TEM) facilities, which was instrumental in characterizing the synthesized materials. Additionally, we acknowledge the financial support of Brno University of Technology (BUT) under whom this study was conducted.

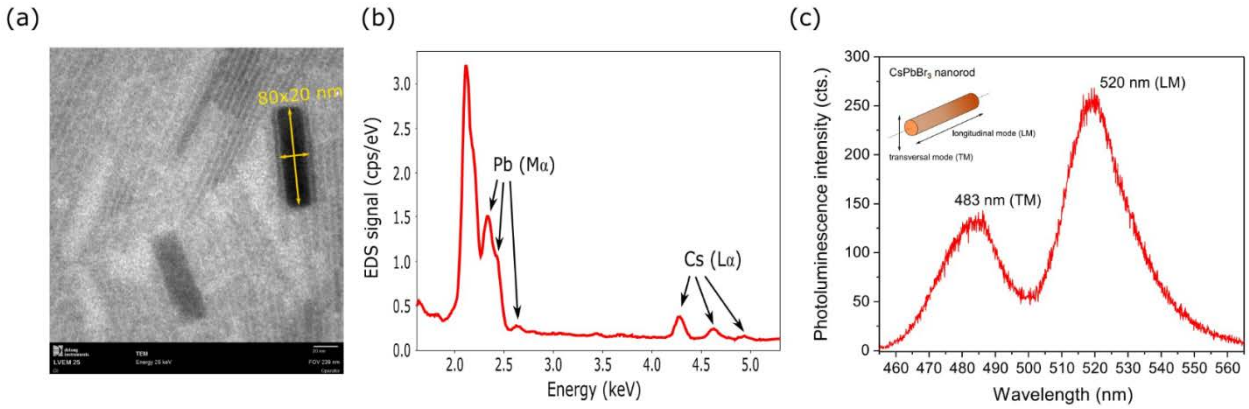

Fig. 1: (a) TEM image, (c) EDX spectrum, (c) and PL spectrum of $CsPbBr_3$ nanorods.

Evidence of the pretreatment solution transfer to the cataphoretic bath using EDS analysis

Koutová Z.[1], Novotná M.[1]

[1] MemBrain s.r.o., Stráž pod Ralskem, Czech Republic

Email of the presenting author: Zuzana.Koutova@membrain.cz

Introduction

Generally, the automotive industry is one of the most overloaded and stressed in the subject of materials selection, characterization, application and their corrosion prevention and surface protection. One of the used and technologically most advanced method of anticorrosive surface treatment processes for automotive industry is cataphoretic coating. Usually, it is used as surface treatment of metal products, which includes mainly steel, galvanized and aluminium parts. The cataphoretic coating process itself is a set of several steps of pre-treatment, paint application and curing. Each sub-process is rigorously controlled (including production of parts and their storage). Nevertheless, it can occur that the parts with a defective coating are the final product of the cataphoretic coating process. The anti-corrosion protection may be reduced even because of relatively small defects, and thus the safety risk increased. In this contribution, case study of the cause analysis of defects arising during the cataphoretic coating process are shown, where it is necessary to use the method of scanning electron microscopy with energy dispersed X-ray spectroscopy (EDS).

Materials and methods

The defect in cataphoretic coating on the surface of metal parts and a drop sample taken after rinsing of these metal parts were examined by the EDS method. EDS analyses were taken with scanning electron microscope (Quanta FEG 250, FEI) at the regime pressure of the low vacuum mode and high vacuum mode, and measured with TEAM™ Software Suite, coupled with the Octane Plus System.

Results and conclusion

The defects in cataphoretic coating on the surface of metal parts were examined to prove the cause of these defects. As these were parts with cavities, contamination of the cataphoretic bath with the pre-treatment solution was suspected. Therefore, it was further analysed a drop sample taken after rinsing of these metal parts. There were detected elements, which are usually present in pretreatment solutions, in both samples. In the sample of the defect of cataphoretic coating on the surface of the metal part, elements usually contained in the cataphoretic bath were also detected. In the case of parts with cavities in the immersion system, where is possible to flow pretreatment solutions to into the cavities and their incomplete flushing in the rinsing bath, the transfer of the pretreatment to the coating bath itself may occur. On the overall composition of the coating bath, these transfers do not need to be measurable. However, local precipitation may occur when the solution transferred in the cavities is mixed with the cataphoretic bath solution. These precipitates can then clog the ultrafiltration modules or cause defects on the part itself.

References:

[1] Brüggemann M. et al.: Electrocoat: Formulation and Technology (2020), Vincentz Network GmbH & Co. KG ISBN: 978-3-7486-0105-0.
[2] Weldon D. G.: Failure Analysis of Paints and Coatings, Revised Edition (2009), John Wiley & Sons, Ltd. ISBN: 978-0-470-69753-5.
[3] Streitberger H.-J. et al.: Automotive Paints and Coatings, Second, Completely Revised and Extended Edition (2008), Wiley-VCH Verlag GmbH & Co. KGaA ISBN: 978-3-5273-0971-9.

Acknowledgement:

The work was carried out within the framework of the project "A long-term concept for the development of the research organization" supported by the Ministry of Industry and Trade of the Czech Republic, using the Membrane Innovation Centre infrastructure.

TEM characterization of the catalytic system for the Suzuki-Miyaura cross-coupling reaction monitored by the SERS

Kožíšek J.[1,2], Šloufová I.[1], Pavlova E.[2,3], Michalcová A.[3]

[1] Charles University, Faculty of Science, Department of Physical and Macromolecular Chemistry, Hlavova 2030, 128 40 Prague 2, Czech Republic
[2] Institute of Macromolecular Chemistry ASCR, Heyrovsky Sq. 2, 162 06 Prague 6, Czech Republic
[3] Department of Metals and Corrosion Engineering, University of Chemistry and Technology Prague, Technická 5, 166 28 Prague 6, Czech Republic

Email of the presenting author: kozisekja@natur.cuni.cz

Introduction. The cross-coupling reactions leading to formation of a new C-C bond and catalyzed by transition metals have been studied intensively for over the last few decades. The importance of cross-coupling reactions has been widely recognized and their authors, R. Heck, E. Negishi and A. Suzuki, were awarded by the Chemistry Nobel Prize in 2010. These reactions opened a new synthetic pathway for products which cannot be easily synthetized. For designing novel reactions it is very important to understand its mechanism [1]. The main aim of this study is monitoring of Suzuki-Miyaura cross-coupling reaction (SMCR) between aryl halide and arylboronic acid in the presence of a base on the surface of the plasmonic nanoparticles [2] via surface-enhanced Raman scattering spectroscopy (SERS) together with characterization of the active system by transmission electron microscopy (TEM).

Experimental. The catalytic system for SMCR was prepared by mixing of palladium (II) salt and silver nanoparticles (Ag NPs), which were prepared by reduction of silver nitrate with hydroxylamine hydrochloride following the procedure described by Leopold and Lendl [3]. At first, system with Ag NPs precoated with arylboronic acid and/or aryl iodide was prepared. Subsequently, 10 ul of Pd^{2+} ions (1 mM) were added into this system.

TEM results. The Pd^{2+} ions oxidized Ag atoms on the surface of the Ag NPs and at the same time they reduce themselves. This electrochemical exchange of atoms on the nanoparticle surface led to the formation of a“core-shell” type of nanoparticles (core-Ag, shell-Pd). Figure 1 shows an active catalytic system of a mixture of both the original symmetrical Ag NPs and the newly formed “hairy” bimetallic AgPd nanoparticles.

Conclusions. TEM has proven to be one of powerful technique for characterization of morphological changes of the metallic nanoparticles in SERS active systems.

References:

[1] Kadu, B. S., Catal. Sci. Technol., 11 (2021), 1186–1221.
[2] Zhao, Y.; et al.: J. Phys. Chem. Lett., 10 (2019), 1286–1291.
[3] Leopold N., et al.: J. Phys. Chem. B., 107 (2003), 5723–5727.

Acknowledgement:

The authors acknowledge funding from Project TN02000020 (TA CR), Charles University Grant Agency 237823 (GAUK).

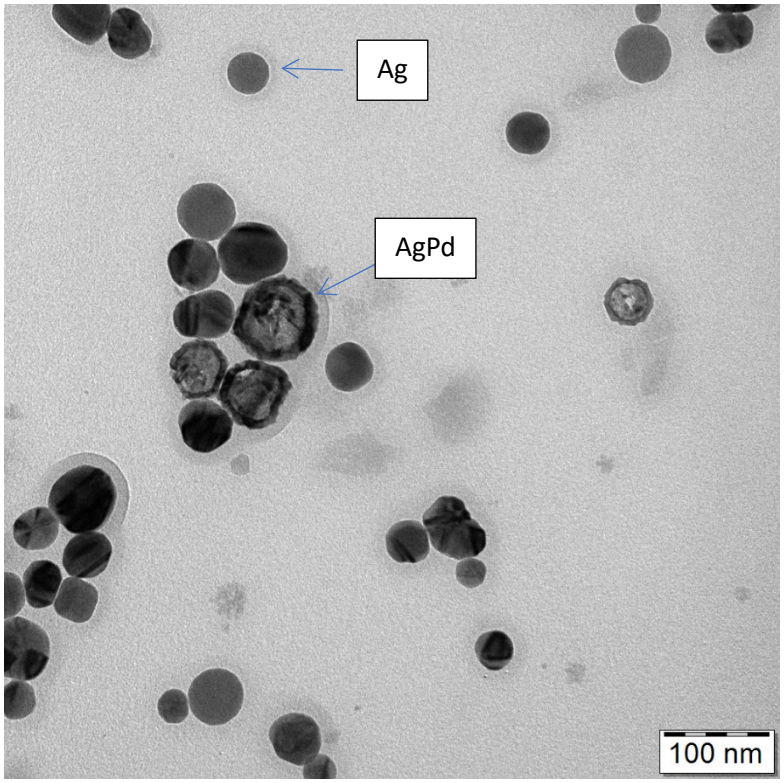

Fig. 1: TEM figure of a catalytic system prepared by mixing Pd^{2+} ions with Ag nanoparticles for the SMCR monitored by the SERS.

Preparation, rheology, and morphological characteristics of thermoplastic material from wheat starch with maltodextrin for bio-medical applications

Rana L.[1], Nemecek P.[1], Gajdosova V.[1], Kouka S.[1], Pavlova E.[1], Strachota B.[1], Konefal M.[1], Stary Z.[1], Slouf M.[1]

[1] Institute of Macromolecular Chemistry CAS, Praha, Czech Republic

Email of the presenting author: nemecek@imc.cas.cz

Introduction. We report the modification of thermoplastic starch (TPS) by the addition of maltodextrin (MD). The purpose of the modification was to get a material with lower viscosity. TPS with lower viscosity can be processed at lower temperatures. This is an important advantage for the biomedical applications, which employ TPS mixed with antibiotics (ATB), as the ATB activity can be compromised at elevated temperatures [1, 2].

Experimental. TPS was prepared from wheat starch (Skrobarny Pelhrimov a.s., Czech Republic) by our two-step preparation [3] that comprises solution casting (SC; device: laboratory-scale mixer; Heidolph (RZR 2020); conditions: mixing of starch, water and glycerol at 67˚C-70˚C until gelatinization) followed by melt mixing (MM; device: Brabender Plasti-Corder; Duisburg, Germany; conditions: 60 rpm at 120˚C for 8 min). Morphology of TPS samples was visualized by light microscopy (LM; Nikon Eclipse 80i; Nikon, Japan) and SEM microscopy (SEM; MAIA; Tescan, Brno, Czech Republic). Crystalline structure changes were assessed from wide-angle X-ray scattering (WAXS: GNR Analytical Instruments, Italy). Rheological and thermomechanical properties were characterized by rheometry (Anton Paar GmbH, Austria).

Results and conclusion. Figure 1 documents that the combination of SC and MM is necessary to achieve highly homogeneous TPS. SC only (Fig. 1a) and MM only (Fig. 1b) contained non-plasticized starch granules (elongated bright spots), while the combination of SC+MM (Fig. 1c) yielded highly homogeneous material. Figure 2 shows rheological properties of TPS: storage modulus (*G*'; Fig. 2a), loss modulus (*G*"; Fig. 2b) and absolute value of complex viscosity (|η*|, Fig. 2c) as a function of frequency (ω). The addition of MD (red and blue curves in Fig. 2) decreased both modules (G' and G'') as well as the complex viscosity |η*|, which confirmed that MD decreased the resistance of TPS towards shear deformation and suggested that the material could be processed at lower temperatures. The fact that *G*' was higher than *G*'' in the whole frequency range for all investigated materials documented that the elastic and solid character dominated in both TPS and TPS/MD. The difference between rheological properties of TPS prepared by MM and by SC+MM was small. The addition of TiO_2 did not influence the rheological properties significantly. Figure 3 displays representative cryo-fractured surfaces of TPS without addition of MD (Fig. 3a), with 5% of MD (Fig. 3b), and with 10% of MD (Fig. 3c). Non-plasticized TPS granules were observed in both TPS/MD samples (Fig. 3b-c). The lower viscosity of the TPS matrix due to MD addition seemed to result in lower overall homogeneity after SC+MM, probably due to lower shear forces during MM. We conclude that TPS/MD preparation followed by two step process (SC+MM) could effectively produce lower viscosity TPS material. The viscosity of the final material lowers at the cost of homogeneity. In our future work, we will try to optimize the processing conditions and maltodextrin/plasticizers ration so that the final material exhibited both lower viscosity and high homogeneity.

References:

[1] Masters, E. A. et al.: Bone Res. 2019, 7, 20.
[2] Gajdosova V. et al.: Materials 2022, 15.
[3] Ostafinska A. et al.: Int. J. Biol. Macromol. 2017, 101, 273-282.

Acknowledgment: Projects TN02000020 (TA CR) and NU21-06-00084 (AZV CR).

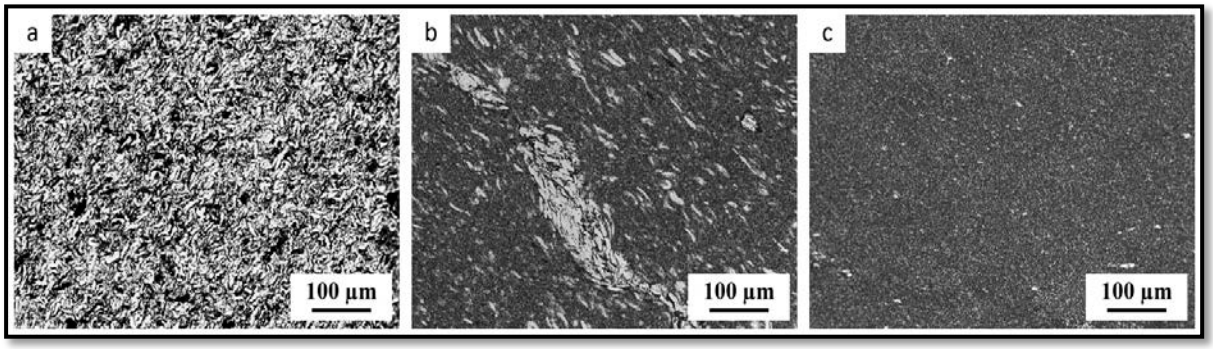

Fig. 1. Light micrographs of thermoplastic starch containing TiO_2 nanoparticles comparing the homogeneity of the processing techniques including (a) solution casting, (b) melt mixing (MM) and (c) SC+MM.

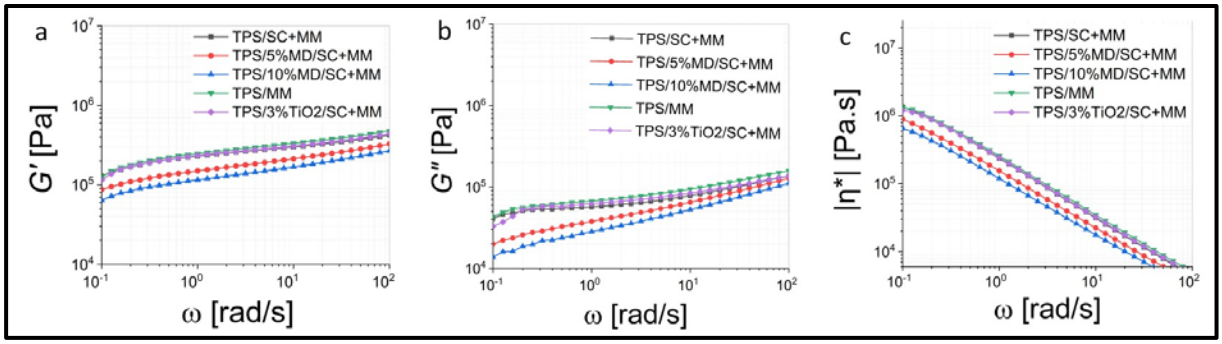

Fig.2. Frequency sweeps from oscillatory shear flow rheometry: (a) Storage modulus G' and (b) loss modulus G'' (c) absolute values of complex viscosities at 120◦C and strain of 0.1%

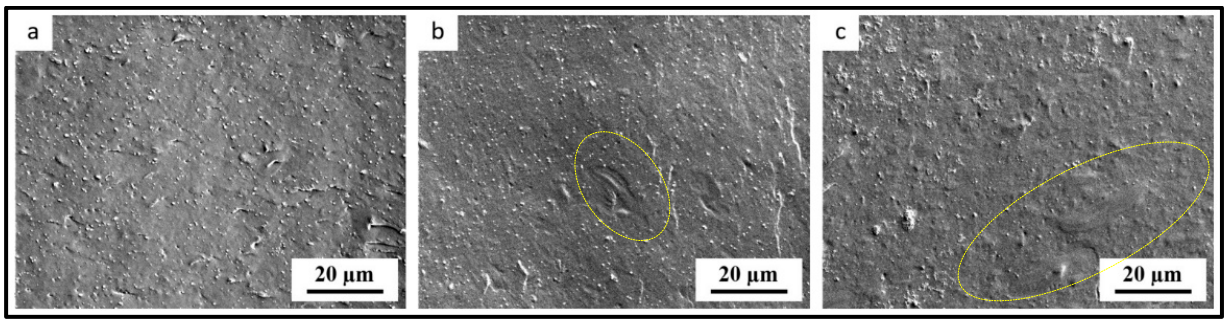

Fig.3. SEM micrographs of TPS/MD/TiO_2, documenting non-homogeneous morphology of TPS after the addition of 5% and 10% of maltodextrin. (a). TPS/3%TiO_2 (b). TPS/5%MD/3%TiO_2 (c) TPS/10%MD/3%TiO_2

Laboratory rocking curve X-ray diffraction imaging of semiconductor wafers

Mikulík P.[1], Caha O.[1], Meduňa M.[1]

[1] Department of Condensed Matter Physics, Faculty of Science, Masaryk University, Brno, Czech Republic

Email of the presenting author: mikulik@physics.muni.cz

Rocking curve imaging (RCI) is a full-field X-ray diffraction imaging technique which combines X-ray digital topography and Bragg- or Laue-diffraction rocking curve recording. A large (almost) parallel monochromatic beam irradiates a crystalline sample with a misorientation distribution characterized by local tilt angles of the crystal lattice, see figure 1. Series of digital topographs are measured by a two-dimensional detector at different sample orientations from which peak characteristics of millions of local Bragg peaks from each series are extracted. The field of view and lateral resolution is given by the camera size, its pixel size and the Bragg angle, while the angular resolution is given by the rocking curve width being typically much smaller than the misorientation angles of the studied crystal. Simultaneous high spatial resolution provided by the two-dimensional detector and high angular resolution (0.001°) allows to quantify crystalline structure perfectness over large sample area which scales with the area of the detector. Therefore the rocking curve imaging is an imaging method with faster recording compared to usual laboratory scanning area diffractometry which requests measurement of the rocking curve at each surface point.

Synchrotron RCI [1,2] profits from large parallel beam, high flux and small detector pixel size down to one micrometre. For small misorientations of the crystal lattice, detector can have any distance from the sample, while larger misorientations due to inherent focusing and defocusing of the diffracted (micro)beams require a dedicated reconstruction procedure.

Laboratory RCI [3] with a slightly diverging beam requires small misorientation angles and very small sample to detector distance, thus a home-made extension for a commercial diffractometer is necessary. Current two-dimensional detectors available at laboratory diffractometers have typical spatial resolution downto 0.1 mm which make it possible to analyze a large sample area at once.

On several examples, we will demonstrate the RCI technique for structure characterisation of several large-area semiconductor wafers, such as silicon, silicon carbide, gallium nitride or overgrown silicon-germanium microstructures, see figures 2 and 3.

References:

[1] P. Mikulík, D. Lübbert, D. Korytár, P. Pernot, T. Baumbach, Journal of Physics D: Appl. Phys. 36 (2003), A74.
[2] D. Lübbert, C. Ferrari, P. Mikulík, P. Pernot, L. Helfen, N. Verdi, D. Korytár, T. Baumbach, Journal of Applied Crystallography 38 (2005), 91.
[3] M. Meduňa, O. Caha, E. Choumas, F. Bressan, H. von Känel, Journal of Applied Crystallography 54 (2021), 1071.

Acknowledgement:

The authors acknowledge funding from the project “Quantum materials for applications in sustainable technologies (QM4ST)”, reg. no. CZ.02.01.01/00/22_008/0004572 by OP JAK, call Excellent Research.

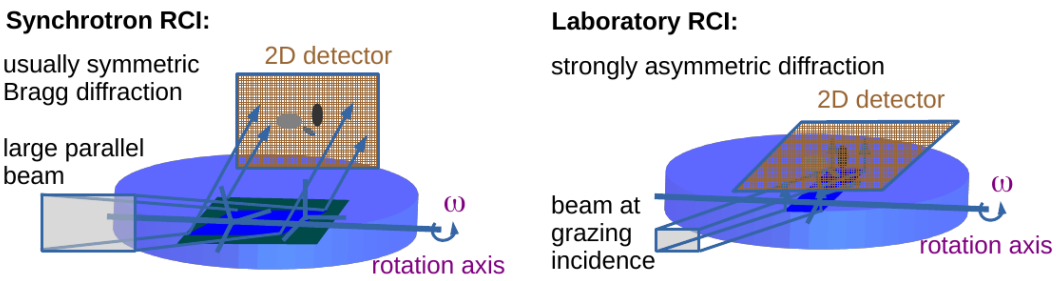

Fig. 1: Schemes comparing the synchrotron radiation and laboratory X-ray rocking curve imaging methods.

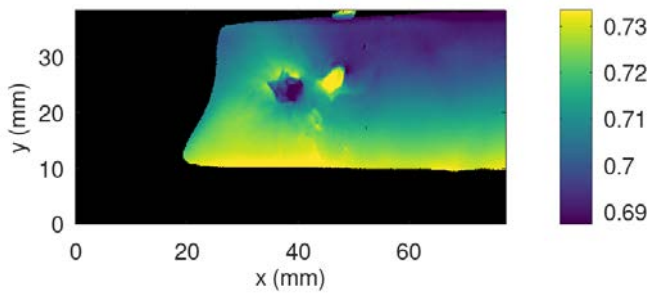

Fig. 2: Image of a relative Bragg peak position (in degrees) on a semiconductor wafer with slightly misoriented grains.

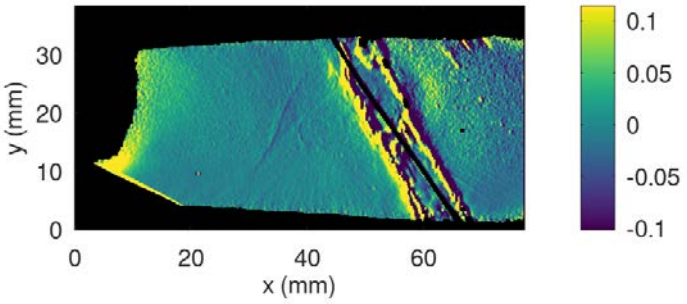

Fig. 3: Calculated image of local curvature (1/m) in a semiconductor wafer with a fracture.

Further optimization and testing of the novel embedding resins with higher resistance to e-beam damage

Pavlova E. [1], Strachota B. [1], Strachota A. [1], Nemecek P.[1], Gajdosova V. [1], Nebesarova J. [2], Tyc J. [2], Krzyzanek V. [3], Slouf M. [1]

[1] Institute of Macromolecular Chemistry CAS, Heyrovskeho nam. 2, 162 06 Prague 6, Czech Republic
[2] Institute of Parasitology, Biology Centre CAS, Branisovska 31, 37005 Ceske Budejovice, Czech Republic
[3] Institute of Scientific Intruments CAS, Kralovopolska 147, 612 64 Brno, Czech Republic

Email of the presenting author: pavlova@imc.cas.cz

Electron microscopy (EM) is one of the main techniques for characterization of soft biological materials, such as tissues, cells and their components. The key decision before the analysis is the choice of an appropriate method for sample preparation, which provides an efficient protection and fixation of the biological specimen structure. One of the well-established biological sample preparation methods is their embedding in synthetic polymer resins. The commercially available embedding resins are optimized for transmission electron microscopy (TEM), which detects high-energy transmitted electrons, but they are not appropriate for the recently popular volume EM visualization techniques that employ scanning electron microscopy (SEM). The reason is that SEM microscopes use lower primary electron energies and higher electron doses. The common embedding resins in SEM tend to suffer from charging and electron beam damage. Therefore, have developed two types of polymer resins with expected higher resistance to e-beam damage: (a) commercial resins with different types of chemical stabilizing agents and (b) resins based on more e-beam resistant polymers.

This contribution is focused on in-depth testing of the new resins for embedding various types of biological samples (such as mouse brain, cerebellum, lungs and other). Furthermore, we tested selected samples from materials science (such as magnetic polymer microspheres), which are even more difficult for SEM analyses due to their non-conductive character. The *commercially-available embedding resins* were modified with three types of stabilizing agents which were marked as A, B and C. It is worth mentioning that different commercial resins (epoxy, acrylic etc.) require different type of stabilizing agent. The *laboratory-prepared new polymer resins* were gradually optimized by means of small chemical modifications in order to improve their adhesion to biological samples and their cutability in microtomes and ultramicrotomes. Moreover, we tried to improve and simplify the resin preparation protocol so that they could be used in common biological laboratories. All prepared resins were characterized by SEM, STEM and TEM microscopy from the point of view of their homogeneity, cuttability, mechanical properties, stability under electron beam and contrast of the embedded testing specimens.

We conclude that both *modified carbon-based embedding resins* and *novel polymer-based resins* outperform the common, non-modified, commercially-available resins. Therefore, the details of the chemical modifications are not revealed at the moment (patent pending). Nevertheless, we will show multiple examples of the improved e-beam resistance, lower charging, and higher contrast, which was achieved with both types of the newly developed resins.

Acknowledgement:

Financial support through grant TN02000020 (TA CR) is gratefully acknowledged.

Microstructural characterization of thermally treated asbestos

Kusiorowski R.[1], Kujawa M.[1], Gerle A.[1]

[1] Łukasiewicz Research Network – Institute of Ceramics and Building Materials, Cementowa 8, 31-983 Cracow; Center of Refractory Materials, Toszecka 99, 44-100 Gliwice, Poland

Email of the presenting author: robert.kusiorowski@icimb.lukasiewicz.gov.pl

Asbestos is a term that refers to a group of natural minerals with special chemical and physical properties and specific fibrous habits. One of the most popular varieties of asbestos minerals widely used in the past was chrysotile. Chrysotile (or white asbestos) is the most commonly encountered form of asbestos, accounting for approximately 95% of the world's asbestos production. It is a fibrous silicate mineral in the serpentine subgroup of phyllosilicates. Its idealized chemical formula is $Mg_3(OH)_4Si_2O_5$. On the other hand, the deleterious effects of asbestos and all asbestos-containing materials began to be highlighted in the first part of the 20th century. Currently, the danger resulting from the use of asbestos materials is known, especially their carcinogenic properties. This is the main reason why asbestos materials have been recognized as hazardous waste in some countries and their disposal has been confined to special hazardous waste landfills. This is not the final solution to the asbestos problem because we do not destroy the fibrous form of asbestos. One of the proposed methods widely investigated and described in the literature could be thermal treatment [1-3].

Due to the fact, that chrysotile asbestos belongs to a group of hydrated silicates, it undergoes easily thermal decomposition process. As a result of the thermal processing of chrysotile asbestos, chemically bound water is released, which in turn leads to a change in the crystal structure. In consequence, the creation of new mineral phases occurs. Chrysotile loses chemically bound water and transforms into an anhydrous phase around 500–800°C (with a maximum rate above 700°C during non-isothermal treatment). Rapid crystallization of the anhydrous phase occurs after this stage above 800°C. The first main product of this transformation is forsterite (Mg_2SiO_4) and amorphous silica. Enstatite ($MgSiO_3$) can be formed at higher temperature, also when the temperature has reached 1000 °C or higher. The above transformations could be simplified and represented by the following overall reaction: $Mg_3(OH)_4Si_2O_5 \rightarrow Mg_2SiO_4 + MgSiO_3 + 2\ H_2O$ [4,5]

The research aimed to determine the microstructure changes that occur as a result of heat treatment of chrysotile asbestos. As a result of isothermal calcination, a change in the microstructure of chrysotile asbestos fibers was found (Fig. 1). As a result of thermal treatment the newly formed mineral phases preserve the original external fibrous habit although a complete modification of the structure at the molecular scale has occurred. Due this phenomenon named as pseudomorphosis the original asbestos fiber irreversibly loses its strength. It is easily fragmented into spherical grains of new silicate minerals which are clearly visible on the primary bundle of asbestos (Fig. 2). With this in mind, thermal methods can be considered as a possible and easy method to solve the problem of asbestos waste.

References:

[1] Spasiano D. et al.: Journal of Environmental Management 204(2017), 82–91.
[2] Paolini V. et al.: Journal of Material Cycles and Waste Management 21(2019), 205–226.
[3] Gualtieri A.F. et al.: Waste Management 31(2011), 91–100.
[4] Kusiorowski R. et al.: Journal of Thermal Analysis and Calorimetry 109(2012), 693-704.
[5] Bloise A. et al.: European Mineralogical Union Notes 18(2017), 215-260.

Acknowledgement:

This research was funded in whole by the National Science Centre, Poland under "Sonata 17" grant number UMO-2021/43/D/ST5/00356.

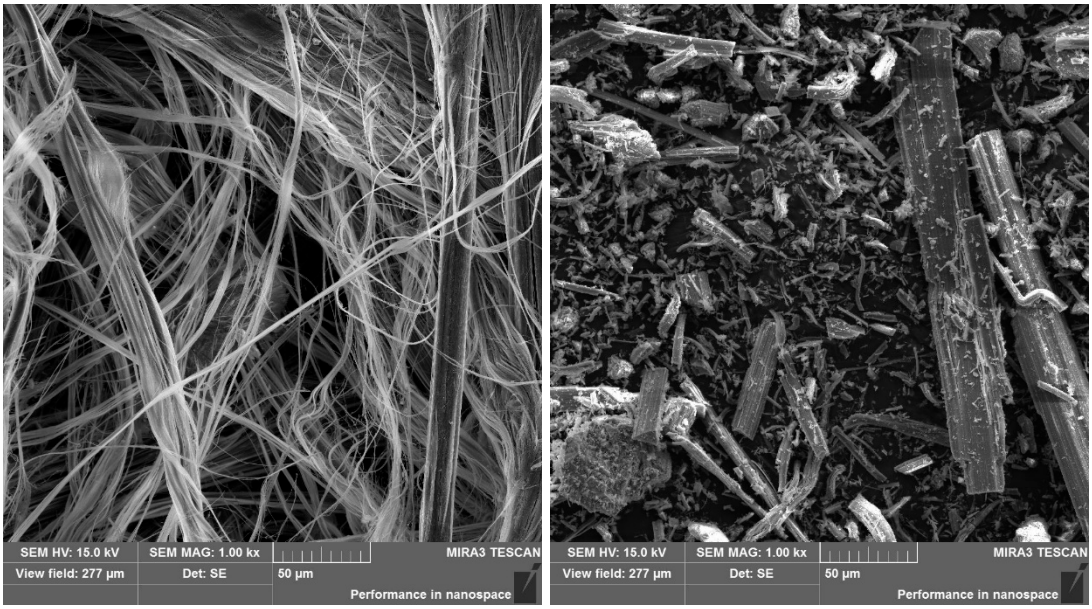

Fig. 1: Microstructure changes of chrysotile asbestos during thermal treatment: raw (left) and after 1200°C (right); magn. 1000x

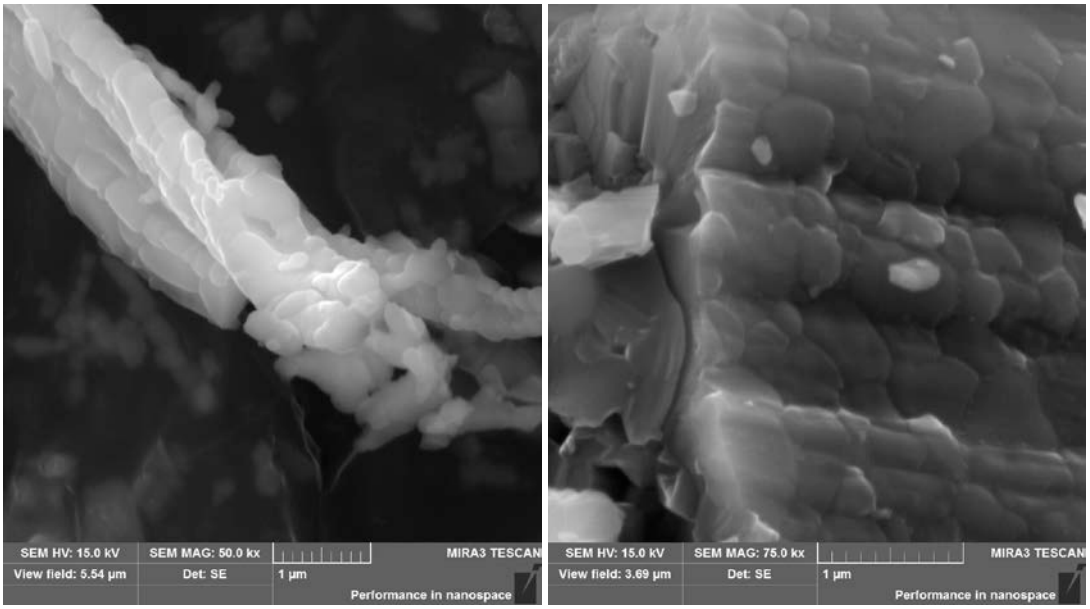

Fig. 2: Example of chrysotile asbestos fibres after thermal treatment at 1200°C. The pseudomorphosis phenomenon is clearly visible; magn. 50000x and 75000x

Microscopy methods for analysis of novel organic materials for gas sensing applications

Haško D.[1]

[1] Slovak Centre of Scientific and Technical Information - International Laser Centre, Ilkovičova 3, 841 04 Bratislava, Slovak Republic

Email of the presenting author: daniel.hasko@cvtisr.sk

Introduction

Recently in addition to scanning electron microscopy the advanced microscopy methods are increasingly coming to the fore with the aim of obtaining comprehensive information about the investigated samples in a shorter time [1]. The properties of organic transistors for gas sensing or the whole complex sensor systems are highly dependent on the surface roughness, defects within the synthesized advanced organic materials and fabricated layers local nanomechanical properties. It was shown that atomic force microscopy (AFM) is a powerful tool for analysis of soft specimens [2]. Unique is also his flexibility in terms of coupling with different spectroscopic methods (e.g. Raman, IR). However, those attractive features are associated with the complexity of the experimental set-up. The ease-of-use methods that quickly determine the morphology and mechanical properties of developed organic materials are therefore of a great interest. This contribution deals with suitable microscopy methods for characterization of the organic materials and structures prepared by the inkjet technology.

Materials and methods

In our laboratory for mapping and evaluation of surface morphology of investigated layers and structures the AFM (NT-MDT, Solver P47H-PRO), working in semicontact mode, is usually employed. For this study a combination of different methods - interferometric microscopy and nanoindenter have been used due to their sufficient spatial and force resolutions. For measurements of surface morphology, optical uniformity and defects in layers the non-contact 3D optical microscope (3D OM - Bruker, Contour GT-K1), operating in vertical scanning interferometry (VSI) and phase shifting interferometry (PSI) modes, has been used. In addition to this, for evaluation of the mechanical behaviour of prepared materials, the nanoindentation tests were performed with an in-situ indenter (Bruker - Hysitron, BioSoft) fixed on an inverted optical microscope (Zeiss, Axio Observer 3) using the adaptor ring. Several organic polymer and semiconductor layers with electron and hole conductivity which have been typically used in organic field effect transistors (OFET's) have been analysed. Using novel synthesized organic materials opens the new possibilities for applications of developed complex integrated devices with the functionalities that were not possible to achieve with inorganic materials [3].

Results

The study of basic physical phenomena concerning to organic semiconductors and the developments of new organic materials are constantly promising areas of research. For this purpose, the 3D OM operating on white light interferometry principle (Fig. 1) was utilized because of the possibility of measuring transparent layers and obtaining the results relatively quick, while maintaining the spatial resolution given by principle of the method. The VSI scanning mode is suitable for measuring inhomogeneities with nanometer vertical resolution in contrast with PSI scanning mode which allows accurate measurements of smooth surfaces with angström vertical resolution. The main difference between those modes is that in VSI mode the stepping motor moves the measuring head with the micro-interferometers while in PSI mode the piezo translator is used to move the objective for precise variation of optical path in the interferometer. The CCD camera periodically records, in each step, the images and the evaluation software subsequently reconstruct 3D image of the samples surface. The basic test technique of mechanical behaviour of materials is the quasistatic nanoindentation which induces the local sample surface deformation. The in-situ indenter BioSoft (Fig. 2) has been specifically designed for multiscale quantitative mechanical testing of soft specimens. The indentation force and displacement were recorded by the three-plate transducer attached to a piezo flexure. The collected data of investigated layers were

processed, and the Young's moduli were calculated by fitting the force-displacement data using an appropriate contact mechanics model.

Fig. 1: 3D optical microscope Contour GT-K1

Fig. 2: In-situ indenter BioSoft - Axio Observer3

Conclusions

Novel organic materials and design and development of the integrated sensing and monitoring devices seems to be a promising strategy to gaining new functionalities. In the terms of flexibility and possibility to tune the properties have organic materials several advantages. Mostly the bottom-up approach at the molecular level permits adjustment of required parameters for each application. On the other hand, it leads to an increase in requirements for analysis of their properties. The obtained results show that VSI and PSI modes of 3D OM offer unique possibilities to characterize organic films flatness with satisfactory lateral resolution. For quantitative analyses of the mechanical properties of examined layers the in-situ indenter proves to be a one of valuable tools. The measurements were taken with flat punch probe and the elastic properties were evaluated by analysis of the unloading segment using Oliver-Pharr model. Both microscopy methods can be used for investigation of advanced organic materials and the complex sensor systems fabricated by the inkjet technology.

References:

[1] Peng X. et al.: Nature Communications 13 (2022), 5197.
[2] Whitehead A. J. et al.: Methods in Molecular Biology 2299 (2021), 217.
[3] Nasri A. et al.: Material Science in Semiconductor Processing 128 (2021),105744.

Acknowledgement:

This work was financially supported by the Slovak Research and Development Agency under the contract No. APVV-20-0310.

AFM-in-SEM can visualize and quantify electron beam damage of polymer materials

Gajdošová V.[1], Pavlova E.[1], Kouka S.[1], Hegrová V.[2], Patočka M.[2,3], Pientka Z.[1], Šlouf M.[1]

[1] Institute of Macromolecular Chemistry ASCR, Heyrovsky Sq. 2, 162 06 Prague 6, Czech Republic
[2] NenoVision, Purkyňova 649/127, Brno, 61200, Czech Republic
[3] Faculty of Mechanical Engineering, Brno University of Technology, Technická 2896/2, Brno, 61669, Czech Republic

Email of the presenting author: gajdosova@imc.cas.cz

Introduction. Synthetic polymers are the most widely used (albeit not very popular) materials in modern era. Before the end of the previous century, the worldwide total volume of synthetic polymers exceeded the total volume of produced metals and alloys [1]. In current research, new polymeric materials are usually available in low amounts. Therefore, the preliminary studies of their morphology and properties are frequently performed in micro- or nanoscale [2].

Experimental. In this contribution, we studied common polymers with a broad range of properties: from the softest, semicrystalline and ductile high-density polyethylene (PE), through somewhat harder polypropylene (PP), to the hardest amorphous and brittle polystyrene (PS) and polymethyl-methacrylate (PMMA). The above-listed polymers are also known to exhibit various resistance to electron beam damage. We prepared smooth surfaces of all four polymers by ultramicrotomy and/or smoothing under liquid nitrogen [3]. The quality of the prepared surfaces and morphology of the polymers before and after the e-beam exposure was studied by light microscopy (LM) and scanning electron microscopy (SEM). The micromechanical properties were characterized by instrumented microindentation hardness testing (MHI). Finally, the morphology and e-beam damage were characterized by means of recent and modern correlative method - AFM-in-SEM (device LiteScope by NenoVision, Czech Republic attached to an SEM microscope Versa by ThermoFisher Scientific, Czech Republic).

Results. SEM micrographs (Fig. 1) illustrated the different extent of electron beam damage in various polymers. Measurement of micromechanical properties by means of MHI (Fig. 2, left) documented that the polymers exhibited broad range of properties. The *F-h* curves in Fig. 2 confirmed that all polymers had been subjected to the same maximum loading force applied to the indentation tip (F_{MAX} = 500 mN), but the tip penetration depths (*h*) varied from ca 20 μm for PE to ca 10 μm for PMMA. The comparison of micro- and nanomechanical properties (Fig. 2, right) proved that micromechanical properties obtained from MHI (with the high penetration depths above 10 μm) were not affected by e-beam irradiation, while the nanomechanical properties assessed from AFM-in-SEM (with low penetration depths well below 1 μm) were affected significantly. This is further illustrated by raw *F-z* curves from AFM-in-SEM measurements (Fig. 3).

Conclusions. AFM-in-SEM is a powerful technique for polymer characterization. One of its advantages consists in the possibility to select the region of interest (using SEM), study detailed surface morphology (using AFM, topography measurements), and quantify micromechanical properties (using AFM, indentation measurements). This contribution has demonstrated that the e-beam irradiation during the SEM characterization of the polymer materials should be minimized in order not to influence the nanomechanical properties assessed by AFM. On the other hand, this phenomenon can be turned into an advantage: the carefully conducted AFM-in-SEM measurements can both visualize and quantify the effect of e-beam irradiation on the investigated materials.

References:

[1] Raab M. et al.: Vesmír. 88 (2009/3) 186.
[2] Encyclopedia of Polymer Science and Technology. DOI: 10.1002/0471440264.pst199.pub2
[3] Slouf M. et al.: Polymer Engineering and Science 47 (2007) 582–592.

Acknowledgement: Projects TN02000020 (TA CR) and NU21-06-00084 (AZV CR).

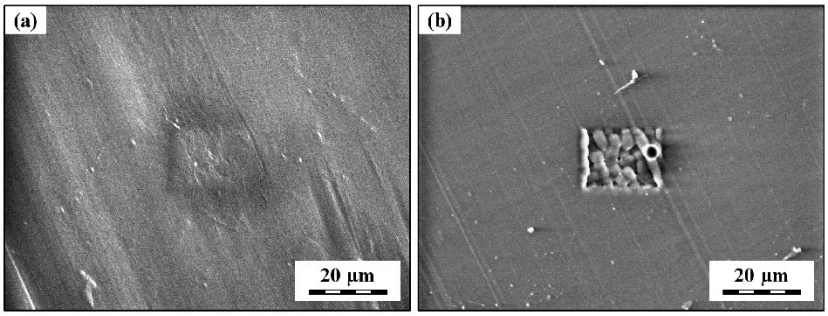

Figure 1: *SEM micrographs of the smooth polymer surfaces after the e-beam irradiation: (a) HDPE (b) PMMA. The whole image was irradiated with a minimal radiation dose (1.9 e/nm^2), while the central rectangular regions have been irradiated by a higher dose (148 e/nm^2 for HDPE and 47 e/nm^2 for PMMA).*

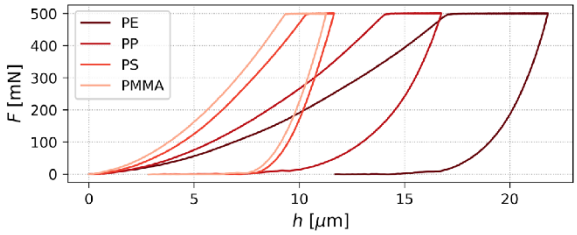

Micro and nanomechanical properties					
Sample	Microindentation			AFM-in-SEM	
	H_{IT} [MPa]	E_{IT} [GPa]	S [mN/nm]	S^0 [nN/nm]	S^{IRR} [nN/nm]
PE	49.92	1.988	0.249	47 ± 11	94 ± 36
PP	91.93	2.129	0.197	x	x
PS	202.34	3.625	0.225	x	x
PMMA	204.15	4.168	0.258	x	x

Figure 2: *Representative F-h curves of selected polymers (left) and table of selected micro and nanomechanical properties (right). The micro/nanomechanical properties are: indentation hardness (H_{IT}), indentation module (E_{IT}), indentation stiffness (S), minimal stiffness (stiffness of outside area) and maximal stiffness (stiffness of the hard crust).*

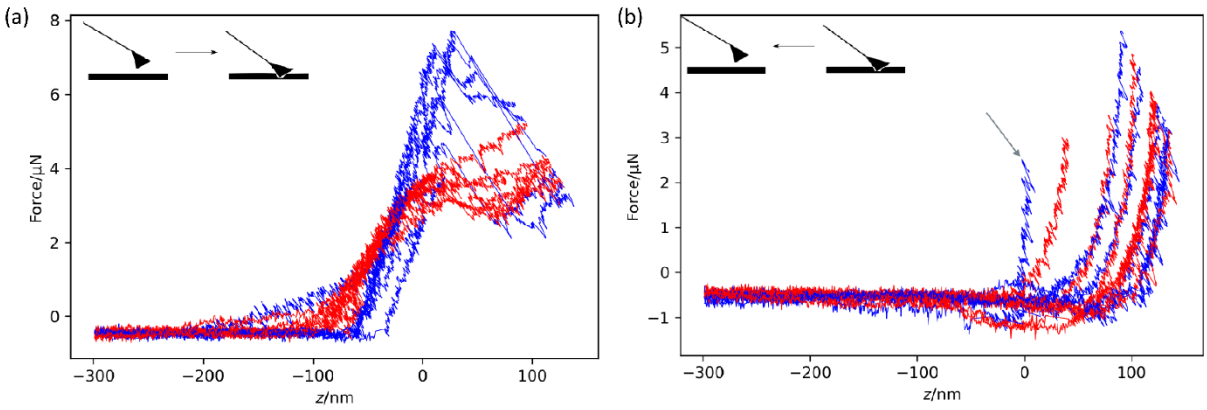

Figure 3: *F-z curves of HDPE sample showing the e-beam hardening effect: (a) approach curves (b) retract curves. Red lines = outside area, blue lines = area affected by e-beam irradiation. Approach curves (a) in the irradiated area indicate the presence of a thin hard crust (about 100 nm thick) that is breached by the probe. The retract curves (b) both inside and outside the area affected by the e-beam are similar as the crust has already been breached. The grey arrow in (b) indicates an anomalous curve, which probably corresponds to a probe that failed to breach the crust.*

Advancing Material Science: AFM-in-SEM for Battery Analysis

Dao R.[1], Hegrová V.[1], Schánilec V.[1], Novák L.[2], Zakopal P.[2], Neuman J.[1]

[1] NenoVision s.r.o., 612 00 Brno, CZ
[2] Fisher Scientific Brno s. r. o., 627 00 Brno, CZ

Email of the presenting author: vojtech.schanilec@nenovision.com

Introduction

In the ever-evolving landscape of materials science, the need for more comprehensive and complex analysis arises. For a better understanding of the complexity of studied materials, the combination of Atomic Force Microscopy (AFM) and Scanning Electron Microscopy (SEM) is often used, as the techniques based on individual microscopies provide necessary complementary information. The implementation of AFM LiteScope inside the SEM allows us to combine the benefits of both microscopies, as we are able to conduct measurements with all techniques in the same place under the same conditions without any need for sample transfer. We present how real in-situ measurements can be utilized in the analysis of battery materials, especially focusing on cathode active materials and the functional cathode itself.

Materials and Methods

The studied materials in this use case were cathode active material powder, which was analyzed both for determining the surface conductivity of the particles as well as the cross-sectional analysis of interparticle conductivity and the cross-sectional analysis of the functional cathode. The battery cathode was made from nickel cobalt aluminum (NCA) and nickel cobalt manganese (NCM) particles. All measurements were conducted without removing the sample from the SEM chamber. The LiteScope microscope was installed directly in the SEM chamber, allowing for subsequent analysis using all techniques. The SEM was used to localize the region of interest and to identify microscopic defects. Chemical analysis was performed using the Energy Dispersive X-ray Spectroscopy (EDS) extension of the SEM to distinguish between NCA and NCM particles. The final analysis was conducted by conductive AFM (C-AFM) to measure the local electrical properties of individual particles. Our AFM-in-SEM solution provide a combination of validated approaches in material science and battery analysis done previously on similar battery components [1-3].

Results

The results presented in our work show how easily we can provide complex information about battery materials with our AFM-in-SEM solution. By revealing the localized chemical and electrical properties, we are able to derive correlated information about failures in the battery structure. Additionally, we can easily analyze the changes in battery materials caused by usage, thereby providing a better understanding of the processes behind the decrease in lifespan and efficiency.

Conclusion

The need for understanding how materials function and what changes they undergo when used in applied sciences requires new methods of analysis. The pioneering AFM-in-SEM solution is one of the emergent techniques that can provide new insights into material behavior. By combining the strengths of separately accessible methods, we are providing another stepping stone, paving the way for researchers to achieve excellence in their field.

References:

[1] KEMPAIAH, Ravindra; VASUDEVAMURTHY, Gokul; SUBRAMANIAN, Arunkumar. Scanning probe microscopy based characterization of battery materials, interfaces, and processes. Nano Energy, 2019, 65: 103925.

[2] ZHANG, Zhenyu, et al. Characterizing batteries by in situ electrochemical atomic force microscopy: a critical review. Advanced Energy Materials, 2021, 11.38: 2101518.
[3] WALTHER, Felix, et al. The working principle of a Li2CO3/LiNbO3 coating on NCM for thiophosphate-based all-solid-state batteries. Chemistry of Materials, 2021, 33.6: 2110-2125.

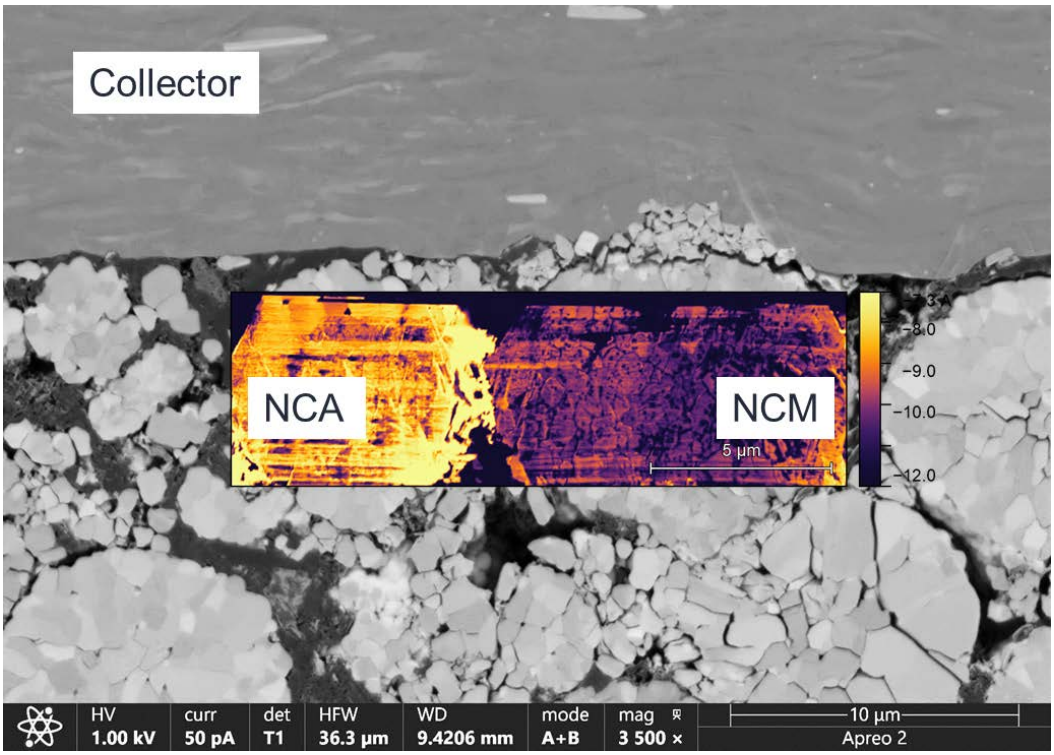

Fig. 1: Result of correlative analysis of cathode. Individual parts were identified by EDS chemical analysis. C-AFM was used to measure the local conductivity of the cathode particle.

3D printed exchangeable SPM tips: a tool for multipurpose correlative microscopy

Zezulka L.[1,2], Nováček Z.[1,2], Konečný M.[1,2], Matějka M.[3], Černý Š.[4], Spousta J.[1,2]

[1] University of Technology, Faculty of Mechanical Engineering, Institute of Physical Engineering, Brno 61669, Czech Republic
[2] Brno University of Technology, Central European Institute of Technology, Purkyňova 123, 61200 Brno, Czech Republic
[3] Institute of Scientific Instruments of the Czech Academy of Sciences, Královopolská 147, 61264 Brno, Czech Republic,
[4] IQS nano s.r.o., Hlavní 130, 25068, Husinec, Czech Republic

Email of the presenting author: lukas.zezulka@vutbr.cz

Introduction: The combined instrument of atomic force microscopy (AFM) and in situ scanning electron microscopy (SEM) allows for comprehensive sample analysis including imaging and spectroscopy and poses an ideal candidate for the introduction of in situ nanofabrication capabilities. We propose the adaption of a photonic crystal fibre (PCF) based scanning probe microscopy (SPM) probe to expand the instrument's capabilities. Namely, the correlated SEM, AFM, and scanning near-field optical microscopy (SNOM) image acquisition as well as the introduction of working media via the optical fibre capillaries, directing intense light near the tip, and establishing an electric potential difference between the sample and the tip (see Figure 1). Thus, making for a multipurpose tool for in situ characterisation, modification, and fabrication of nanostructures.

However, the inner capillary structure of the PCF poses a significant challenge for conventional wet etching-based tip fabrication. We overcome this challenge by mounting an exchangeable two-photon polymerisation (2PP) 3D printed tip onto the optical fibre making it a novel approach within the field of fixedly 2PP 3D printed SPM tips with various demonstrated applications including AFM [1], microfluidic AFM [2], and SNOM [3]. Here we show the developed exchangeable SPM tips and their proof-of-concept application in topography and cathodoluminescence (CL) image acquisition.

Materials and methods: The proposed multipurpose correlative microscopy, in principle depicted in Figure 1, was realised as a combination of LiteScope™ AFM in SEM solution for Correlative Probe and Electron Microscopy (CPEM™) from NenoVision s.r.o. and SEM TESCAN Vega2. For the fabrication of the exchangeable tips was employed direct laser writing system IQNANO3D (IQS nano s.r.o.) and 2PP resist OrmoComp®. Printouts were post-processed with 1:1 O_2+SF_6 etching using PlasmaPro 80 (Oxford Instruments) and metalized using magnetron sputtering (Leica Microsystems EM ACE 600). The tip mounting process was facilitated by custom-built micromanipulator setup with feedback via optical stereomicroscope.

Results and Conclusions: We successfully developed a self-tightening socket-based SPM tip mountable as an endpiece onto an optical fibre. This endpiece consists of two distinct parts: the socket, designed as a spring mountable onto the optical fibre, and the SPM tip itself, with a design adaptable to specific applications such as AFM, SNOM, working media delivery, or their combination in the proposed multipurpose tip (Figure 2a). These are fabricated using the 2PP 3D printing (Figure 2b, c). The application of a multipurpose hollow tip was successfully demonstrated with proof-of-concept topography and CL signal measurements (Figure 2d, e). However, the in situ acquisition of correlated images as well as the advanced functionalities remain the subject of ongoing development.

In summary, we have proposed a novel multipurpose correlative microscopy technique for SEM in situ characterisation, modification, and fabrication of nanostructures based on exchangeable 2PP 3D printed tips mountable onto photonic crystal fibre. The viability of the concept is proved by proof-of-concept CL and topography measurements, however correlative image acquisition and proposed advanced functionalities remain to be demonstrated.

References:

[1] Novotna V. et al.: Microscopy Today 28(2020), 38-46.
[2] Sun L. et al.: Nature Communications 11(2020). 5732.
[3] Kramer R. C. L et al.: Lab on a Chip 20(2020), 311-319.
[4] Jung B. J., H. J et al.: Optics Communications 286(2013), 197-203.

Acknowledgement: This work was supported by the Technology Agency of the Czech Republic (TACR FW03010504-INCHAR). We also acknowledge CzechNanoLab Research Infrastructure supported by MEYS CR (LM2023051). We also acknowledge the NenoVision s.r.o. for providing the LiteScope™ microscope. Furthermore, Brno Ph.D. Talent Scholarship – Funded by the Brno City Municipality is acknowledged.

Figures:

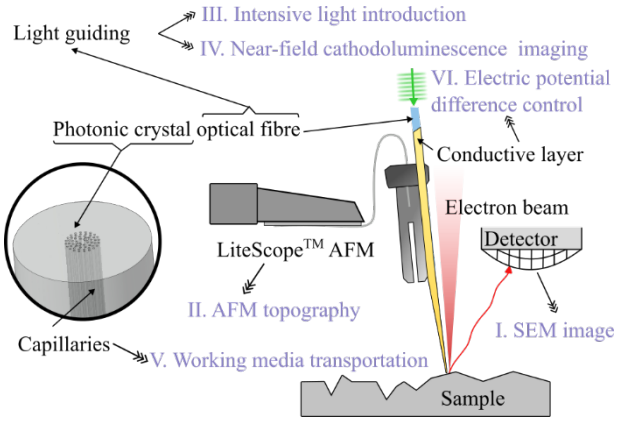

Fig. 1: Multipurpose SPM: *Illustration of the experimental setup with highlighted capabilities introduced by the multipurpose probe (III-VI) to the correlative SEM/SPM microscopy (I, II).*

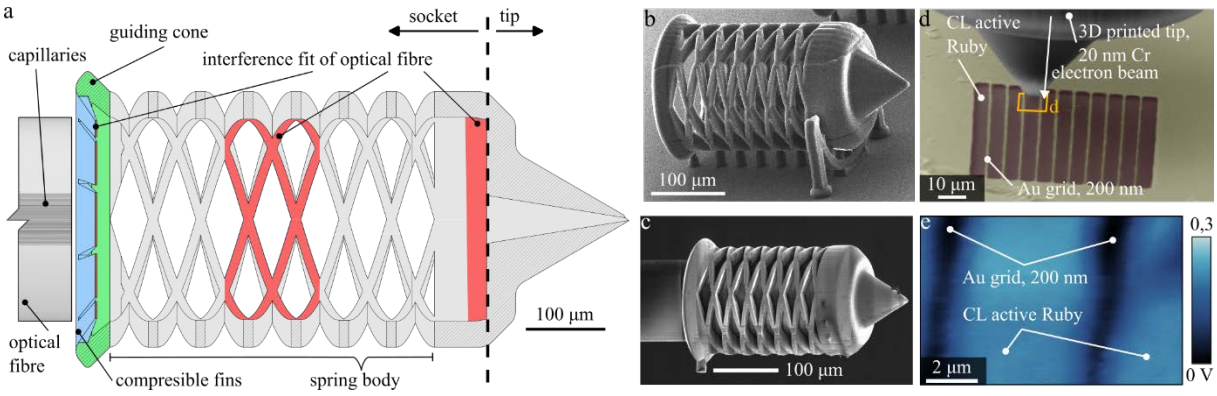

Fig. 2: Two-photon polymerisation 3D printed exchangeable SPM tip: ***(a)*** *Exchangeable tip design consisting of the socket section used for mounting on an optical fibre and tip section adjustable for the specific application (AFM, microfluidic AFM, SNOM, multipurpose tip).* ***(b, c)*** *SEM image of SPM tip 2PP 3D printed on a silicon wafer and mounted on an optical fibre, respectively.* ***(d)*** *Colourised SEM image of the tip during proof-of-concept measurement of a 200nm thick gold grid fabricated on CL active Ruby substrate with a constant tip to electron beam offset.* ***(e)*** *Acquired CL image with visible alternating stripes of gold and CL active Ruby.*

Enhanced Cathodoluminescence Decay in Garnet Scintillators via Defect Engineering

Lalinský O.[1], Rathaiah M. [2], Kučera M.[2]

[1] Institute of Scientific Instruments of the CAS, Královopolská 147, 612 64 Brno, Czech Republic
[2] Charles University, Faculty of Mathematics and Physics, 121 16 Prague, Czech Republic

Email of the presenting author: xodr@isibrno.cz

Recently, significant acceleration of cathodoluminescence (CL) decay has been achieved in garnet epitaxial films [1]. This was accomplished using a method known as "defect engineering," wherein partial substitution of trivalent ions in the dodecahedral position (Lu^{3+}, Gd^{3+}) with divalent ions (Mg^{2+}, Ca^{2+}) can lead to the stabilization of luminescent centers Ce^{3+} into the 4+ valence state [2, 3]. This raises the question of whether the reverse process is feasible: stabilizing already stable Ce^{4+} centers back into the 3+ valence state using tetravalent ions (Si^{4+}).

Samples were prepared via liquid phase epitaxy employing lead-free BaO-B_2O_3-BaF_2 flux [4]. Two series of cerium-activated lutetium aluminum garnet (LuAG:Ce) were grown, as depicted in Fig. 1. One series consisted of LuAG:Ce,Ca with a constant Ce content (6000 ppm = 0.6%, relative to the dodecahedral position), but with increasing Ca content up to 0.6%. The second series comprised LuAG:Ce,Ca,Si with constant Ce and Ca content (both 0.6%), but with increasing Si concentration up to a Si/Ca ratio of 1.

Cathodoluminescence (CL) was investigated using a specially adapted CL apparatus [5]. CL spectra, CL decays following pulsed e-beam excitation, thermoluminescence, and other CL characteristics were studied at various temperatures. These results, supported by optical absorption findings, will be presented at the conference.

In Fig. 1, the gradual loss of yellow coloration observed in the first series corresponds to the Ce^{3+} absorption transition. For sample 1LCa5, a significant portion (or all) of Ce^{3+} ions is stabilized in the Ce^{4+} valence state. In the second series, an increase in yellow coloration with rising Si/Ca concentration ratio can be observed. This phenomenon can be explained by the re-stabilization of Ce^{4+} centers into the 3+ valence state.

In conclusion, our research successfully stabilizes cerium centers in garnet films through defect engineering. By elucidating these mechanisms, our work contributes to optimizing garnet-based scintillators, advancing detection capabilities in fields from electron microscopy or medical imaging to high-energy physics.

References:

[1] Lalinský O. et al.: Phys Status Solidi A 216 (2019), 1801016.
[2] Liu S. et al. Phys. Status Solidi RRL 8 (2014), 105–109.
[3] Wu Y. et al.: Phys. Rev. Applied 2 (2014), 044009.
[4] Kučera M. et al.: J. Cryst. Growth 312 (2010) 1538–1545.
[5] Bok J. et al.: Rev. Sci. Instrum. 82 (2011) 113109.

Acknowledgement:

The research was supported by the Technology Agency of the Czech Republic (TN02000020); the infrastructure by the Czech Academy of Sciences (project RVO:68081731).

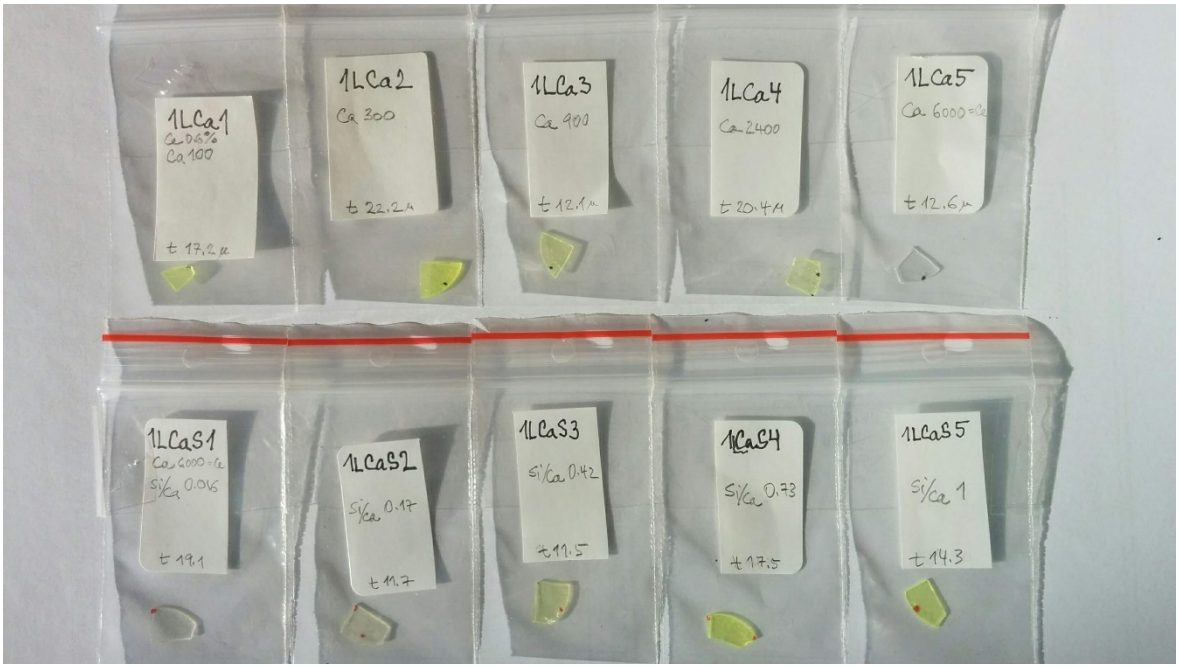

Fig. 1: Color demonstration of the LuAG:Ce,Ca (1LCa) and LuAG:Ce,Ca,Si (1LCaS) specimens. In the 1LCa, the Ca concentration (shown in ppm) grows from left to right; in the 1LCaS the Si/Ca concentration ratio grows from left to right.

Setting up an experiment for iterative ptychography using simulations

Jílek Z.[1]

[1] Institute of Scientific Instruments of CAS, Brno, Czech Republic

Email of the presenting author: jilek@isibrno.cz

With the increasing accessibility of fast pixelated detectors, there is a growing interest in novel 4D scanning transmission electron microscope (4D-STEM) imaging techniques, particularly ptychography, which will be explored in this work. Ptychography is a computational coherent diffraction imaging technique that can recover the transmission function of the sample together with the illumination probe. In 4D-STEM, ptychography uses a set of far-field diffraction patterns acquired with a small probe at different locations on a sample. Contrary to traditional techniques, ptychography recovers the transmission function of the sample at a higher resolution as its resolution is limited by the cut-off angle of the diffraction patterns and beam coherence rather than by the probe size [1]. Another significant advantage of ptychography is its high dose efficiency [2].

The main goal of this work is to optimise the parameters of SEM for ptychography reconstruction using microscopical simulations, which were performed using the Python library abTEM [3]. With this library, it is straightforward to simulate diffraction patterns for ptychography. The simulation was performed for an uncorrected SEM with a spherical aberration of third-order of 0.88 mm and a beam energy of 30 keV. It also covers the beam's temporal and spatial incoherence and finite electron dose. The number of pixels in the simulated diffraction pattern was 256x256 and the pixel pitch was 56 μm. The sample atomic model shown in Fig.1 consists of two graphene layers, which are slightly rotated with respect to each other, and on top of those layers are three carbon nanotubes. Simulations were conducted for a range of aperture angles, defocus values and camera lengths.

Simulated diffraction patterns were then processed with an extended ptychographical iterative engine (ePIE) algorithm [4]. The reconstructed transmission function converted to a phase image is shown in the Fig. 2 for increasing incoherence levels. There are shown only results with an aperture angle of 18 mrad, a defocus of 200 nm and a camera length of 120 mm, which were found to be optimal for high resolution (it is worth noting that the optimal probe for standard SEM applications would be close to an aperture angle of 12 mrad and a defocus of 40 nm with a d50 resolution of 0.4 nm). At this camera length, the first order diffraction disks are visible in the diffraction patterns and contribute to high resolution. Also at this aperture angle and defocus diffraction patterns are still appropriately sampled by the detector. In the figure, one can see how the incoherences worsen the phase image, but at a current of 50 pA and a dwell time of 1 ms, the reconstruction is still retaining small features in the image, especially the moire pattern - formed by two graphene layers - is still visible.

Suppose the preference is dose efficiency rather than high resolution. In that case, one may opt for a smaller aperture as lower-dose diffraction patterns contain scattering data only in a bright field (when the sample is weakly scattering). The diffraction cut-off at the bright field would then determine the attainable resolution, and the dose would be spent only on a smaller span of spatial frequencies, as in [2].

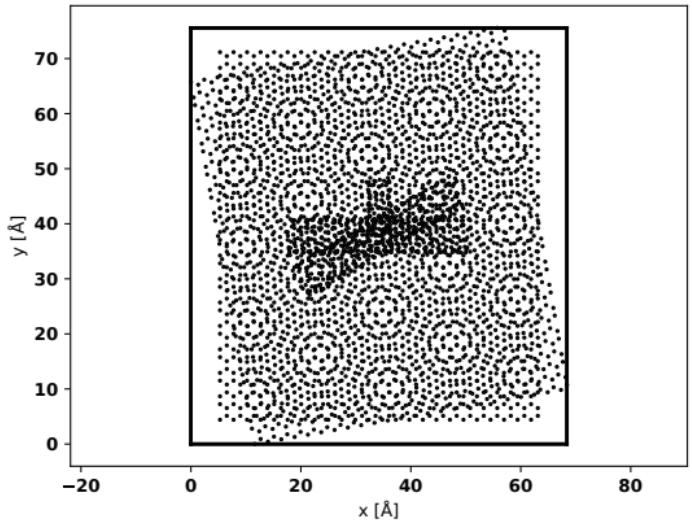

Fig. 1: Atomic model of the sample

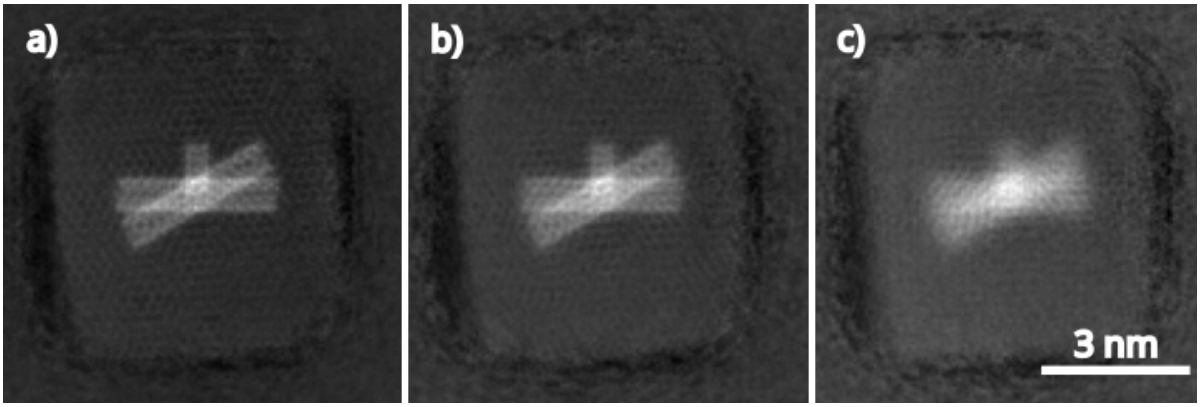

Fig. 2: Reconstructed phase of the sample using the ePIE. a) coherent case with a current of 50 pA and a dwell time of 1 ms b) incoherent case with a current of 50 pA and a dwell time of 1 ms c) incoherent case with a current of 400 pA and a dwell time of 0.125 ms

References:

[1] Chen, Z. et al.: Nature Communications 11 (2020)
[2] Zhou, L. et al.: Nature Communications 11 (2020)
[3] Madsen, J. et al.: Open Res Europe 1 (2021), p. 24
[4] Maiden, A. et al.: Ultramicroscopy 109 (2009), p. 1256-1262

Acknowledgement:

The author acknowledges funding from the Czech Science Foundation (project 21-13541S) and the Technology Agency of the Czech Republic (project TN02000020).

Second-harmonics generation microscopy for visualisation of collagen

Chorvat D.[1]

[1] International Laser Centre of SCSTI, Bratislava, Slovakia

Email of the presenting author: dusan.chorvat@cvtisr.sk

Collagen is the most abundant structural protein in mammals and it plays an important role in many physiological processes. The assessment of collagen morphology can provide important information about the examined tissue and it can be used as biomarker for several pathologies. In this regard, second-harmonic generation (SHG) microscopy is becoming increasingly popular method of high-resolution label-free approach for non-invasively detecting collagen organization. Previously we used SHG microscopy to visualize structural and functional changes in rat aorta accompanying cardiovascular disease development [1] and tested the applicability of newly synthesized organic dyes with nonlinear optical properties to enhance SHG signals and two-photon fluorescence from collagen structures of rat aorta [2].

In this study, we imaged samples of equine pericardium (EP), a standardized collagen scaffold used in tissue engineering applications, with inverted microscope Axiovert 200M with confocal laser scanning head LSM 510 Meta NLO. The microscope was utilized with two femtosecond oscillators with different parameters (1040 nm vs 780 nm wavelength). SHG images recorded from EP were analyzed using two different algorithms: gray-level co-occurrence matrix (GLCM), a method widely used for texture analysis, and curvelet transform (CT-FIRE) as an alternative to Fourier transform approach [3]. By examining SHG images of collagen by GLCM approach we targeted information about periodical structures in the image, as well as changes of regularity of a fibrillar structure. CT-FIRE approach was used for evaluating the average width of collagen fibers. Overall our experiment demonstrates that SHG microscopy combined with advanced image processing algorithms represents a powerful diagnostic tool for characterization of various parameters of collagen structure at supramolecular to tissue levels.

References:

[1] M. Uherek, et al., Laser Physics 26 (2016), 105606
[2] A. Čibová, et al., Dyes and Pigments 149 (2018), 597–611
[3] R. Cicchi, et al., Journal of Biophotonics, submitted manuscript

Acknowledgement:

Supported by LASERLAB-EUROPE (grant agreement no. 871124, European Union's Horizon 2020 research and innovation programme)

Prototype of cryo assembly for FIB-SEM HELIOS G4

Laznicka T.[1], Krutil V.[1],. Brauner T.[1,2], Hanzelka P.[1], Urban P.[1], Hrubanova K.[1], Krzyzanek V.[1]

[1] Institute of Scientific Instruments, The Czech Academy of Sciences, v.v.i., Kralovopolska 147, 612 00 Brno, Czech Republic
[2] Faculty of Mechanical Engineering, Brno University of Technology, Technicka 2896/2, 616 69 Brno, Czech Republic

Email of the presenting author: lazna@isibrno.cz

Microscopy is increasingly favouring the use of advanced technologies for detailed analysis of biological samples [1]. In this respect, the scanning electron microscope (SEM) equipped with a focused ion beam (FIB-SEM) plays an important role, allowing high-resolution and detailed imaging of structures. One of the critical factors for the practical analysis of biological samples is maintaining their stability and integrity during observation. This paper presents a newly developed functional setup for sample cooling that has been tested in the FIB-SEM HELIOS G4 (Thermo Fisher Scientific).

The setup was designed to allow the cooling of mainly biological samples in the SEM and their subsequent analysis using other techniques. The key components of this assembly are a Dewar vessel with a connected conductive finger and a table with an anti-contamination shield. The Dewar vessel serves as a reservoir for liquid nitrogen, the primary refrigeration source for the cooling system [2]. The conductive finger connects the Dewar vessel to the microscope chamber, dissipating excess heat from the stage into the liquid nitrogen reservoir. The stage with the anti-contamination shield is connected to the conductive finger by flexible cooling braids, allowing movement in all three axes, tilt and rotation of the stage with the sample.

The assembly also includes temperature sensors located in the Dewar vessel and on the table, allowing stable temperature conditions to be monitored and maintained during sample analysis. In addition, the table is equipped with a heating element to help maintain a constant temperature and the possibility to raise temperature to further sublimation of the sample surface. The theoretical value of the temperature that the assembly is able to reach is 130 K. Experimentally, a temperature of 142 K was reached on the surface of the table, confirming the efficiency of the cooling system.

This work resulted in the development of a functional and reliable device for cooling biological samples in the FIB-SEM HELIOS G4. This setup represents an important tool for scientific research, particularly in the field of biology, and allows the study of structures at the microscopic level while maintaining their integrity and stability.

References:

[1] Dykstra, M. J., et al.: Biological Electron Microscopy: Theory, Techniques and Troubleshooting, 2011
[2] Brauner T., et al.: in Microscopy 2023

Acknowledgement: The research was supported by the Czech Science Foundation (GA23-07962S), the Technology Agency of the Czech Republic (TN02000020) and the Czech-BioImaging large RI project (LM2023050 funded by MEYS CR).

The influence of supporting films on LVEM micrograph quality

Bačovský J.[1], Hrabalová V.[1], Štěpán P.[1], Mrázová K.[2], Hrubanová K.[2]

[1] Delong Instruments, Brno, Czech Republic
[2] Institute of Scientific Instruments of the Czech Academy of Sciences, Brno, Czech Republic

Email of the presenting author: jaromir.bacovsky@delong.cz

Introduction:

The spatial resolution is often considered to be the determinative parameter of electron microscopy imaging. However, the evaluation of micrograph quality is inherently more complex and must be based on a combination of spatial resolution and image contrast. The most natural way to increase and thus achieve a sufficient level of contrast is to reduce the energy of the electron beam. Although this approach allows us to deal with the lack of contrast typical for conventional microscopy, it requires careful consideration of sample preparation methods. Especially some routines in sample preparation can negatively affect the quality of imaging because once the issue of lack of contrast is solved by sufficient scattering in the sample, the same physical phenomena cause the increased sensitivity of image quality on the thickness of the sample. One of these persistent stereotypes is the redundant usage of supporting film beneath biological sections or the use of excessively thick films when imaging nanoparticles.

Materials and methods:

This study explores the impact of various commonly used supporting films on micrograph quality and investigates how these supporting films affect imaging results. Imaging ultrathin section of *Candida tropicalis*, we assessed the level of detail imaging achieved with a low-voltage transmission electron microscope LVEM 25E, using both TEM at 25 keV and STEM at 10 keV and 15 keV. The effect of supporting films on spatial resolution are further analyzed by LVEM 5 [1] in TEM mode at approximately 5 keV using standard carbon nanotube sample in accordance with the main application areas of these instruments.

Results:

While low-voltage transmission electron microscopy offers excellent image contrast, it is more susceptible to chromatic aberration compared to conventional transmission electron microscopy. This sensitivity becomes particularly relevant when thicker samples cause a significant broadening of the energy spectra of the primary electron beam. As a result, proper sample preparation—avoiding unnecessary extra layers—is crucial to achieve optimal imaging quality in TEM mode. The collection of investigated supporting layers with different mechanical properties includes formvar, carbon film of various thicknesses (10 nm, 15-25 nm) and novel LUXfilm. We also discussed the results from scanning modes designed to address the challenge of blurry TEM images caused by excessively thick samples. We also examined the related issue of sample contamination and differences in volume information through the transmission and SEM modes.

Conclusion:

Our results highlight the need for optimal sample preparation, demonstrating that redundant or overly thick supporting films can significantly degrade image quality, and, on the other hand, the optimized sample preparation provides extraordinary image clarity. We also demonstrated the benefits of complex LVEM solution providing the STEM modes to deal with additional chromatic aberration contribution given by the broadening of energy spectra.

References:

[1] Delong A. et al.: Electron Microscopy vol. 1 (1992), 79-82.

Acknowledgement:

Sample preparation was provided by CF ISI EM which is supported by the Czech-BioImaging large RI project (LM2023050 funded by MEYS CR).

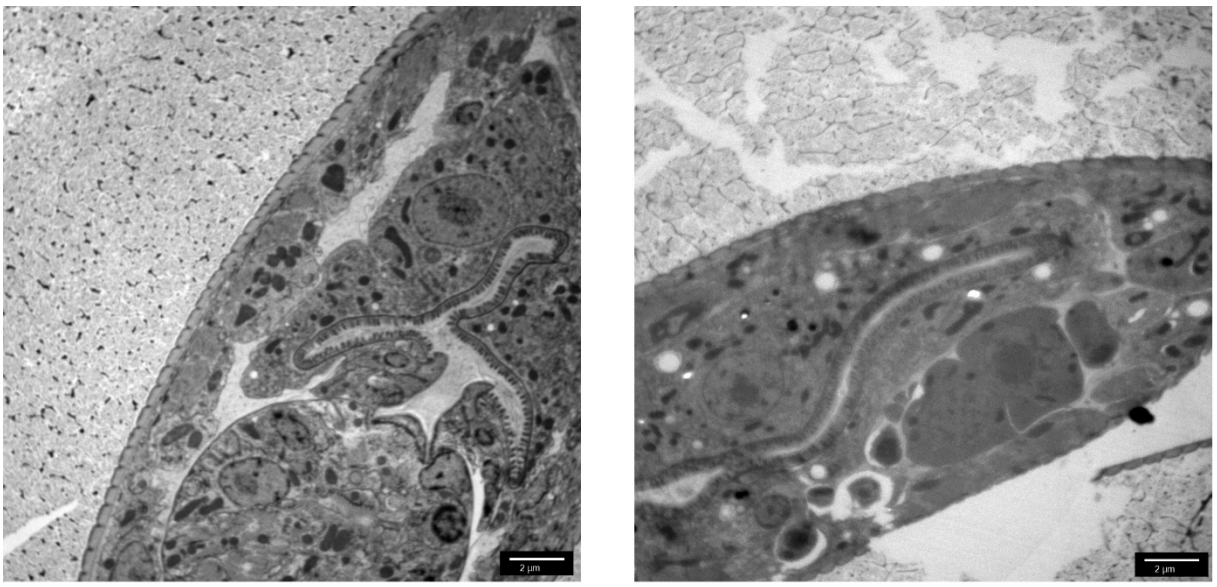

Fig. 1: Ultrathin section on the grid without supporting film (left); ultrathin section on formvar (right). LVEM 25E, TEM at 25 keV.

Looking inside a complex biological condensate - the structure of avian reovirus replication factories

Durinova E.[1,2], Bily T.[1,2], Kitzberger F.[1,2], Franta Z.[1], Mojzes P.[3], Chlanda P.[4], Tuma R.[1]

[1] Faculty of Science, University of South Bohemia in České Budějovice, Czech Republic
[2] Biology Centre, Czech Academy of Sciences in České Budějovice, Czech Republic
[3] Faculty of Mathematics and Physics, Charles University, Ke Karlovu 5, Prague 2, Czech Republic
[4] Department of Infectious Diseases, Virology, Heidelberg University Hospital, Heidelberg, Germany

Email of the presenting author: evadurinova12@gmail.com

Avian reovirus (ARV) belongs to *Reoviridae* family with segmented dsRNA genomes. ARV is responsible for significant economic losses to the poultry industry by causing tenosynovitis and chronic respiratory disease in chicken. ARV virion exhibits an outer protein shell enclosing an inner core which contains 10 unique dsRNA segments and multiple copies of viral polymerase. ARV assembly takes place in so-called viroplasms or viral factories (VF). They are cytoplasmic membrane-less inclusions which accumulate viral proteins and RNA, and assist capsid assembly, genome packaging and replication. VFs also provide protection from the host cell defense mechanisms by sequestering viral RNA. Given the dense nature of VFs, little is known about ARV assembly and packaging intermediates. Using previously developed host cell lines and imaging techniques [1-2] we demonstrate that ARV VFs are inhomogeneous biological condensates in which the inner, fluid phase is surrounded by densely packed virion arrays. The inner phase concentrates viral non-structural proteins and assists assembly of viral cores. The larger, RNA-filled and double-layered particles are excluded and emanate from the inner fluid phase at the periphery. This suggests that ARV VFs are functionally compartmentalized: the inner fluid phase assists RNA assortment and core particle assembly while the peripheral phase is the site of RNA replication inside viral cores and virion completion.

References:

[1] Durinova et al. (2023) Shedding light on reovirus assembly-Multimodal imaging of viral factories. Adv Virus Res 116, 173-213.
[2] Zimmermann & Chlanda (2023) Cryo-electron tomography of viral infection—from applications to biosafety. Curr. Op. Virology 61, 101338.

Acknowledgement:

The project was supported by MEYS CR (LM2023050 Czech-BioImaging and OP VVV CZ.02.1.01/0.0/0.0/18_046/0016045) and the Czech Science Foundation GACR 22-25396S.

Application of Raman microspectroscopy for the detection and identification of organic matter and mineral structures of the bone tissue and eggshells of extinct organisms

Jurašeková Z.[1], Fabriciová, G.[1], Kundrát M.[2]

[1] Department of Biophysics, Faculty of Science, P. J. Šafárik University, Jesenná 5, 040 01 Košice, Slovakia
[2] Center for Interdisciplinary Biosciences, Technology and Innovation Park, P. J. Šafárik University, Jesenná 5, 040 01 Košice, Slovakia

Email of the presenting author: zuzana.jurasekova@upjs.sk

Raman microspectroscopy (RMS; micro-Raman) is a non-destructive and non-contact analytical technique that combines microscopy and spectroscopy, thus providing a potential for non-invasive and *in situ* molecular identification even over heterogeneous and rare samples such as fossilized tissues. Recently, chemical imaging techniques have become an increasingly popular tool for characterizing trace elements, isotopic information, and organic markers in fossils. RMS also shows a growing potential for understanding bone microstructure, chemical composition, and mineral assemblance affected by diagenetic processes. Thus, RMS is a valuable and promising analytical tool in molecular paleontology.

In the present study, we have investigated a wide range of different fossil tissue samples, mainly Mesozoic vertebrates (from Jurassic through Cretaceous), in order to map organic composition and understand the diagenetic alterations undergone. Generally, we are focused on understanding the taphonomic selectivity in the long-term preservation of fossil biomolecules (i.e., organic residues) as well as in the mineral replication of soft tissues due to different climatic and ecological factors. We recorded and discussed in detail the characteristic Raman bands of both modern and diagenetically altered bone tissues [1]. Besides standard spectra of sedimentary rocks, including pigment contamination, the Raman spectra also exhibit interesting spectral features in the 1200-1800 cm-1 spectral zone, where Raman bands of proteins, nucleic acids, and other organic molecules can be identified. We discuss both a possible origin of the observed bands and difficulties with the definition of the specific spectral markers in fossilized soft and hard tissues. Consequently, we have used them to predict the preservation state of sub-fossilized and fully-fossilized bones.

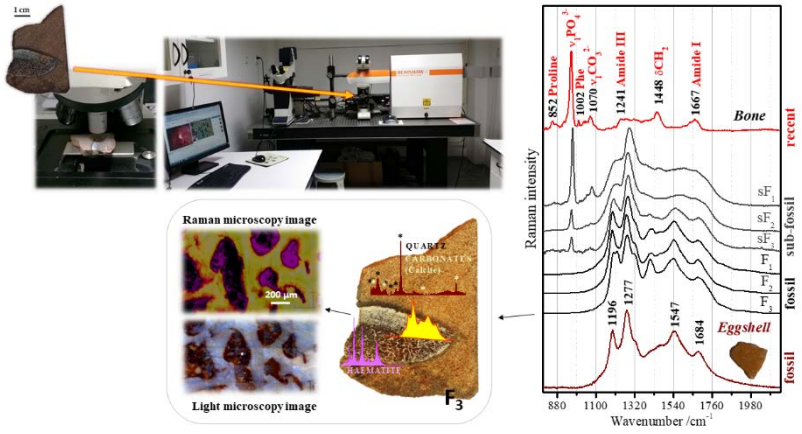

Fig. 1: Micro-Raman analysis of the recent, sub-fossil and fossil bone and eggshell samples

References:

[1] Jurašeková, Z. et al. International Journal of Molecular Science 23(18) (2022) 10689.

Acknowledgement:

The authors acknowledge funding from APVV-21-0319 and VEGA 1/0075/22 projects.

Morphological and functional properties of neuronal SH-SY5Y cells: implication for Wolfram Syndrome

Adnan M.[1], Novotová M.[1], Cagalinec M.[1]

[1] Dept. of Cellular Cardiology, Institute of Experimental Endocrinology, Biomedical Research Center, Slovak Academy of Sciences, Bratislava, Slovakia

Email of the presenting author: mohd.adnan@savba.sk

Introduction: Wolfram syndrome (WS) is a rare disorder characterized by diabetes mellitus, diabetes insipidus, optical atrophy and deafness. Although originally classified as mitochondrial disease, later it became clear the mutations of the Wolframin 1 protein (Wfs1), located in the membrane of the endoplasmic reticulum (ER) are responsible for WS [1]. Wfs1 is highly expressed in the brain and pancreas. In neurons, it has been shown that Wfs1 regulates ER stress, calcium signalling and mitochondrial metabolism [2]. To study complete knock-out of Wfs1, neuronal SH-SY5Y cell line represents suitable model of neuronal complications in WS. Therefore, the aim of this study was to optimize sample preparation protocols for transmission electron microscopy (TEM) and for calcium entry and release using fluorescence laser scanning confocal microscopy in control SH-SY5Y cells.

Materials and methods: For TEM sample preparation, the protocol described before [3] was applied with modifications described in the results. To analyze cytoplasmic calcium dynamics, cells were loaded with the fluorescent calcium indicator Fluo-3/AM at a concentration of 2.5 µmol/l at room temperature for 40 min. The cells were then washed with HBSS (138 mM NaCl; 5.3 mM KCl; 0.34 mM Na_2HPO_4; 0.44 mM KH_2PO_4; 4.17 mM $NaHCO_3$; 4 mM $MgCl_2$, pH = 7.4). Fluo-3 fluorescence (ex/em 488/505-560 nm) was recorded by Leica SP2 AOBS inverted confocal microscope equipped with a 63×/1.4 NA objective. For calcium entry experiments [4], cells were first perfused with HBSS for one minute, then with HBSS with added KCl of 90 mM+5 mM $CaCl_2$ for 2 min, and then returned to HBSS for 2 min (Fig. 2). For calcium release experiments [4], cells were perfused first with HBSS for 2 min, then with HBSS containing thapsigargin (TG) for 6 min followed by perfusion with HBSS containing TG+$CaCl_2$ in concentrations described in the results for 2 min. Images were taken every 3 s. Acquired data were processed in Figi image analysis software. Here, from the image stack, 8 to 10 cells were chosen, the signal at the cell nucleus was omitted and cell cytoplasm was marked as a region of interest. Time plots of the fluorescence intensity from the individual cells were then visualized in MS Excel.

Results: For the TEM, we had to obtain a sufficiently large pellet of the cells (roughly 0.5 mm^3), therefore growing the cells in various volumes was tested first and the T75 flask was optimal. Second, the time for trypsin digestion is an important step in the procedure, where we have found 30 s as the optimal time. Third, the gentle centrifugation was tested, here 100 g RPM was sufficient to keep the pellet intact. After finishing the steps, we obtained images with sufficient contrast (Fig. 1). For the Fluo-3 fluorescence imaging, we first tested the laser intensity, where 80% was optimal to minimize the bleaching. For the calcium release experiments, we tested two options: 1µM TG+2mM $CaCl_2$ and 2µM TG+5mM $CaCl_2$ where both options provided sufficient fluorescence signal (Fig. 3).

Conclusion: With the experimental protocols optimized as described above we were able to visualize in high contract membrane structures of the SH-SY5Y cells. For the calcium dynamics we optimized measuring of response to plasma membrane depolarization and ER calcium release. With these protocols we plan to reveal changes in morphology and calcium signalling in Wfs1 knock-out SH-SY5Y cells.

References:

[1] Fonseca S.G. et al.: J Biol Chem 280(47) (2005), 39609-15.
[2] Cagalinec M. et al.: PLoS Biology 14(7) (2016), e1002511.
[3] Novotova M. et al.: Sci Rep 10(1) (2020) 8076.
[4] Pascual-Caro C. et al.: J Mol Med (Berl) 6(10) (2018), 1061-79.

Acknowledgement: The authors acknowledge funding from APVV-21-0473 project.

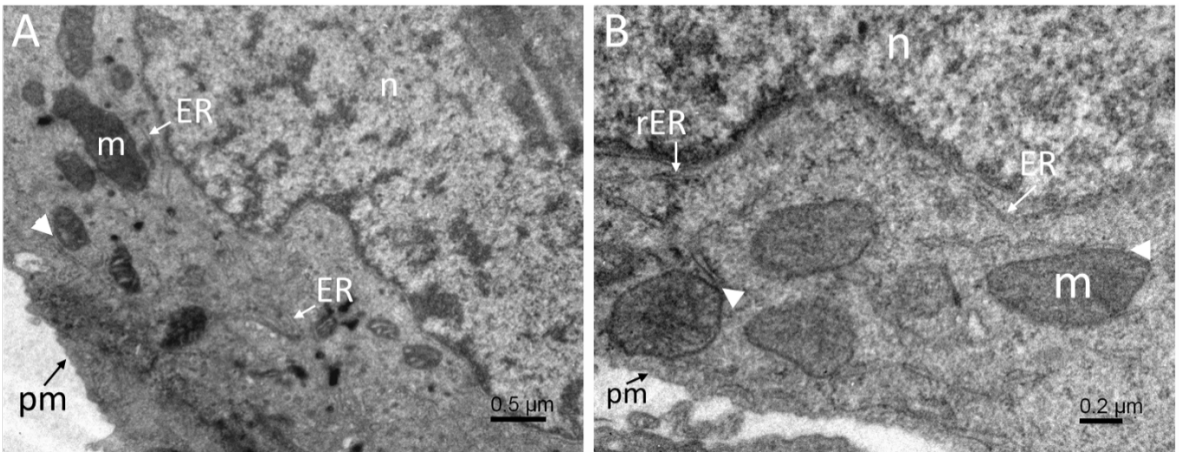

Fig. 1: Transmission electron microscopy visualization of SH-SY5Y cells at 20- (A) and 40,000x magnification. n – nucleus, m – mitochondria, ER – endoplasmic reticulum, rER – rough ER, pm – plasma membrane. Arrowheads depict ER-mitochondria contacts.

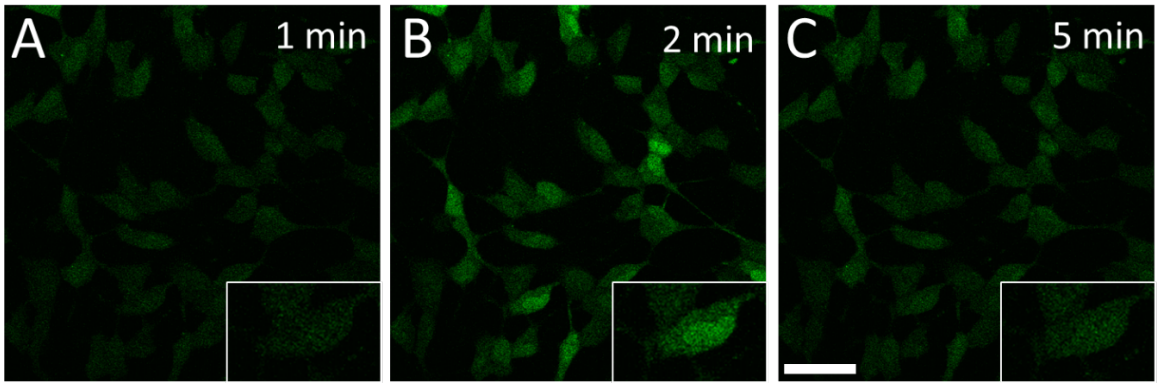

SH-SY5Y cells stained with the fluorescent indicator Fluo-3 under control condition (A), after depolarization with KCl+ $CaCl_2$ (B) and after return to control conditions (C). Bottom right: detail of a single representative cell. Bar: 10 µm.

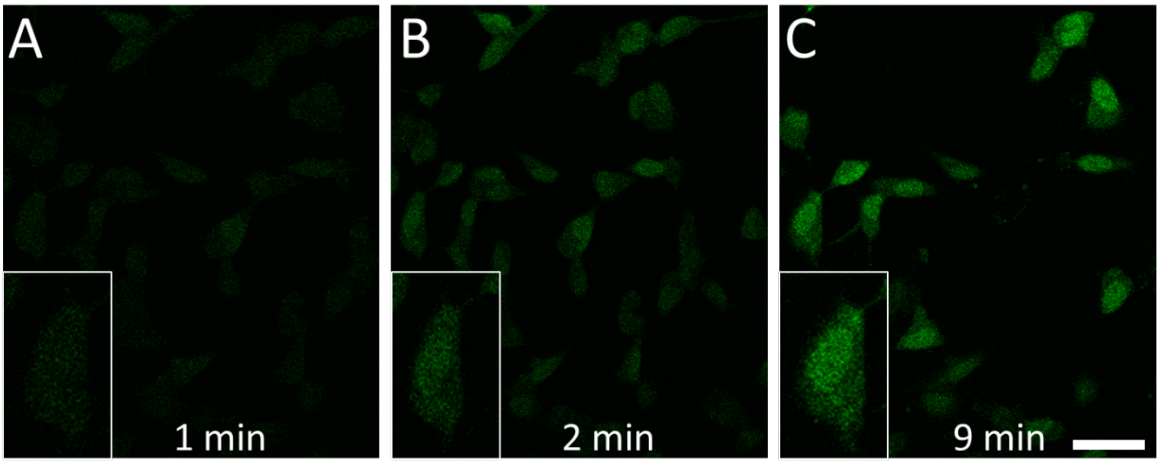

SH-SY5Y cells stained with the fluorescent indicator Fluo-3 under control condition (A), after application of 2 µM thapsigargin (B) and after application of 2 µM thapsigargin + 5 mM $CaCl_2$ (C). Bottom left: detail of a single representative cell. Bar: 10 µm.

Effect of mitochondrial ATP dependent potassium channels in cellular model of neurodegeneration

Pokusa M.[1] , Rovňaníková R.[2], Dibdiaková K.[2], Péčová R.[2], Račay P.[3], Evinová A.[1]

[1] Biomedical Centre Martin, Jessenius Faculty of Medicine, Comenius University in Bratislava, Slovakia
[2] Department of Pathophysiology, Jessenius Faculty of Medicine, Comenius University in Bratislava, Slovakia
[3] Department of Medical Biochemistry, Jessenius Faculty of Medicine, Comenius University in Bratislava, Slovakia

Email of the presenting author: michal.pokusa@uniba.sk

Introduction

Modulation of ATP-sensitive potassium channels (KATP) shows increasing potential in managing of neurodegeneration. Majority of already obtained data about KATPs effects are related to treatment by their well-known modulators- glibenclamid (blocker of surface and mitochondrial KATPs) and diazoxide (specific agonist of mitochondrial KATPs). Distribution of KATP channels throughout the intracellular membranes is therefore a factor, which needs to be investigated. In order to judgment of distinct roles of especially mitochondrial KATPs, their selective modulators of KATP (diazoxide, 5-hydroxy decanoate) could be involved in experimental procedures beside the non-selective modulators (pinacidil, glibenclamide).

Methods

In our experiments, we worked with human SH-SY5Y neuroblastoma cells ordinary used in research of Parkinson´s disease. The process of neurodegeneration is ordinary induced by the toxic effect of rotenone, as an inhibitor of mitochondrial respiratory complex I. Effect of KATPs located in mitochondria was explored by their specific vs non-specific modulators, to which cells were exposed for 24 hours. The functional impacts on cellular physiology were analyzed by quantification of intracellular calcium located separately in and out of mitochondria using fluorescent confocal microscopy. Beside the basal calcium concentrations, attention was devoted also to immediate calcium increase response to excitation of cells in described experimental condition. For this purpose, calcium imaging in real time was employed.

Results

Calcium plays an indispensable role as a second messenger of gene expression regulation, effector of exocytosis as well as regulation of apoptosis onset. Our results indicate that selective modulation of mitochondrial KATPs using their agonist diazoxide and 5-hydroxydecanoate as an antagonist modulate calcium homeostasis inside the cell in different manner as was observed after use of non-selective KATP modulators (pinacidil and glibenclamide). Specific features of selective mitochondrial KATPs modulation is evident after comparison of calcium changes in control and pathological conditions as well.

Conclusion:

In vitro experiments brought evidence about significant difference between effects mediated by mitochondrial and cytoplasmic membrane KATP in control condition as well as after initialization of neurodegeneration. Except that, we confirmed lowered concentration of calcium inside the mitochondria, when compared to cytoplasm in control conditions. According to our results, shifts in mitochondrial vs cytoplasm signal ratio of calcium is modified according to chosen treatment. This observation could serve as a platform for establishment of a novel procedure for evaluation of apoptosis risk in future experimental science.

Acknowledgement:

Supported by VEGA-1/0085/24 and VEGA 1/0183/23

Solutions for preparation and visualization of vitrified biological samples at IMG Electron Microscopy Core Facility

Pinkas D.[1], Vlcak E.[1], Raabova H.[1], Filimonenko V.[1,2]

[1] Electron microscopy core facility, Institute of molecular genetics, Prague, Czechia
[2] Laboratory of Biology of the Cell Nucleus, Institute of molecular genetics, Prague, Czechia

Email of the presenting author: Dominik.pinkas@img.cas.cz

Continual advancement in a broad range of interconnected cryo-electron microscopy pipelines has made the preservation and subsequent visualization of sensitive biological samples in close-to-native state more reliable and convenient than ever before. Cryo-electron microscopy has therefore, become the new standard for dependable analysis of biological objects. Our facility has been continually updating the cryo-workflows to stay up-to-date with these advancements and to provide professional solutions for current scientific demands.

A 200 kV Jeol JEM-F200 transmission electron microscope with cryo polepiece, cold field emission electron gun, sensitive 4k CMOS camera TVIPS XF-416, and phase plate provides optimal configuration for a broad range of cryoTEM applications. The latter include observation of morphology of small objects sensitive to dehydration, such as e.g. small organisms or DNA origami, quality check of purified protein samples prior to SPA analysis, collection of diffraction patterns of frozen protein crystals, and cryo-electron tomography of subcellular structures.

The whole workflow of cryo-TEM tomography of frozen hydrated lamellae is currently available at the core facility due to the running collaborative project with TESCAN Company. The optimized on-grid workflow includes plunge freezing with Leica EM GP2, quality check in Leica THUNDER cryo-CLEM, mounting and transfer of sample to TESCAN Amber Cryo FIB-SEM for lamella fabrication, and final transfer of lamella into cryoTEM for tilt series acquisition. Larger samples vitrified using high-pressure freezing in Leica EM ICE HPF machine with light-stimulation module can also be imaged in frozen hydrated state after cryo FIB lift-out procedure or alternatively processed to resin blocks upon freeze-substitution in Leica EM AFS2 machines. Successful observations and volume reconstructions of subcellular structures of C. elegans, S. cerevisiae, Chlamydomonas, Chlorella, and HeLa cells were performed using the workflow. Several other skill-demanding workflows utilizing sample vitrification, such as freeze-fracture replica immunolabeling using multi-purpose sputter coater Leica EM ACE900, cryo-CLEM imaging with reliable correlation of images from both modalities, or cryo-sectioning followed by immunolabeling after Tokuyasu are established at the core facility.

The EM CF, being a part of large imaging infrastructures Czech-BioImaging and Euro-BioImaging, provides open access to all described technologies with professional support on all steps of the user project.

Acknowledgement:

Electron Microscopy Core Facility, IMG ASCR, Prague, CR, is supported by MEYS CR (LM2023050 Czech-BioImaging),OP RDE (CZ.02.1.01/0.0/0.0/18_046/0016045, CZ.02.1.01/0.0/0.0/16_013/0001775) and IMG grant (RVO: 68378050).

Comparison of various versions of Imaris software for creating 3D models of insect tissues from microCT images

Podlahová Š.[1,2], Krejčová G.[1], Bajgar A.[1,2], Sehadová H.[1,2]

[1] Faculty of Science, University of South Bohemia, Ceske Budejovice, Czech Republic
[2] Biology Centre of the Czech Academy of Sciences, Institute of Entomology, Ceske Budejovice, Czech Republic

Email of the presenting author: sarka.podlahova@entu.cas.cz

Micro-computed tomography (microCT), a technology based on X-ray imaging, is a non-invasive method that enables high-resolution three-dimensional (3D) visualisation and characterisation of small biological objects. MicroCT can be applied to morphological and anatomical studies of insects[1,2]. The advantage of microCT imaging is that it allows detailed in situ projection of internal structures, organs or exoskeletons without destroying the specimen. However, the high resolution comes with a large amount of digital data and requires powerful analysis software such as Imaris (Bitplane AG, Oxford Instruments, UK). Here we compare the advantages of the Surface module for segmentation and surface rendering in three different versions of Imaris software (Imaris 9.3, Imaris 10.0 and Imaris 10.1). Our research on the caterpillars of Lepidoptera shows that Imaris 9.3 is excellent at creating semi-transparent surfaces with adjustable transparency, while the latest Imaris 10.1 does not allow this. On the other hand, Imaris 10.1 uses Machine learning segmentation based on Artificial Intelligence (AI), which makes surface creation much faster and easier. The combination of Imaris 9.3 and Imaris 10.1 provides suitable tools for 3D models of biological objects.

References:

[1] Schoborg, T.A.: J. Vis. Exp. 163, e61515(2020), 17 p.
[2] Smith, D. B. et al.: Scientific Reports 6, 21768 (2016), 10 p.

Acknowledgement:

The work was supported by Biology Centre CAS, Institute of Entomology (RVO 60077344).

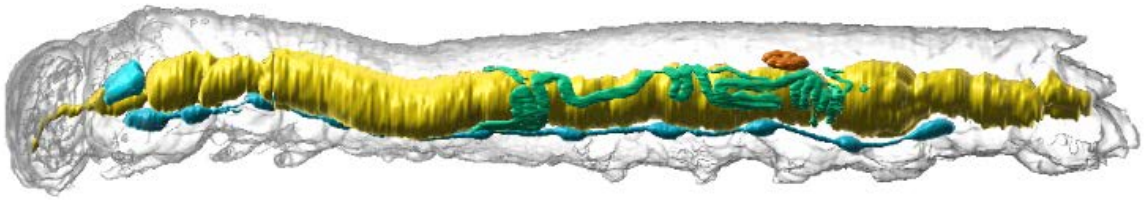

Fig. 1: 3D model of a Smerinthus ocellatus L2 instar larva with internal tissues created in Imaris software (Bitplane AG, Oxford Instruments, UK)

Interactome and forces guiding barrier transmigration of Lyme disease Borrelia

Strnad M.[1,2], Kopecká J.[1], Týč J.[1], Kitzberger F.[1], Hain L.[3], Oh YJ.[3], Hejduk L.[2], Rathner A.[4], Rego R.[1,2], Vancová M.[1,2]

[1] Biology Centre ASCR, v.v.i., Branisovska 31, 370 05 Ceske Budejovice, Czech Republic
[2] Faculty of Science, University of South Bohemia, Branisovska 31, 370 05 Ceske Budejovice, Czech Republic
[3] Institute of Biophysics, Johannes Kepler University Linz, Linz, Austria
[4] Institute of Biochemistry, Johannes Kepler University Linz, Linz, Austria

Email of the presenting author: martin.strnad.cze@gmail.com

Systemic dissemination of microbial pathogens permits pathogens to spread from the initial site of infection to target tissues. A key step in dissemination is transmigration from vasculature into extravascular tissues and further across various mechanical barriers before reaching the target tissues, which is mediated by surface adhesion proteins. *B. burgdorferi* is a bacterial pathogen and the causative agent of Lyme disease in humans. After tick transmission, the spirochetes need to escape from the high immune pressure in the blood stream and traverse through the endothelial cell lining into extravascular tissues. On its way, *B. burgdorferi* is able to squeeze through dense, gel-like matrices and cellular junctions with pore sizes much smaller than the diameter of their body. Using atomic force microscopy-based single-molecule force spectroscopy, we have shown that this is achieved by forming transiently stable interactions with several protein components of the extracellular matrix. We have observed that a subset of borrelial surface proteins, particularly Decorin binding protein DbpA/B, can enhance the translational movement of spirochetes in the extracellular matrix of the host. Using nuclear magnetic resonance, we study in-detail the specific interactions of DbpA/B with GAG molecules present in the extracellular matrix of the host. To complement the mechanical studies of borrelial migration, we visualize *in-vitro* the transmigration of *Borrelia* through endothelial cells using advanced electron microscopy techniques such as serial block-face electron microscopy.

Acknowledgement:
We acknowledge the GACR projects (22-18647K; 23-06525J) and BC CAS core facility LEM supported by MEYS CR (LM2023050 Czech-BioImaging and OP VVV CZ.02.1.01/0.0/0.0/18_046/0016045).

Directionality of two-photon absorption by fluorescent proteins

Myšková J. [1], Brynda J. [2], Khoroshyy P. [1,2], Lazar J. [1]

[1] First Faculty of Medicine, Charles University, Prague, Czech Republic
[2] Inst. of Organic Chemistry and Biochemistry CAS, Prague, Czech Republic

Email of the presenting author: jitka.myskova@lf1.cuni.cz

Fluorescent proteins (FPs), the basis of thousands molecular biosensors, exhibit pronounced optical directionality. Directionality of single-photon (1P) light absorption and emission of several FPs has recently been experimentally determined [1]. However, two-photon (2P) optical directionality of FPs is more pronounced than 1P directionality and yields more information on molecular orientation [2]. Despite these advantages, little is currently known about 2P optical directionality of FPs, due to its more complex physical nature and mathematical description. Our present work aims to fill this gap. We have now carried out 2P measurements of crystals of several FPs. We have also developed a mathematical description allowing detailed interpretations of our optical measurements. By combining our experimental data with information on molecular structure of the observed crystals, we have now unambiguously determined the 2P absorptivity tensors of the fluorescent proteins mTurquoise2, eGFP and mCherry. The comprehensive knowledge of 2P optical directionality of these FPs will allow determinations of molecular orientations in living cells and better FP-based biosensors [3].

References:

[1] Myšková J. et al.: PNAS 117 (2020), 32395-32401.
[2] Bondar A. et al.: Communications Biology 4(2021), 1-12.
[3] Lazar J. et al.: Nature Methods 8(2011), 684-690.

Acknowledgement:

The authors acknowledge funding from Czech Science Foundation grant 23-05983S to J. Myšková.

Liposomes and gels as delivery system for joint – recalibration of multimodal tomography monitoring by quantitative fluorescence microscopy

Skopalík J.[1,4], Trávník J.[2], Sekora J.[3], Čudek P.[3], Průcha J.[4], Parák T.[1]

[1] Department of Pharmacology and Toxicology, Faculty of Pharmacy – MU, Brno, Czech Republic
[2] Department of Traumatology - Trauma Hospital Brno, Faculty of Medicine, Masaryk University, Brno, Czech Republic
[3] Faculty of Electrical Engineering and Communication, Brno University of Technology, Brno, Czech Republic
[4] Department of Information and Communication Technology in Medicine, Faculty of Biomedical Engineering, Czech Technical University in Prague, Prague, Czech Republic

Email of the presenting author: j.skopalik@seznam.cz

Introduction: Liposomes and exosomes (nature variant of liposomes) are lipid nano-size unit, which can play role of the delivery "trojan horse" for bioactive factors and drug molecules into the problematic parts of the joint. The continual application of liposomes into the proximity of cartilage is problematic, only effective method is periodical injection till today [1]. However compact gel body implanted in the join can bring effect of continual delivery.

Methods: Gels and liposomes inside the gel structure can be used as bioactive factors deposit directly to the surface of knee cartilage. The goal of the study was understanding of "gel + liposomes complex" stability and also descrition of liposome transport to the cartilage and synovial tissue on rabbit knee joint. Liposomes were labeled by double-contrast: gadolinium and red fluorescence nanoparticles [3,4]. Three monitoring scanning methods were used at days 5 - 30 after implantation: S1 - non-invasive fluorescence scanner on joint in vivo (em. 600 and 650 nm), S2 - contactless non-invasive RTG scanner on joint ex vivo, S3 - fluorescence scanner for open joint focusing to synovial tissue on joint in vivo (ilustration of joint – Fig. 1.). The signal of initial gel drop was recorded also by all three method before implantation for quantitative calibration of signal.

The histological pictures from twenty areas (4 mm^2) of cartilage and synovial membrane was recorded by fluorescence microsopy. The signal from tissue was recomputed to absolute number of liposomes per cube millimeters in different joint location. The graphical comparison of results from fluorescence and RTG scanners and absolute number of exosomes derived from microscopic scan are presented in Fig. 2.

Results and conclusion: Each scanning method S1 – S3 bring real pictures of redistribution of liposomes from gel in joint, however the signal is partially distorted by overlying tissue (skin for *in vivo* variant). The absolute signal from microscopy was used to compute "correction coefficient 2D matrix" for all scanner. Scanners with recomputing by correction coefficients can bring exact summary of compartment statistic (Fig. 2), the method can be used now for real animal and human clinical tests of liposome application into knee joints, and curative effects can be correlated with quantitative map of particle redistribution.

References:

[1] Michalek J. et al. *Journal of clinical orthopaedics and trauma* 10(1) (2019), 234-241
[2] Malina T. et al. *Carbon* 152 (2019), 434-443
[3] Průcha, J., Physiological Research, 68 (2019), 114-126

Acknowledgement: The authors acknowledge Technology Agency of the Czech Republic – project FW01010106 „Development of new generation medical devices by means of the translational medicine and physical interventions principle".

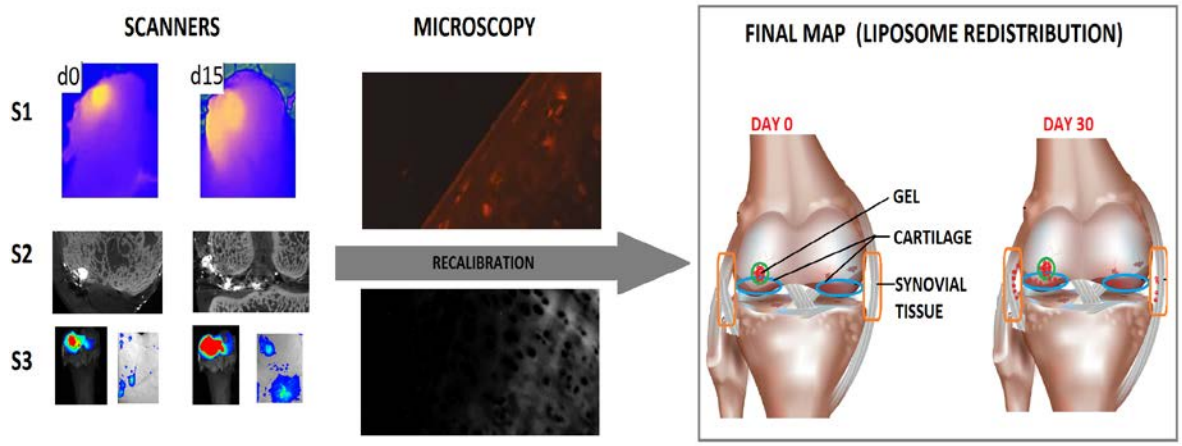

Fig. 1: Datasets from scanners (S1, S2 and S3) and recomputing the liposomes redistribution to final kinetic map of joint

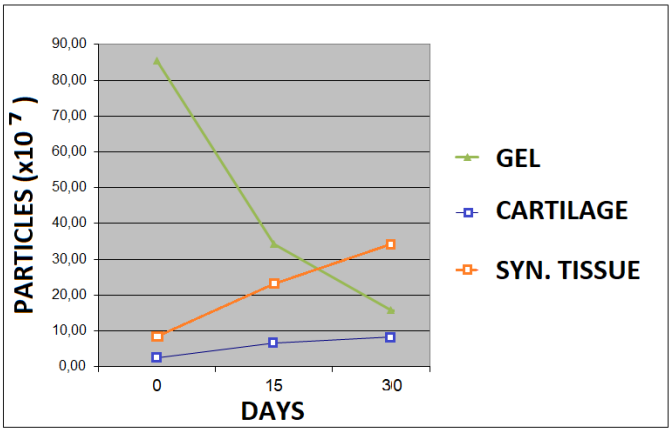

Fig. 2: Kinetic of liposomes redistribution in days 0 – 30.

In Vivo TBEV Replication in Mouse Brain: Investigating Cellular Alterations

Bílý T.[1,2], Tesařová M.[1], Prančlová V.[1,2], Dvořáková M.[1], Hönig V.[1,3], Kamiš J.[1,2], Vancová M.[1,2], Palus M.[1,3]

[1] Institute of Parasitology, Biology Centre CAS, Branišovská 31, CZ-37005 České Budějovice, Czech Republic
[2] Faculty of Science, University of South Bohemia, Branišovská 31, CZ-37005, České Budějovice, Czech Republic
[3] Department of Virology, Veterinary Research Institute, Hudcova 70, CZ-62100 Brno, Czech Republic

Email of the presenting author: thomass@paru.cas.cz

Tick-borne encephalitis virus (TBEV) causes serious infections of the central nervous system in humans. The initial phase of infection typically presents with nonspecific influenza-like symptoms. In the second phase, meningitis, meningoencephalitis or meningoencephalomyelitis can occur, possibly leading to a post-encephalitic syndrome. TBEV belongs to the Flavivirus genus within the Flaviviridae family. Flaviviruses are characterized by lipid-enveloped particles with an outer diameter of approximately 50 nm. These virions contain an inner electron-dense nucleocapsid composed of capsid protein C and a positive-sense RNA genome. Upon entry into the host cell, the RNA genome is translated into a polyprotein, which is subsequently cleaved into structural proteins C (Capsid), M (membrane), E (envelope), as well as non-structural proteins NS1, NS2A, NS2B, NS3, NS4A, NS4B, and NS5.

The replication of the virus is enabled by the formation of replication complexes, involving non-structural proteins, which induce alterations in the rough endoplasmic reticulum (RER). These alterations manifest as convoluted membranes, smooth membrane structures, and induced vesicles.

In this study, samples from mouse brains infected with TBEV strain Neudörfl were analyzed. The infected cells were rare, but replication complexes were repeatedly localized in areas within larger cells exhibiting electron-dense cytoplasm, numerous mitochondria, and irregularly shaped nuclei. Tubular structures were identified within the altered RER, consistent with previous findings in cultured neurocytes and astrocytes Palus et al. (2014) and Bily et al. (2015). This comprehensive analysis sheds light on the cellular alterations induced by TBEV replication in the mouse brain, providing valuable insights into the virus-host interactions.

The 3D structure of these tubules was visualized using electron tomography, employing a TEM Jeol 1400 Flash equipped with a CMOS camera EMSIS Xarosa and controlled by Serial EM software. Tomogram reconstruction and 3D model generation were conducted using the Imod software package.

Acknowledgement:

This work was supported by the Czech-BioImaging large RI project (LM2023050 and OP VVV CZ.02.1.01/0.0/0.0/18_046/0016045 funded by MEYS CR) and from the Czech Science Foundation (grant No. 20-30500S and 23-08039S).

Observing Conformational Changes in the Insulin Receptor Using Excitation Polarization-resolved Fluorescence Microscopy

Sakhi A.[1,3], Paul M.[2], Lazar J.[1,2]

[1] Institute of Organic Chemistry and Biochemistry CAS, Flemingovo nam. 2, 160 00 Prague 6, Czechia
[2] First Faculty of Medicine, Charles University, Katerinska 1660, 121 08 Prague 2, Czechia
[3] Faculty of Science, Charles University. Albertov 6, 128 43 Prague 2, Czechia

Email of the presenting author: alinasakhi@gmail.com

The insulin receptor (IR) is a receptor tyrosine kinase crucial for insulin signalling. Upon binding of insulin, IR undergoes a series of conformational changes that ultimately lead to activation of the intracellular kinase domain and to phosphorylation. In order to observe the conformational changes in IR in living cells, we have now developed a genetically encoded molecular biosensor. The biosensor converts the conformational changes in the extracellular domain of the receptor into changes in orientation of a fluorescent protein, detectable by polarization microscopy. Here we present the results of our observations of conformational changes in the insulin receptor in response to agonists, antagonists, as well as to kinase inhibitors.

References:

[1] Lazar, J., et al. (2011). "Two-photon polarization microscopy reveals protein structure and function." Nature Methods 8(8): 684-690.
[2] Bondar, A. and J. Lazar (2017). "The G protein Gi1 exhibits basal coupling but not preassembly with G protein-coupled receptors." Journal of Biological Chemistry 292(23): 9690-9698.
[3] Bondar, A., et al. (2021). "Quantitative linear dichroism imaging of molecular processes in living cells made simple by open software tools." Communications Biology 4(1).
[4] Myšková, J., et al. (2020). "Directionality of light absorption and emission in representative fluorescent proteins." Proceedings of the National Academy of Sciences 117(51): 32395-32401.

Acknowledgement:

The research was supported by European Regional Development Fund project ChemBioDrug (CZ.02.1.01/0.0/0.0/16_019/0000729) (J.L., J.J.) and EIC PathFinder project UniSens (J.L.).

Optimization of cryoSEM for quantitative and qualitative analyses of trichomes on different varieties of potato leaves

Samcová N. [1,2], Sehadová H. [1,2], Moos M. [1], Vaněček J.[3], Skoková Habuštová O.[1], Doležal P.[4]

[1] Biology Centre CAS, Institute of Entomology, Branisovska 31, 370 05 Ceske Budejovice, Czech Republic
[2] University of South Bohemia in Ceske Budejovice, Faculty of Science, Branisovska 31, 370 05 Ceske Budejovice, Czech Republic
[3] Biology Centre CAS, Institute of Parazitology, Branisovska 31, 370 05 Ceske Budejovice, Czech Republic
[4]Potato research Institute Ltd, Dobrovského 2366, 580 01 Havlíčkův Brod, Czech Republic

Email of the presenting author: sehadova@entu.cas.cz

Colorado potato beetle is currently a very important pest in potato plants in the Czech Republic. Every year it causes huge damage and the yield loss of potato crops. The use of potato varieties with a high density of glandular trichomes could create an environmentally friendly natural biological shield providing high protection of plants against pest attacks [1]. We have developed the optimal methodology and necessary material equipment for the most efficient quantification of trichome density and determination of trichome types on potato leaves. We designed and constructed an object holder for Jeol JSM-7401F scanning electron microscope (Joel, Akishima, Japan) that allows maximizing the monitored area, mounting a leaf and its freezing in the horizontal plane, and the puncher of corresponding dimensions ensuring to cut out the same areas from the leaves. We standardized the sublimation process as well as sputter coating to unify protocol conditions for the whole experiment. To evaluate the density of trichomes, we optimize the scanning method for capturing the largest possible area of leaves with sufficient resolution. The optimized scanning method was used in our research project investigating trichome density on leaves from 12 potato varieties. We investigate whether the frequency of occurrence of glandular trichomes on both abaxial and adaxial leaf surfaces of commonly cultivated potato varieties can affect the occurrence of Colorado potato beetle larvae and/or adults. From each variety both abaxial and adaxial side of 3 leaves from an identical location on the plant were tested i.e. a total of 6 samples of each variety. The data obtained were analyzed by counting the number of glandular and non-glandular trichomes using the Cell counter tool in the Fiji software. We compared the obtained data with the rate of feeding on individual potato varieties by the Colorado potato beetle.

References:

[1] Cho, K.S. et al.: Horticul. Environ. Biotech. 58(2017), 450-457.

Acknowledgement:

The work was supported by the Czech-BioImaging large research infrastructure project (LM2023050 funded by MEYS CR), National Agency for Agricultural Research (NAZV) Project No. QK1910270 and by Biology Centre CAS, Institute of Entomology (RVO 60077344). We acknowledge the core facility Laboratory of Electron Microscopy, Biology Centre CAS.

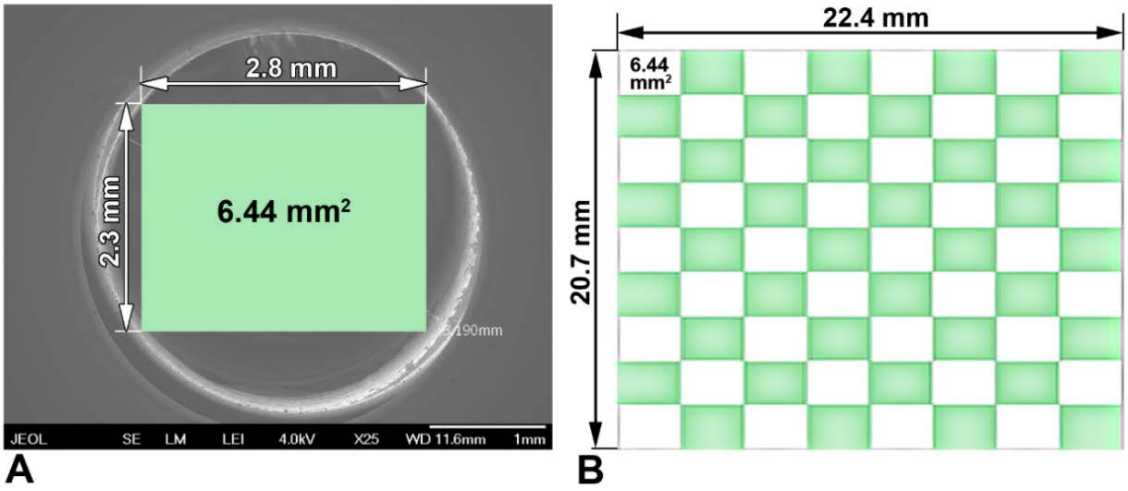

The capture template. (A) An image of the field of view of a Jeol JSM-7401F scanning electron microscope. (B) Checkerboard template for scanning potato leave surface.

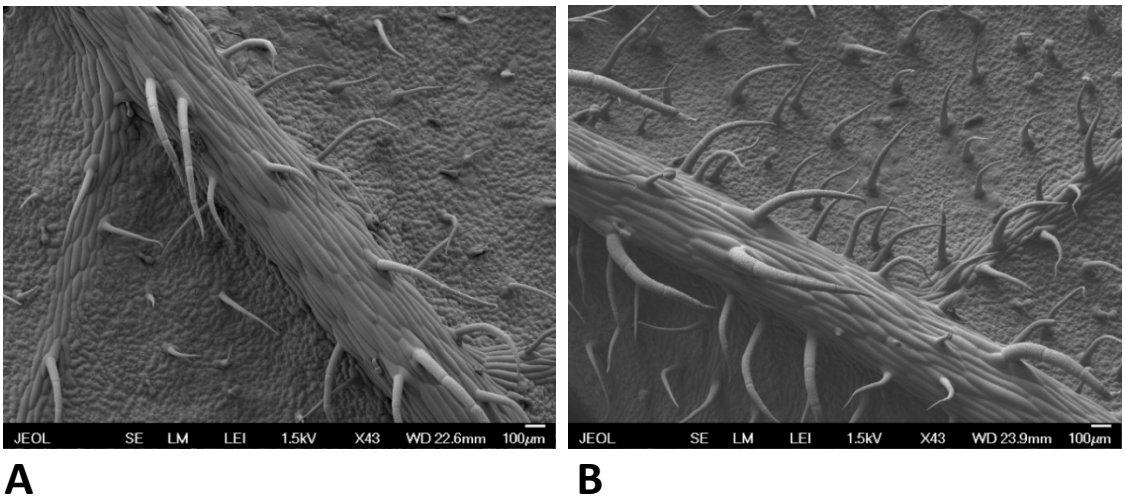

Examples of scanning microscopy image of abaxial side of the leaf of variety Carrera (A) and variety Magda (B) at magnification 43x and 40 seconds per image at image size 1280x1024 pixels.

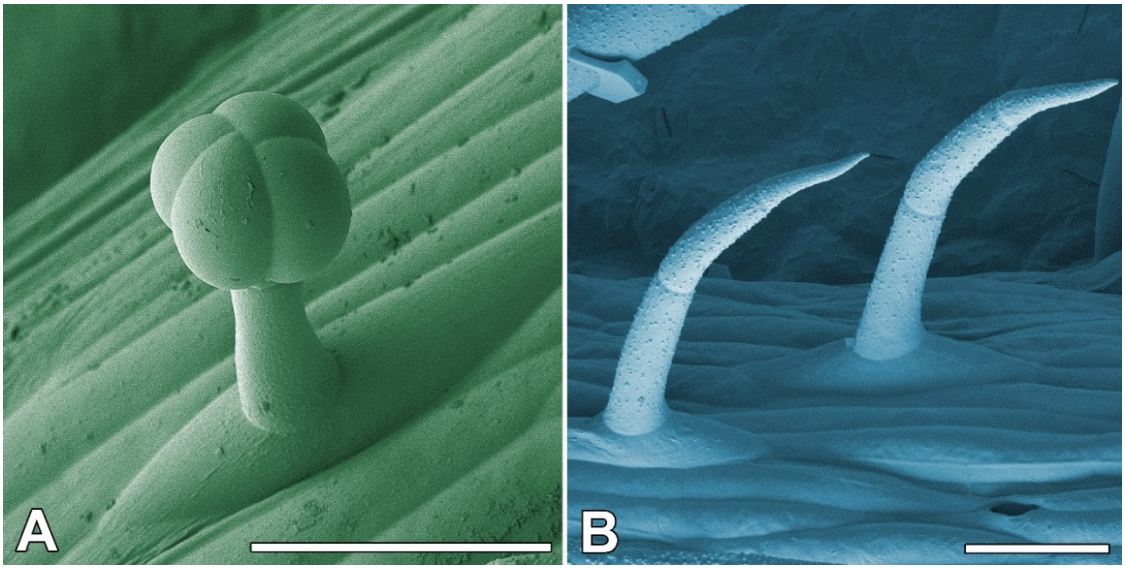

Hight magnification of a grandular (A) and nongrandular (B) trichomes. Scale bar 100 µm.

Comprehensive capture of the chromatin structure

Molínová P.[1], Dalecká M.[2, 3], Benda A.[2], Chmúrčiaková N.[1], Cmarko D.[1]

[1] Institute of Biology and Medical Genetics, First Faculty of Medicine, Charles University and General University Hospital in Prague, Prague, Czech Republic
[2] Imaging Methods Core Facility at Biocev, Faculty of Science, Charles University, Prague, Czech Republic
[3] Department of Genetics and Microbiology, Faculty of Science, Charles University, Prague, Czech Republic

Email of the presenting author: pavla.bazantova@gmail.com

Important nuclear functions concerning gene expression include DNA replication and repair, as well as RNA synthesis, maturation, and movement towards nuclear pores. These activities are linked to non-membrane chromatin-containing domains. Generally accepted opinion is that chromosomes reside in a certain area of the nucleus known as the chromosomal territories (CT). On the other hand, there is still disagreement over the interchromatin compartment, which is the DNA-poor nuclear region surrounding each individual CT.

Our study set out to examine the distribution of DNA and chromatin inside the interphase nuclear region, taking into account 3D nuclear architecture and its functional role over spatial and temporal gene expression.

Estimates of 3D chromatin compaction and organisation can be obtained using light microscopy and fluorescent labeling. For higher resolution analysis, electron microscopy is required. To differentiate chromatin from other structures including ribonucleoproteins, the cells were treated by pre-embedding staining where chromatin is observed as a highly contrasted structure. NAMA-Ur is method based on the extraction of RNA and phosphate groups from phosphoproteins by a weak alkali hydrolysis (NA) which does not affect DNA, followed by blockage of the amino and carboxyl groups by methylation and acetylation (MA). Finally, sections are stained by uranyl (Ur), which can bind to DNA (Testillano, JHC 39, 1991). Furthermore, to reveal the chromatin domains where gene transcription or replication take place, cells were labelled by *in vivo* incorporation of labeled nucleic acid precursors. Structural and functional acquisitions were finally performed using focused ion beam scanning electron microscopy (FIB-SEM). Combinations of FIB-SEM with time-of-flight secondary ion mass spectrometry (SIMS) or transmission EM with nanoscale SIMS (NanoSIMS) were also tested. Moreover, serial sectioning of labeled nuclei is currently in progress for SEM followed by NanoSIMS as well as for array tomography. The obtained data was analysed using Amira software.

We successfully obtained a 3D datasets of NAMA-Ur-labeled nucleus by FIB-SEM acquisition with sufficient resolution and contrast for further analysis. Morphometric analysis showed that DNA/chromatin occupies about half of the total nuclear volume, i.e. a significant part of nucleoplasm belongs to the interchromatin compartment. Furthermore, the analysis of distribution of DNA revealed chromatin domains associated with nuclear periphery (perinuclear chromatin) and chromatin domains associated with nucleolus (chromatin containing ribosomal genes) (see figure). The results demonstrate that this approach performed on nuclei with specifically contrasted chromatin offers an extraordinary opportunity for study of nuclear architecture *in situ*.

Acknowledgement:

This work was supported by Charles University (Cooperatio). We acknowledge the Imaging Methods Core Facility at BIOCEV, institution supported by the Czech-BioImaging large RI projects (LM2015062 and CZ.02.1.01/0.0/0.0/16_013/0001775, funded by MEYS CR) for their support with obtaining imaging data presented in this work.

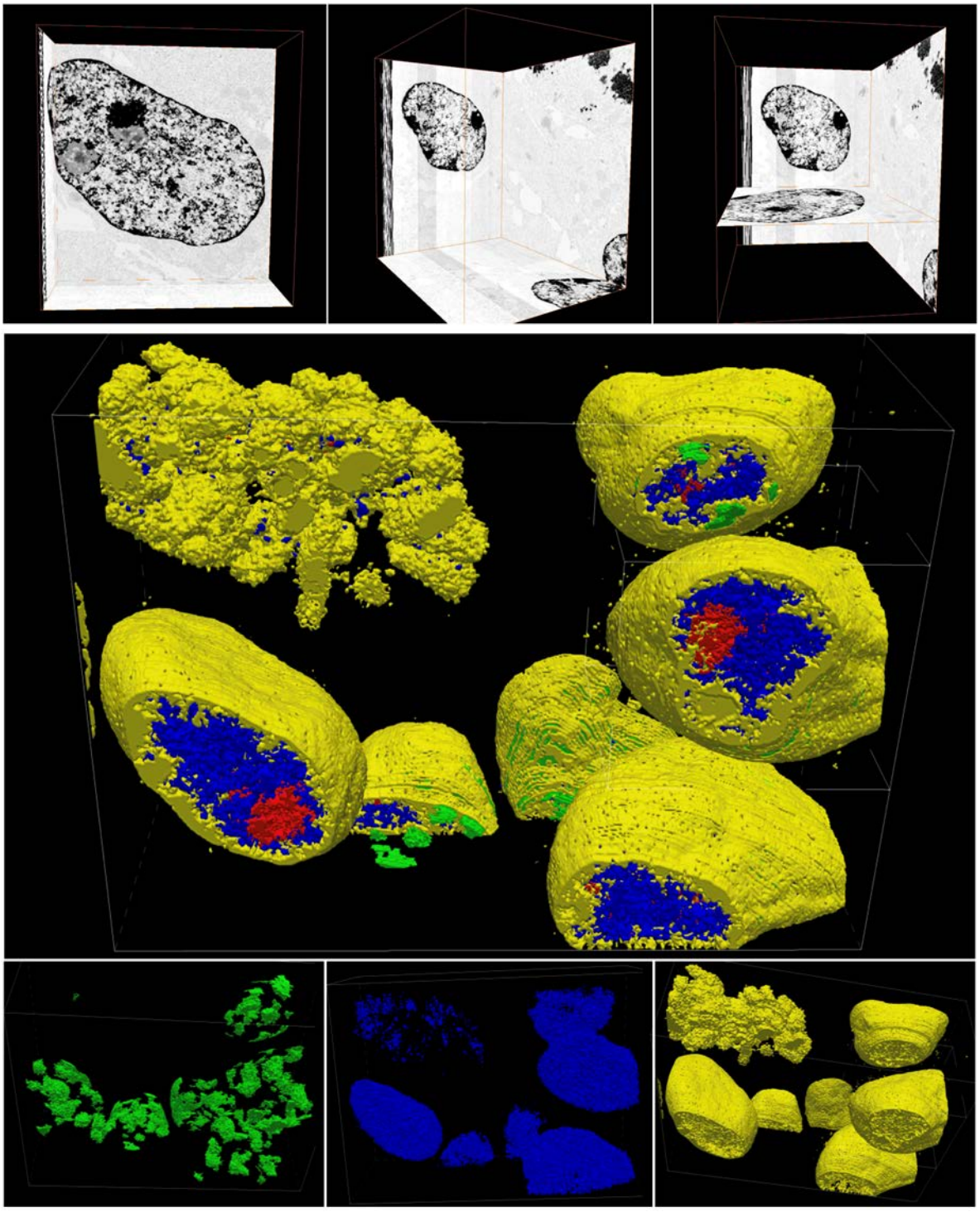

Fig.: Our 3D reconstruction of chromatin arrangement showed occurrence of the chromocentres (green), internuclear (blue) and perinuclear (yellow) chromatin.

Czech-BioImaging: Empowering Through Education, Engagement, and Events

Klimešová D.[1]

[1] Institute of Molecular Genetics of the Czech Academy of Sciences, Prague, Czech Republic

Email of the presenting author: daniela.klimesova@img.cas.cz

Our main focus at Czech-BioImaging, the national research infrastructure for biological and medical imaging, is providing open access to our core facilities. We strive to simplify the process for users to reach out and utilize our resources effectively. Through our website, users can easily fill out a form or directly contact the core facility leaders. Their feedback is invaluable to us, which is why we send satisfaction surveys annually to gather insights and continually improve our services.

Czech-BioImaging dedicates a significant portion of its efforts to user education and engagement. Our focus on education ensures that users have the skills to work more efficiently on their research projects. Through a range of courses and workshops, we offer support to researchers at all levels. Aligned with our motto, "Imaging Principles of Life," we stay dedicated to advancing biological and medical imaging in this way.

Engagement is key. We encourage collaboration and help to bridge the gap between scientists, industry leaders, and academia, to create innovative solutions to imaging challenges. Our events, like user meetings at CFs or the annual conference, serve as platforms for networking and idea exchange. Additionally, to keep users engaged and informed, we regularly send out newsletters with updates, news, and upcoming events.

Take advantage of our open access or participate in our scientific courses to become part of the Czech-BioImaging community.

Acknowledgement:
Czech-BioImaging, National Infrastructure for Biological and Medical Imaging is co-funded by the Ministry of Education, Youth and Sports of the Czech Republic (project LM 2023050 and OP JAK infrastructure project "Modernisation of the VVI Czech-BioImaging" CZ.02.01.01/00/23_015/0008205).

Metabolic and Mitochondrial Effects of KATP Modulation in SH-SY5Y Cells: Implications for Neurodegeneration and Parkinson's Disease

Evinova A.[1], Dibdiakova K.[2], Baranovicova E.[1], Racay P.[3], Pecova R.[2], Pokusa M.[1]

[1]Biomedical Center Martin, Jessenius Faculty of Medicine, Comenius University in Bratislava, Slovakia
[2]Department of Pathological Physiology, Jessenius Faculty of Medicine, Comenius University in Bratislava, Slovakia
[3]Department of Biochemistry, Jessenius Faculty of Medicine, Comenius University in Bratislava, Slovakia

Email of the presenting author: andrea.evinova@uniba.sk

Abstract

Inward rectifying potassium channels sensitive to ATP levels (KATP) have garnered extensive research attention over the past decades due to their established role in metabolic and cardiovascular diseases. Emerging experimental evidence suggests the potential therapeutic relevance of KATP modulation in neurodegenerative disorders. However, the existing data on the effects of KATP agonists/antagonists in neurodegeneration experiments exhibit inconsistencies, primarily attributable to variations in experimental models employed.

This study seeks to present a comprehensive analysis of the impacts of both activating and inhibiting KATP channels in two distinct forms of SH-SY5Y cells. Our findings provide valuable insights into the metabolic variances between differentiated and non-differentiated SH-SY5Y cells, particularly within the context of glibenclamide and diazoxide effects under normal physiological conditions and during the initiation of pathological processes mimicking Parkinson's disease in an in vitro setting. Special emphasis is placed on assessing mitochondrial functions and alterations in mitochondrial network morphology.

The observed heightened expression of KATP channel proteins in non-differentiated SH-SY5Y cells appears to create a foundation for a more pronounced influence of KATP modulators in this cell subtype. Furthermore, the efficacy of rotenone treatment in inducing morphological changes in the mitochondrial network depends on the differentiation status of SH-SY5Y cells.

Funding:

Experiments were funded by VEGA 1/0085/24 and 1/0183/23 grants of Scientific grant agency of Ministry of Education, Science and Sports of Slovak Republic

IMG Electron Microscopy Core Facility

Raabová H.[1], Pinkas D.[1], Vlčák E.[1], Filimoněnko V. V.[1,2]

[1] Core Facility for Electron Microscopy, Institute of Molecular Genetics CAS, Prague, Czech Republic
[2] Laboratory of Biology of the Cell Nucleus, Institute of Molecular Genetics CAS, Prague, Czech Republic

Email of the presenting author: helena.raabova@img.cas.cz

The Electron Microscopy Core Facility offers services in a wide range of both advanced and routine techniques, focused mainly on biological samples. The team's expertise is supported by state of the art equipment for sample preparation and ultrastructural imaging. Our high-end transmission electron microscope (TEM) operates at up to 200 kV and offers high-resolution TEM, imaging in STEM mode, 3D analysis by TEM- or STEM tomography, cryo-electron microscopy and STEM-EDS elemental analysis. For routine observation, a standard 120kV TEM with a user friendly Limitless panorama application is used. Recently we have incorporated FIB-SEM instrument and developed a cryo-lamella lift-out workflow.

Standard and advanced techinques are tied up also with the sample preparation. Starting from routine chemical fixation and resin embedding, or negative staining of weakly observable samples, we can proceed to better preservation of natural sample appearance by cryofixation using plunge-freezing or high-pressure freezing, followed by freeze-substitution, cryosectioning or freeze fracture replica labeling. For even more advanced applications we can provide cryoCLEM technique using a specialized microscope. Another field forms pre- and post-embedding immunolabeling techniques using gold nanoparticles of different sizes.

Users as well as potential applicants can think of service processing and imaging of various biological samples – in the core facility we can deal with human and animal cell cultures, plant and animal tissues, worms, microorganisms, lipid micelles, isolated DNA, or purified proteins. We provide development and optimization of sample preparation, based on a long expertise and fruitful collaborations with companies providing equipment for electron microscopy.

The Electron Microscopy Core Facility is part of the IMG Czech-BioImaging node and Prague Euro-BioImaging node. We provide open access to our technologies and expertise and are ready to welcome users from all fields.

Acknowledgement:

We acknowledge funding from MEYS CR (LM2018129, LM2023050), ERDF (CZ.02.1.01/0.0/0.0/18_046/0016045, Z.02.1.01/0.0/0.0/16_013/0001775) and IMG grant (RVO: 68378050).

Novel genetically encoded probes for functional imaging of cell signalling

Miclea P.[1], Nagy Marková V.[1], Sakhi A.[2], Bondar A.[1], Myšková J.[1], Khoroshyy P.[1,2], Lazar J.[1]

[1]1st Faculty of Medicine, Charles University, Albertov 4, 128 00 Prague 2, Czech Republic
[2] Inst. of Organic Chemistry and Biochemistry CAS, Flemingovo nám. 2, 160 00 Prague 6, Czech Republic

Email of the presenting author: sebastian.miclea@lf1.cuni.cz

Genetically encoded fluorescent probes convert specific biomolecular events into optically detectable signals. Typically, such probes work by modulating the absorption or emission spectrum of the fluorophore, through a suitable fluorescence quenching process. Here we present a very different, widely applicable design of genetically encoded fluorescent probes that takes advantage of an unrelated detection principle: directionality of optical properties of fluorescent proteins. The probes offer an extremely simple design, high sensitivity, multiplexing capability, ratiometric output, resilience to bleaching artifacts, without requiring any modifications to the proteins of interest. The probes are applicable to imaging cellular activity of G protein coupled receptors, G proteins, arrestins, receptor tyrosine kinases and other signaling proteins.

Changes in the hydrogel structure depending on the crosslinking agent seen by electron microscopy

Mrazova K.[1,2], Havlickova A.[2], Cernayova D.[2], Hrubanova K.[1], Sedlacek P.[2], Krzyzanek V.[1]

[1] Institute of Scientific Instruments of the CAS, v. v. i., Brno, Czech Republic,
[2] Faculty of Chemistry, Brno University of Technology, Brno, Czech Republic

Email of the presenting author: mrazova@isibrno.cz

Hydrogels are materials consisting of crosslinked polymer chains capable of binding substantial amounts of water. Even though several types of hydrogels can be of synthetic origin, there are also hydrogels found in nature [1]. For example, the bacterium *Azotobacter vinelandii*, belonging to the group of plant growth-promoting bacteria, produces biopolymer alginate to form a polysaccharide capsule, which protects the cell from drying out. Since *A. vinelandii* can be used as bioinoculants, their production of alginate can be also an advantage in their agricultural utilization. Bacteria encapsulated in hydrogel can be further processed into the final form of bioinoculant and since *A. vinelandii* produces its own alginate, it is possible to add just the crosslinking agent to the cultures and thus reduce the costs for bioinoculant production [2,3]. To make the production of hydrogel-encapsulated bioinoculant, it is necessary to choose the most suitable crosslinker since depending on the crosslinking agent the final hydrogel changes its structure. In our study, we have focused on determining the changes in the structure of the alginate-based hydrogel depending on the use of different crosslinkers, namely $CaCl_2$ and glucono-D-lactone together with $CaCO_3$. To observe the structure of hydrogels cryogenic scanning electron microscopy was used. Samples were fixed using a high-pressure freezing method (EM ICE, Leica Microsystems), followed by freeze-fracture and sublimation for 7min at -95°C (ACE600, Leica Microsystems). Samples were then observed in a scanning electron microscope (Magellan 400/L, FEI) equipped with a cryo-stage, at −120 °C using a 1–2 keV electron beam. It was possible to distinguish the difference in the hydrogel structure based on the crosslinker used. For 2% $CaCl_2$ solution, the hydrogel formed a polymeric net surrounding the cells where individual fibres could be seen, while samples crosslinked using 1M solution of lactone together with 0,5M $CaCO_3$ formed dense mass. Similar results were also observed in the preliminary STEM study of the same hydrogel-based samples processed using the freeze substitution procedure, supporting our initial findings.

References:

[1] Ahmed E. M. et al.: Journal of Advanced Research 6(2015), p. 105-121.
[2] Santos M. S. et al.: AMB Express 9(2019), p. 205.
[3] Noar J. D. et al.: Microbiology 164(2018), p. 421-436.

Acknowledgement:

The authors acknowledge funding from GACR (project GA23-06757S), and TACR (project TN02000020). Microscopic analysis was provided by CF ISI EM which is supported by the Czech-BioImaging large RI project (LM2023050 funded by MEYS CR).

The Impact of Dietary Haemoglobin on Nymphal Stages of Ixodes ricinus: The volume reconstruction of the gut via Volume EM

Kitzberger F.[1, 2], Urbanová V.[1], Kopáček P.[1], Sojka D.[1], Perner J.[1], Vancová M.[1]

[1] Institute of Parasitology, Biology Centre of the Czech Academy of Sciences, Branišovská 31, 370 05, České Budějovice, Czech Republic
[2] Faculty of Science, Department of Physics, University of South Bohemia, Branišovská 1645/31a, 37005 České Budějovice

Email of the presenting author: Frantisek.kitzberger@paru.cas.cz

The tick is a ubiquitous parasite, whose survival relies heavily on its host's haemoglobin, as it has lost the ability to synthesize its own haem group during the evolution. However the haem group plays a crucial role in the tick's reproductive process, being deposited on its eggs. While previous research has demonstrated that adult females can survive without the haem group, the necessity of this component for nymphs remains unclear.

Our study utilized SBF-SEM to examine the morphology of tick nymph gut, followed by 3D reconstruction of granules, identified through immunolabelling of host albumin and haemoglobin. Employing MIB/deepMIB [1, 2], we reconstructed a total volume of 0.003 mm^3, visualized using AMIRA (Thermo Fisher Scientific).

Our findings reveal the distribution of haemoglobin and albumin in midgut cells, alongside lipid droplets which predominate during feeding. These components play crucial roles in nymph metamorphosis and subsequent survival of adult ticks.

[1] Microscopy Image Browser: A platform for segmentation and analysis of multidimensional datasets
I. Belevich, M. Joensuu, D. Kumar, H. Vihinen and E. Jokitalo
PLoS Biology 2016 Jan 4;14(1):e1002340. doi: 10.1371/journal.pbio.1002340
[2] DeepMIB: User-friendly and open-source software for training of deep learning network for biological image segmentation
I. Belevich and E. Jokitalo
PLoS Comput Biol. 2021 Mar 2;17(3):e1008374. doi: 10.1371/journal.pcbi.1008374

Acknowledgement:

The study was supported by MEYS CR (LM2023050 Czech-BioImaging and OP VVV CZ.02.1.01/0.0/0.0/18_046/0016045) and GAČR (No. 21-08826S – P. I. Kopáček).

The dawn of phase-contrast microcinematography: Kurt Michel, polytene chromosomes and meiosis

Pelc R.[1,2]

[1] Institute of Biochemistry & Organic Chemistry, Czech Academy of Sciences, 16610 Prague, Czech Republic
[2] Third Faculty of Medicine, Charles University, 10000 Prague, Czech Republic

Email of the presenting author: radek.pelc@seh.oxon.org

Imaging of chromosomes in living (unstained) cells had drastically improved by the invention of phase-contrast microscopy in 1932. Initially, polytene (giant) chromosomes in the salivary glands of non-biting midges (*Chironomidae*) were observed by this technique (**Fig. 1A**). This was easy given their huge size and thus relatively large optical thickness [1].

Attempts to follow mitosis and meiosis proved much more challenging as the chromosomes are of normal size, i.e., hard to see unless stained. It took Kurt Michel (Carl Zeiss Mikrolaboratorium, Jena, Germany) three years only to establish a reliable protocol of keeping insect spermatocytes alive and dividing for a sufficiently long time to be filmed [2]. His time-lapse recording of chromosomes (Ch) and microtubules (Mt) pulling them apart during meiosis (**Fig. 1B, C**) was instrumental in the acceptance of phase-contrast microscopy by the biological community, and in awarding of the 1953 Nobel Prize to Frits Zernike. He originally invented the phase-contrast method to evaluate the quality of astronomical mirror telescopes, with no cells (dead or alive) in mind [3].

Michel made his film [4] in 1943 (video-still images in [1-3], [4b] and [5], videos in [3] and [4c]). Jointly with a background information (1958 edition), it used to be available from *Institut für den Wissenschaftlichen Film* (IWF, Göttingen, Germany) now incorporated into the German National Library of Science and Technology (TIB, Hannover). At least in the past, a copy of the film was also kept by the Medical Illustration Service of the Armed Forces Institute of Pathology (Silver Spring, MD, USA) as a “professional medical film”, PMF 5036 [6].

The present ‘microscopic archaeology’ paper aims to highlight the now mostly forgotten works of Kurt Michel (1909-2000), a contemporary of Willi (Wilhelm) Kuhl (1892-1972), Ronald G. Canti (1883-1936) and Michael Abercrombie (1912-1979), all of them pioneers of live-cell microcinematography [7,8]. Ronald G. Canti studied cancer cell proliferation using only brightfield and darkfield microscopy [9] as he died before the phase-contrast microscopy became commercially available (1942). His videos have been made available by the Wellcome Trust library [8,9].

[1] Michel K. (1941) *Naturwissenschaften* **29** (4): 61-62 (www)
[2] Brice A.T. (1953) *American Biology Teacher* **15** (5): 124–128 (www)
[3] Pelc R., Hostounský Z., Otaki T. & Katoh K. (2020) *Neuromethods* **153**: 275-323 (www)
[4a] Michel K. (1943) Die Reifeteilungen (Meiose) bei der Spermatogenese der Schnarrheuschrecke (*Psophus stridulus L.*). Hochshulfilm C443/1944. RWU, Berlin (www)
[4b] Michel K. (1943) *Zeiss Nachrichten* **4** (9): 236–251 (www)
[4c] Michel K. (1943) *Cell Image Library*; CIL:39225 to CIL:39229 (5 videos) (www)
[5] Michel K. (1950) *Naturwissenschaften* **37** (3): 52-57 (www)
[6] Jacquez J.A. & Biesele J.J. (1954) *Experimental Cell Research* **6** (1): 17–29 (www)
[7] Bereiter-Hahn J. (1973) *Marine Biology* **23** (1): 1 (www)
[8] Stramer B.M. & Dunn G.A. (2015) *Journal of Cell Science* **128** (1): 9–13 (www)
[9] Canti R.G. (1933) Cultivation of living tissue (Pt 1, 2 and 3). *Wellcome Library*; № b2099803x (www), b20998041 (www) and b21021004 (www)

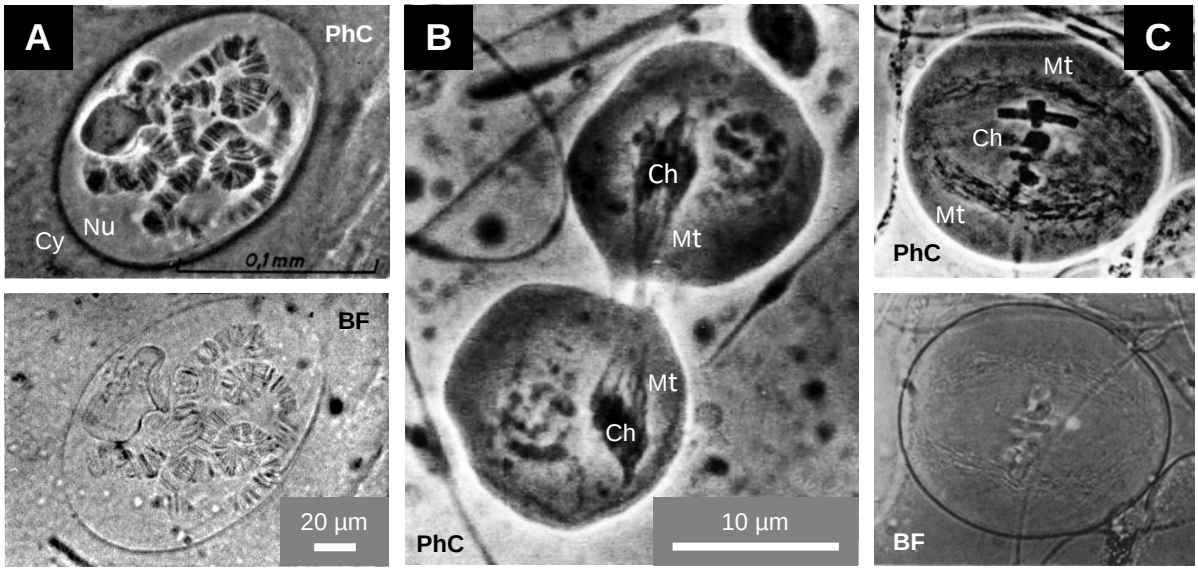

Fig. 1. *Insect chromosomes in phase-contrast (PhC) and brightfield (BF) microscopy.* ***A*** *Giant nucleus (Nu) with polytene chromosomes in the salivary gland of a chironomid. Cy cytosol. Reprinted from [1].* ***B,C*** *Living grasshopper spermatocytes in meiosis. Ch chromosomes. Mt microtubules.* ***B*** *(obj. x40/0.65) reprinted from [4].* ***C*** *reprinted from [2], images by Kurt Michel (≤1945, magnification unknown but expected to be comparable to B)*

Acknowledgement

The author acknowledges support from the European Regional Development Fund (the "ChemBioDrug" project).

Links to References

[1] https://doi.org/10.1007/BF01476461

[2] https://doi.org/10.2307/4438501

[3] https://doi.org/10.1007/978-1-0716-0428-1_10

[4a] http://www.filmarchives-online.eu/viewDetailForm?FilmworkID=e1dc265c54b1521f738a193710c04f46&content_tab=deu

[4b] https://www.archive.zeiss.de//objekt_start.fau?prj=zeiss&dm=Druckschriften&ref=86486&prj=zeiss&dm=Druckschriften&ref=86486

[4c] http://www.cellimagelibrary.org/groups/39225

[5] https://doi.org/10.1007/BF00627160

[6] https://doi.org/10.1016/0014-4827(54)90144-5

[7] https://doi.org/10.1007/BF00394105

[8] https://doi.org/10.1242/jcs.165019

[9] https://archive.org/details/Cultivation_of_living_tissue_Part_X-wellcome (substitute "X" for "1", "2" or "3")

SERS-tags: selective immobilization and detection of bacteria using specific antibodies and surface-enhanced Raman scattering

Benešová M.[1,2], Bernatová S.[1], Pilát Z.[1], Motlová T.[1], Pokorná Z.[1], Mika F.[1], Ježek J.[1], Kizovský M.[1], Mikulová A.[1], Samek O.[1]

[1] Institute of Scientific Instruments of the CAS, v. v. i., Brno, Czech Republic
[2] Faculty of Chemistry, Brno University of Technology, Brno, Czech Republic

Email of the presenting author: benema@isibrno.cz

Raman spectroscopy is a non-destructive instrumental analytical technique based on Raman scattering, which is the inelastic scattering of photons that occurs when they interact with electrons in chemical bonds. Raman spectroscopy can be used to analyze chemical compounds, mixtures of compounds, and biological samples, including living organisms, in a very rapid, non-contact, and non-destructive manner. The measurements made can be compared with spectral databases. The problem with Raman spectroscopy is that samples sometimes give a weak signal that is often overlaid by intense fluorescence. A micro-Raman spectrometer is used to obtain Raman spectra, see *Figure 1*.

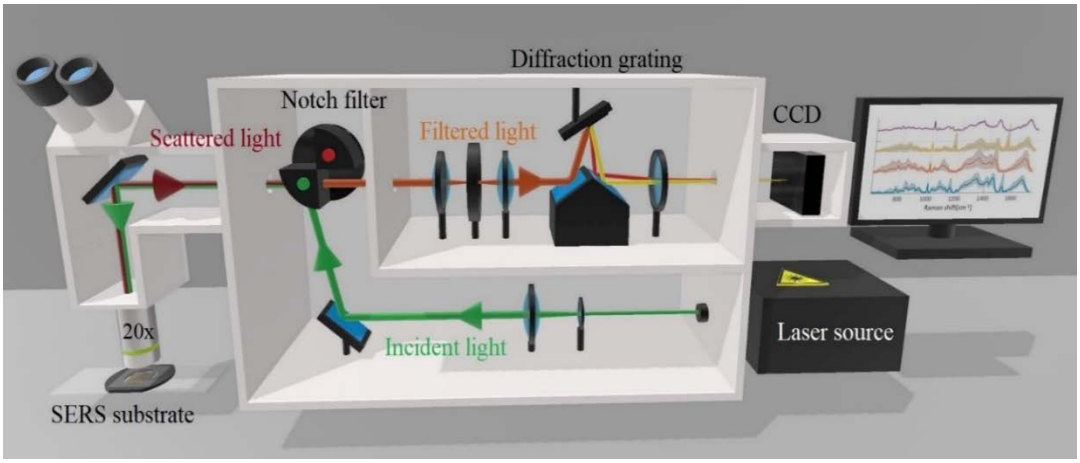

Figure 1: micro-Raman spectrometer – diagram of the experimental setup. The light from the laser passes through the optical elements to the microscope objective and hits the sample. The scattered light is collected by the objective and separated from the excitation radiation on a notch filter. It then passes into the spectrometer and onto the CCD detector.

SERS (surface-enhanced Raman spectroscopy) is used to amplify Raman scattering. Metallic nanoparticles exhibit so-called plasmon resonance, which is a coherent oscillation of conduction electrons produced by the interaction of visible radiation with metallic nanostructures. To enhance Raman scattering, the analyte is most often adsorbed onto the surface of gold or silver nanoparticles. Overall, Raman enhancement of several orders of magnitude can be achieved, commonly 10^3, but in some cases as high as 10^{11}-10^{14}. SERS substrates can take different forms, (*Figure 2 A*) different types of nanoparticles (AuNRs), or a nanostructured planar layer (*Figure 2 B*).

The SERS method enables the rapid identification and discrimination of a wide range of chemical or biological samples, including bacteria. However, differences in the chemical composition of microorganisms may be too small to reliably distinguish related bacterial species. In order to make the identification specific to a particular bacterial species, a technique called SERS-tag can be used in combination with specific immobilization of bacteria using antibodies. SERS-tag Au nanoparticles have a surface modified by a so-called Raman reporter, which provides a specific and very strong response that is enhanced by the SERS principle *(Figure 3)*. The surface of the nanoparticle is also modified by an antibody that binds to the surface of a specific type of bacteria based on antigen-antibody affinity. If the Raman reporter response is observable in the spectrum of the sample, it is clear what kind

of bacteria is present in the sample. These diagnostic nanoparticles can be used to label any type of bacteria, just by modifying the surface with a strain-specific antibody. In following research on bacteria species and bio-markers we plan to include CARS technique (Coherent anti-Stokes Raman scattering).

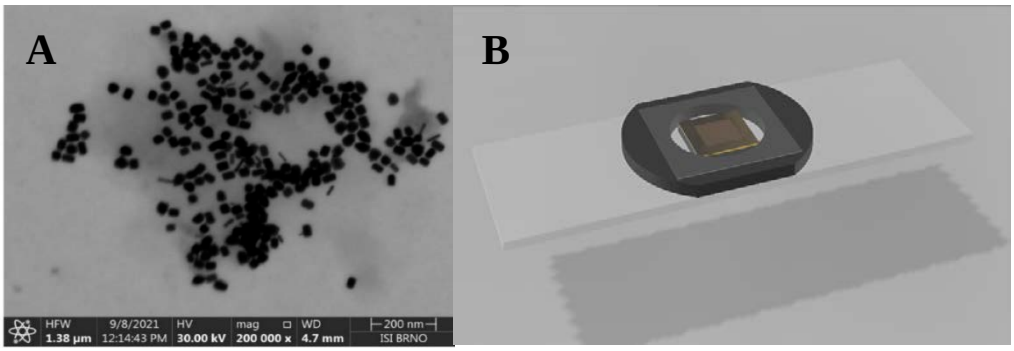

Figure 2: SERS substrates – A. SEM image of synthesized AuNRs [1]; B. Planar SERS substrate with nanostructured layer.

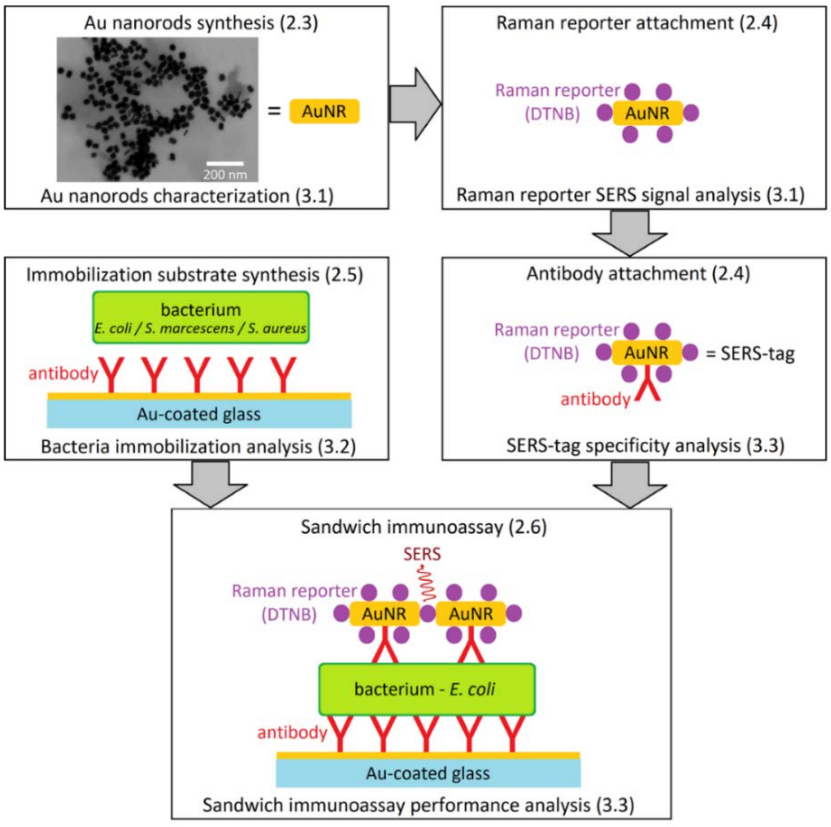

Figure 3: Schematic of the workflow leading to a sandwich immunoassay for the detection of E. coli using SERS markers. Synthesis of AuNRs followed by their characterization by electron microscopy. Raman reporter molecules are then attached to the AuNRs and their SERS signal is analysed. Subsequent attachment of antibodies provides the complete SERS-tag. The Au-coated glass is modified with antibodies and bacteria are immobilized on its surface. In the final step, the branches of the diagram are joined to produce a sandwich immunoassay [1].

Acknowledgment: This project is funded by the EU uCAIR Horizont Europe project no. 101135175. Electron microscopy and Raman spectroscopy analysis provided at Core Facility Electron microscopy and Raman spectroscopy, ISI CAS, Brno, CR, is supported by MEYS CR (LM2023050 Czech-BioImaging).

References:

[1] Benešová, M.; et al. *Biosensors* **2023**, *13*, https://doi.org/10.3390/bios13020182

Workshops

Electron Microscopy and Artificial Intelligence

Sykora V.[1,2]

[1] First Faculty of Medicine Charles University, Prague, Czech Republic
[2] Faculty of Science, Charles University, Prague, Czech Republic

Email of the presenting author: viktor@sciencephoto.eu

With the explosive development of its capabilities, AI (artificial intelligence) finds its use in many fields and microscopy/electron microscopy is no exception. Microscopy, with its ability to provide detailed, high-resolution images, is key to understanding material structures and biological processes. Combined with AI, which enables advanced data processing, pattern detection and automation, it opens up new possibilities for the analysis and interpretation of image data. However, in the context of using AI, it is also important to reflect on potential risks and opportunities for misuse, such as breaches of data protection and privacy, generation of biased results, and loss of human control over results. These potential risks require the establishment of robust ethical and security standards and the ongoing monitoring and evaluation of technologies to ensure that their use is safe and in line with ethical standards.

Deep Learning for Image Segmentation: A Comprehensive Workflow from Raw Images to Complete Models

Belevich I.[1]

[1] University of Helsinki, Helsinki, Finland

Email of the presenting author: ilya.belevich@helsinki.fi

Image segmentation of features from volume Electron Microscopy (vEM) datasets, has long been a challenging aspect of experimental pipelines. This challenge has been amplified by recent advances that have significantly increased the throughput of data collection, leading to an overwhelming amount of data to process. In the cell biology research, the heterogeneity of features of interest, such as organelles, add another layer of complexity to the task. These features are often numerous and diverse, making their segmentation a significant problem. While computer-aided and manual segmentation have provided substantial assistance, they struggle to keep pace with the scale of data now being produced. Luckily, the landscape of image segmentation is being transformed by recent innovations in Artificial Intelligence (AI). Deep learning approaches, which are increasingly accessible to biologists, are emerging as powerful tools to address these challenges.

In this workshop, we will explore the utilization of the Microscopy Image Browser for a comprehensive image segmentation workflow. This will be achieved through the application of deep learning techniques such as segment-anything and convolutional neural networks, with a particular focus on the segmentation of mitochondria from a Focused Ion Beam Scanning Electron Microscopy (FIB-SEM) dataset of a U2OS cell. Our aim is that by the end of this session, you will not only appreciate the transformative power of AI in research but also feel inspired to incorporate these techniques into your own work.

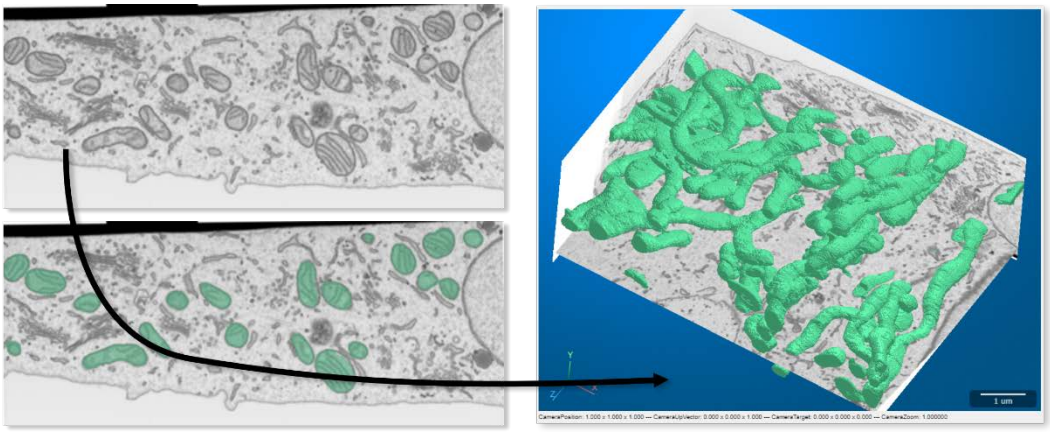

Title: Microscopy 2024. Book of abstracts.

Editors: Vladislav Krzyžánek, Kamila Hrubanová, Dušan Chorvát

Publisher: Czechoslovak Microscopy Society
Královopolská 147, 612 00 Brno, Czech Republic

Edition: 1st, May 2024

Number of pages: 130

ISBN 978-80-909216-0-3

www.mikrospol.cz

ISBN 978-80-909216-0-3